# DEVELOPMENT OF COIR FIBER BASED INSULATIVE COMPOSITE MATERIAL TO REDUCE THERMAL HEAT IN BUILDINGS

Lanka Geeganage Chamath

(208020D)

Thesis submitted in partial fulfilment of the requirements for the degree

Master of Philosophy

Department of Materials Science and Engineering

University of Moratuwa

Sri Lanka

November 2022

## DECLARATION

I declare that this is my own work, and this thesis does not incorporate without acknowledgement any material previously submitted for a Degree or Diploma in any other University or Institute of higher learning and to the best of my knowledge and belief it does not contain any material previously published or written by another person except where the acknowledgement is made in the text.

I hereby grant to The University of Moratuwa the irrevocable, non-exclusive, and royalty free license to archive and make accessible my work in whole or in part in all forms of media, now or hereafter known. I agree that the document mentioned above may be made available immediately for worldwide access unless an embargo applies.

I retain all other ownership rights to the copyright of my work. I also retain the right to use in future works (such as articles or books) all or part of my work. I understand that I am free to register the copyright to my work.

Signature: UOM Verified Signature Date: 24/11/2022

L.G. Chamath

The above candidate has carried out research for the MPhil thesis under my supervision.

Signature of the supervisor: UOM Verified Signature Date: 24/11/2022

Name of the Supervisor: Dr. (Mrs) G.A. Sewvandi

Signature of the supervisor: UOM Verified Signature Date: 2022/11/24

Name of the Supervisor: Dr. L.K.T. Srimal

## DEDICATION

This dissertation is dedicated to my loving parents who always encouraged and motivated me during my ups and downs.

## ACKNOWLEDGMENTS

I would like to express my sincere gratitude to my research supervisor, Dr.(Mrs) A.S. Galhenage, not only for her guidance throughout my research but also for the knowledge and experience that she has shared with me. Her guidance and advice carried me through all the stages of this research she played a major role in my career development also. Next, I would also like to thank my other supervisor, Dr. L.K.T Srimal, Senior Lecturer, Department of Mechanical and Manufacturing Engineering, University of Ruhuna, for closely guiding me in this work and having fruitful discussions throughout the period.

I also thank Mrs. M.M.P.D Samarasekara, former director of the Institute of Technology, University of Moratuwa (ITUM), Major General (Rted.) S.K. Thirunavukarasu, Director/ITUM, and Eng J.M.P. Gunasekara, Head of the Division of Mechanical Engineering Technology, for allowing me to join the staff of the ITUM, and giving invaluable support in administrative issues. Many thanks are due to the academic staff members for reducing my academic workload and permitting me to focus on my research work. I would like to take this opportunity to acknowledge the support given by Mr. K.L.D.J Liyanage of Production Laboratory, and all the academic and non-academic members in Division of Mechanical Engineering Technology, ITUM and Division of Chemical Engineering Technology ITUM.

Special thanks are due to the academic and non-academic staff in the Department of Materials Science and Engineering for their continuous support during my research works. Further, I am thankful to Mrs. T.L.K. Kumari, and Department of Mechanical Engineering, University of Moratuwa. Special thank goes to Department of Physics, The Open University of Sri Lanka, for providing lab facilities for this study.

Finally, my heartfelt appreciation to my family members for taking many hardships to warrant me a disturbance-free environment for successful completion of this study.

L.G. Chamath

## ABSTRACT

Energy consumption is a critical factor in building design. Maintaining a comfortable indoor temperature consumes high energy than other necessities such as lighting and cooking. The building envelope is the main component of the building that transfers heat between indoor and outdoor environments. During the daytime, a proper ventilation system or an air conditioning system can control the heat in a building. Insulation layers are also used under the roofing sheets to control the heat transfer through the roof because a building's roof contributes to a significant heat gain in tropical countries.

Sustainable insulation materials have been more attractive in the last two decades due to biodegradability, low embodied energy, availability, and non-toxicity. Sustainable insulation materials are primarily fabricated using lignocellulose fiber (natural plant fibers). Then it is mandatory to add binder material to adhere to fibers and the material formulated as a composite material, and an air void should be introduced to the combination of fiber and binder to increase insulation properties. Now the whole material can be identified as a three-phase composite material. Thus, the volume fraction of each phase (fiber, binder, and air void) is the most critical factor which controls these composites' insulation properties.

The insulation properties of the material can be analysed using experimental, analytical, and numerical methods. Analytical and numerical methods are more attractive than experimental methods. However, there are limited number of studies on the effect of volume fraction with insulation properties in a three-phase composite. In this study, the effective thermal conductivity ($K_{eff}$) of the composite was analysed through the analytical and numerical models and validated through the experimental results. The results concluded that the experimental results agreed with the numerical and analytical results. Furthermore, a novel mathematical model has been proposed to find the $K_{eff}$ of the three-phase composite using the analytical and numerical methods. The proposed model shows better agreement with the experimental result. Therefore, it can be used to develop this research area further.



**Keywords:** Building insulation, Composites, Coir fibers, Thermal conductivity

# TABLES OF CONTENTS

# LIST OF FIGURES

# LIST OF TABLES

# LIST OF ABBREVIATIONS

| | |
|---|---|
| GHG | Global Greenhouse Gas |
| IEA | International Energy Agency |
| AC | Air Condition |
| MFA | Microfibril Angle |
| TGA | Thermal Gravimetric Analysis |
| DTGA | Derivative Thermal Gravimetric Analysis |
| FWO | Flynn Wall Ozawa |
| FEM | Finite Element Method |
| EMA | Effective Medium Approximation |
| EMT | Effective Medium Theories |
| FTIR | Fourier Transform Infra-Red Spectroscopy |
| SEM | Scanning Electron Microscope |
| NR | Natural Rubber |
| GHP | Guarded Hot Plate |
| DSC | Differential Scanning Calorimetry |
| KAS | Kissinger Akahira Sunose |

# CHAPTER 1

# INTRODUCTION

Reducing energy consumption in the building sector is an essential need today. The building sector consumes approximately one-third of the world's global energy for various applications [1]. As a result, it is responsible for one-third of global greenhouse gas (GHG) emissions. The International Energy Agency (IEA) estimates that the building sector will account for 53% of global energy consumption over the next decade because of the human population growth and the change in the art of living. Therefore, environmental issues are arising with the upsurge in energy demands. $CO_2$ emission primarily contributes to the greenhouse gas effect, which increases the average global temperature. Further, $CO_2$ emissions and rising temperature affect the natural ecosystem and human health [2,3]. Therefore, the energy consumption of the building is a critical parameter to be considered in building design.

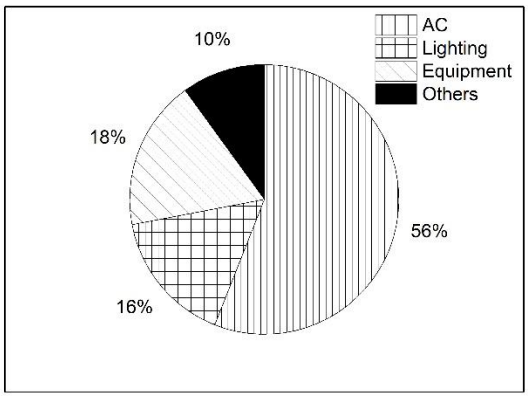


Figure 1.1: Typical building energy consumption in tropical countries [4]

The indoor comfort of a building is an essential objective, equating to other needs such as privacy, security, and weather protection. According to Figure 1.1, a high amount of energy is required to maintain the indoor atmosphere at a suitable thermal comfort level. Therefore, considering the heat transfer through the building is very important for the design work.

The building envelope is the main component contributing to the heat transfer in a building. This is a physical barrier that separates the indoor and outdoor environment of a building and protects the indoor environment from various outdoor conditions such as wind, temperature, ultraviolet radiation, humidity, and precipitation [5,6]. By being a thermal barrier, the building envelope controls the indoor temperature and helps reduce the energy to maintain indoor thermal comfort. Hence, controlling heat transfer through the building envelope can drastically reduce the power requirement for cooling and heating. This decreases the energy required for cooling in hot climates and heating in cold climates [7].

In a tropical country, the indoor temperature changes with the outdoor temperature without an Air Condition (AC) system. Therefore, installing an air conditioning system increases thermal comfort. Moreover, the AC load depends on the heat transfer through the building envelope, and the energy cost highly depends on the nature of the building envelope. In general, the heat transfer through the building envelope can be reduced by the thermal insulation of the building envelope's main components. This method helps to increase energy efficiency by reducing the temperature difference between indoor and outdoor temperatures [2,3]. The main components of the building envelope are the floor, wall, doors, windows, and roof. Among these components, the roof contributes to a significant heat gain to the building. Because the roof is exposed to a direct beam of sunlight during the daytime, 35% of solar thermal radiation enters the building through the roof. Also, the roof represents the highest area of the horizontal surfaces [2,8]. Therefore, controlling the heat transfer through the roof is vital to maintain energy serving.

Typically, the ceiling is limited in the cold climate as an insulator, but in the hot climate, both mass insulators and reflective insulators are used for the insulation [2]. However, the pitched type is the most common roofing method [9]. Therefore, internal insulations are used below the roof structure for the pitch type of roofing structure, where the insulation layers are installed under the roofing sheets [10]. The common types of roofing insulation materials can be identified as conventional materials such as expanded polystyrene, extruded polystyrene, polyethylene, rockwool, and fiberglass [2,3]. Nowadays, researchers are moving to develop

sustainable insulation materials from lignocellulose fibers (natural plant fibers) since various environmental issues occur with conventional materials during raw material supply, manufacturing process, on-site work, building operation, and recycling [9]. These problems can be minimised using sustainable insulation materials foamed by lignocellulose fibers. Sustainable materials are biodegradable, have low embodied energy, and have a low cost for insulation. Therefore, the environmental impact of sustainable materials is neglected, and hence sustainable material is a good candidate for replacing conventional insulation materials [3]. Additionally, lignocellulose fibers have low thermal conductivity, low density, and better mechanical properties, thereby helping to fabricate thermal insulation materials.

However, the insulation material is formulated as a composite material from lignocellulose fibers since it should contain a binder material to adhere to fibers. Also, introducing air void into that combination provides better insulation properties for the final product. Then the composite consists of three phases of the entire structure, and the insulation properties depend entirely on the volume content of these phases. Moreover, finding the behaviour of insulation properties with the volume content of each phase is a huge challenge for scientists.

This research will develop an insulation composite material from a suitable lignocellulose fiber with a natural binder for the roofing insulation. In fact, the literature review will form the basis for selecting the suitable fiber. Next, the behaviour of the thermal conductivity value will be evaluated with different volume fractions of fiber, binder, and void because the composite's thermal conductivity value provides the main idea of heat transfer through the composite. This research work will evaluate these values by analytical, numerical, and experimental analysis. Then the development of a mathematical model based on analytical and numerical results is a new approach for this research work.

With this aim, the following objectives are identified for this study.

## 1.1 Objectives

1. To select suitable bio-degradable natural fiber/s to make thermal insulation composites.
2. To analyse the thermal conductivity of the fiber.
3. To analyse the behaviour of the thermal conductivity with the volume fraction of each phase.
4. To fabricate the composite with high thermal insulation property.

# CHAPTER 2

# LITERATURE REVIEW

The primary objective of this research work is to find an internal thermal insulation material for pitched type roofs. Selecting a suitable insulation material and evaluating the thermal conductivity of the insulation material are the main steps to be followed in this project. Therefore, it is essential to identify the types of roof insulation materials before choosing a material for this application. Section 2.1 discusses the various types of roof insulation materials.

## 2.1 Classification of roof insulation materials

Figure 2.1 illustrates the classification of roof insulation materials.

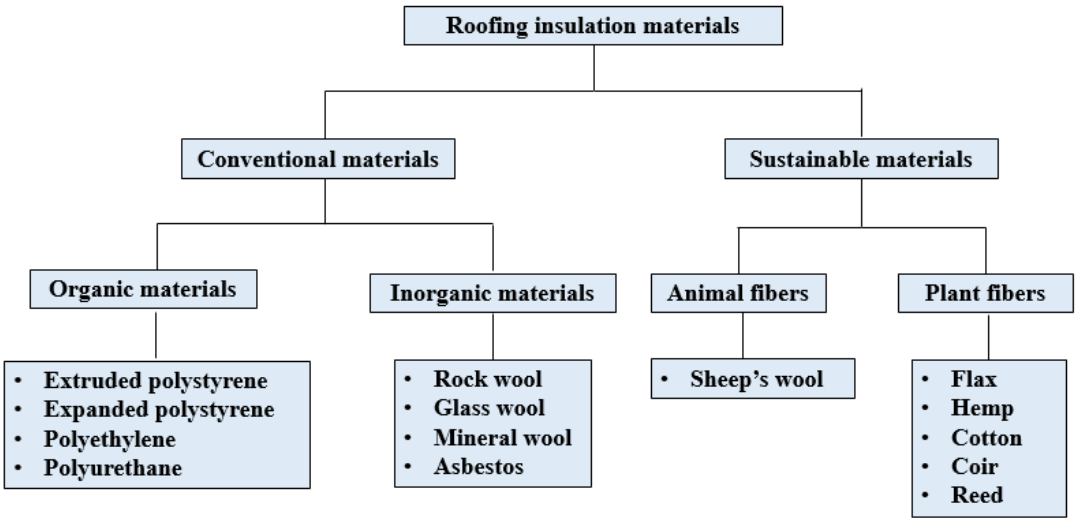


Figure 2.1: Classification of roofing insulation materials [9,11]

According to Figure 2.1, roof insulation materials are mainly categorised into conventional and sustainable. Conventional materials can be subdivided into organic and inorganic materials, while sustainable materials can be categorised into animal and plant fibers [9,11]. According to their internal structure, they can also be classified as fibrous, cellular, and granular [9,12]. Mineral, plant, and animal insulators mainly have

fibrous structures, and conventional organic materials have a cellular structure [9,12]. However, the sheep's wool batts are costly due to high labour costs and loss of material during manufacturing. Therefore, conventional organic, conventional inorganic, and plant fibers are the most suitable materials for roof insulation. Figure 2.2 presents the demand for these insulation materials.

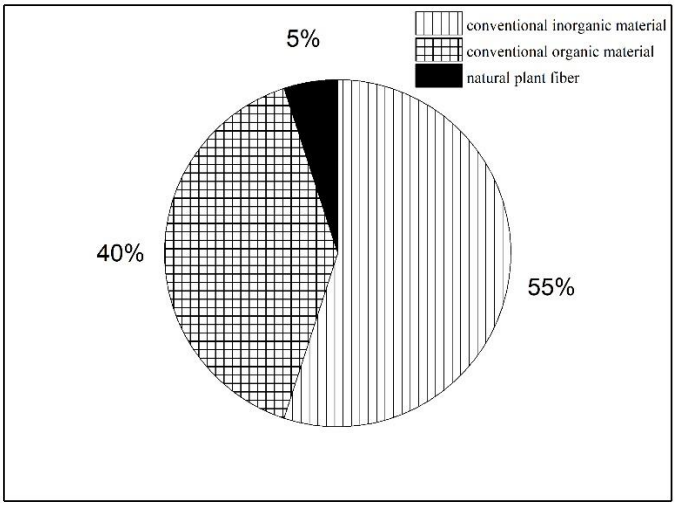


Figure 2.2: The demand for thermal insulation materials [13]

According to Figure 2.2, conventional inorganic insulation products are the most attractive insulation material globally. These materials are abundant in the world but are non-renewable. Glass mineral wools, rock mineral wools, and asbestos fibers are examples of inorganic insulation materials [2,12]. These inorganic materials show very high performance for thermal insulation, high moisture absorption resistance, and fire resistance than other conventional materials and are cheaper than the others [2,13]. However, those materials release toxic dust particles into the environment during manufacturing and installation processes, health issues related to these inorganic fibers were identified after the $20^{th}$ century [13]. Exposure to an air-born concentration of these dust damage lung functions [14]. Several countries have banned these products [13] since the manufacturing process requires a high amount of energy, and environmental pollution can occur due to high temperatures [9].

Conventional organic insulation materials are manufactured from organic materials such as polystyrene, polyurethane, and polyethylene. These insulation materials are used for various industrial applications due to their low price, availability, and high performance as insulation materials. Nevertheless, these materials are much more hazardous to the environment and human health because the addition of toxic substances during the manufacturing process emits dangerous gases [14].

According to Figure 2.2, natural insulation materials represent about 5% of the total market [13]. However, the demand for natural materials has increased over the last twenty years because of the high manufacturing cost, the high energy requirement for manufacturing, and the release of toxic substances during manufacturing and recycling problems with conventional insulation materials [15]. Introducing natural plant fibers can minimise these problems since they help mitigate the landfill problems and reduce energy consumption for manufacturing [15,16]. The amount of $CO_2$ in combustion becomes neutral during their growing time at the end of the lifetime of the fibers [15]. Furthermore, high embodied energy is required to produce conventional materials than natural fiber insulation materials [2]. This can be well explained by comparing the energy required to produce glass fibers and kenaf fibers. A glass fiber takes 54 MJ of energy to produce 1 kg, and a kenaf fiber takes 15 MJ of energy to produce that weight of fiber. In addition, natural fibers are less dense than glass fibers. Therefore, more quantity of natural fiber insulation materials can be manufactured from the same energy.

The maintenance cost of machine tools is less due to the non-abrasive nature of fibers. It provides a good working environment for workers because of the nontoxicity [16]. Additionally, natural fiber materials are readily available as a by-product of agricultural industries. Fiber from oil palm, coconut, cotton, sugarcane, date palm, and other natural fibers could be eco-friendly insulation materials for building applications [17].

According to Section 2.1, lignocellulose fibers (natural plant fibers) can be used to fabricate thermal insulation materials. However, it is mandatorily required to select a suitable fiber for the internal insulation of the pitched type roof. Therefore, Section 2.2

focuses on various factors for the selection criteria for this application, comparing those factors with existing natural fibers and selecting a suitable fiber that meets the research work requirements.

### 2.2 Selection of lignocellulose fiber for roof insulation

The selection and installation of building insulation materials depend on various factors. The application and working conditions of the building are the key factors for selection. The thermal conductivity behaviour, reactance to moisture absorption, mechanical behaviour, durability with thermal and biological resistance, and cost for the given thermal performance should also be considered during the selection process [9].

#### 2.2.1 Application and working conditions

According to European Technical Approvals, the following six parameters should be considered when selecting an insulation product for the building insulation [10].

1. Mechanical stability and resistance
2. Safety in utilisation
3. Safety in case of fire
4. Protection against noises
5. Health and the environment
6. Energy efficiency and heat retention

Therefore, identification of the application and working conditions is the prerequisite for selecting insulation material [9]. The primary purpose of this project is to develop an insulation material to use below the pitched type roofing cover. Natural plant fiber could be selected to fulfil this requirement. Wood fibers, cellulose fibers, hemp, cotton, flax, reed, and coconut fibers can be used under the roofing cover as an insulation material under the above technical parameters of European technical approval [10].

#### 2.2.2 Thermal conductivity of natural fibers

Thermal conductivity less than 0.065 W/mK is referred to as the insulation material in building construction [9]. Figure 2.3 shows the thermal conductivity and density of natural fibers with a thermal conductivity value of less than 0.065 W/mk.

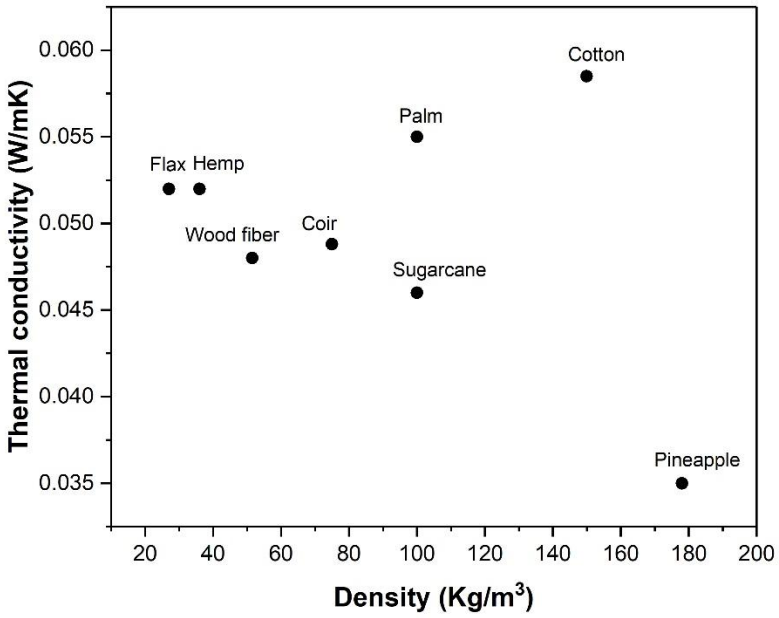


Figure 2.3: Thermal conductivity of natural fibers [1,14,18]

Here, the thermal conductivity values are given for some materials without a binder, while other values are obtained from composites made of natural fibers. However, Figure 2.3 indicates that the above materials can be used for building insulation because their thermal conductivity values are less than 0.065 W/mK [18].

The fiber density of binder-less palm fibers, coconut fibers, and sugarcane fibers gave optimum thermal conductivity values at 100 $kgm^{-3}$, 75 $kgm^{-3}$, and 100 $kgm^{-3}$, respectively. The respective thermal conductivity values were 0.055 W/mK, 0.0480 W/mK, and 0.046 W/mK in Manohar's work [17]. The behaviour of thermal conductivity with the density of the fiber bundle was carried out in this experiment. The thermal conductivity of the fibrous batt was decreased with the density of the fibrous batt until the optimum point and then increased after that point hence the thermal conductivity value of loose-fill material is greater than close-celled materials after the optimum point [17]. Cetiner experimentally investigated the thermal conductivity as 0.0528 W/mK for oven-dried binder-less wood waste materials [19]. According to the literature, binder-less cotton stalk fiberboards were made with

densities of 150 – 450 $kgm^{-3,}$ and the thermal conductivity varied from 0.0585 W/mK to 0.0815 W/mK 117 $kgm^{-3}$.

Sathishkumar reported thermal conductivity values of different fibers with epoxy resin [20]. The smallest thermal conductivity value was 0.03 W/mK, which has cotton, and the tertiary smallest value was 0.047 W/mK for coir fibers. The thermal conductivity of fabricated samples can be arranged in the ascending order of cotton, sisal, coir, flax, palm, and hemp [20]. The thermal conductivity of jute and hemp fiber is higher than in cotton and flax because the lumen size of cotton and flax is larger than hemp and jute, increasing the fiber insulation properties [21].

The thermal conductivity of fiber-reinforced clay bricks was measured according to Rashid's experiment [22]. Brick reinforced with coir fiber had the lowest thermal conductivity. Thereafter, the thermal conductivity values increased in the order of bamboo, sisal, and jute, respectively. Still, the thermal conductivity value of bricks depends on the porosity level, density, and water absorption percentage [22].

Tangjuank investigated the thermal conductivity with pineapple and latex composite [23]. Here, a composite with a density value of 210 $kgm^{-3}$ had a thermal conductivity of 0.035W/mK. The composite is made of fiber: latex with 1:3 ratios. The pineapple and natural rubber latex composite made by Kumfu had a thermal conductivity of 0.057W/mK with 338 $kgm^{-3}$ [24]. Also, coir fiber and natural rubber latex showed good thermal insulation properties for building insulations [25,26].

Composites made from sugarcane, coconut, palm fiber, cotton stalk, wood waste, sisal, jute, pineapple, hemp, and flax can be used as building insulation materials since their thermal conductivity values are less than 0.065 W/mK as explained above. Furthermore, cotton, sisal, coir, bamboo, and sugarcane have lower thermal conductivity values than hemp, flax, jute, and palm, according to the above literature results [17,20,21,22].

### 2.2.3 Density comparison of natural fibers

The thermal conductivity of a material depends on the material density. Therefore, low-density materials can be used for insulation since molecular vibrations occur due to the storing of heat energy in molecules. The temperature increases with molecular

vibration, producing more molecular vibrations at higher temperatures [26]. This argument is well reflected in the density value of solid palm fiber, coconut fiber, and sugarcane fiber compared to thermal conductivity. The fiber density of palm fiber, coconut fiber, and sugarcane fiber were 797 $kgm^{-3}$, 755 $kgm^{-3}$, and 686 $kgm^{-3}$, respectively, with thermal conductivity values of 0.0555 W/mK, 0.0480 W/mK, and 0.0461 W/mK. The fiber density must also be reduced to lower the composite weight [27]. Hence, the analysis of the density variation of natural fibers is an essential parameter for selecting fiber for thermal insulation materials. Figure 2.4 illustrates the density variation of different fibers.

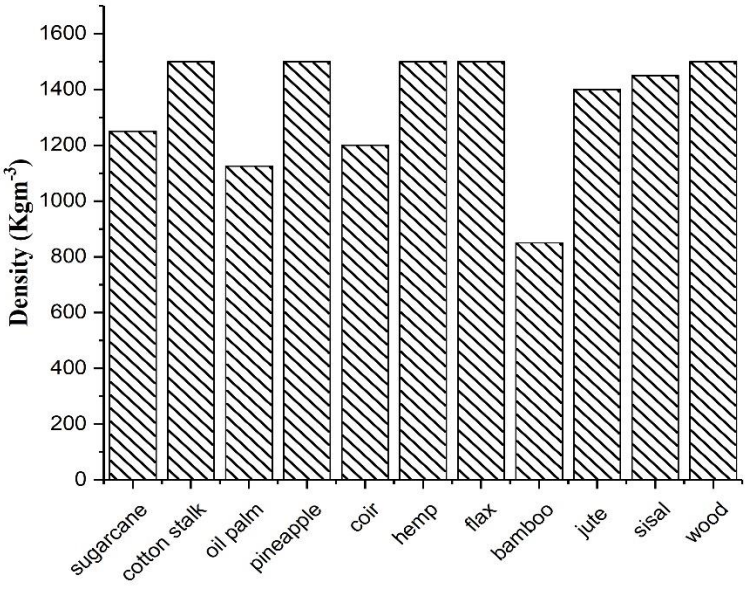


Figure 2.4: Density of natural fibers [15,27,28,29,30]

According to Figure 2.4, bamboo, oil palm, coir, and sugarcane fibers have the lowest density values.

### 2.2.4 Structure of natural fibers

Lignocellulose is the basic constructional substance for the plant cell, and most types of natural fiber structures are formed by lignocellulose substances [31]. Lignocellulose contains cellulose, hemicellulose, lignin, pectin, waxes, and water dissoluble substances [27]. The lignocellulose structure is a natural composite [27], and the microfibril that produces cellulose gives reinforcement for the cell [27]. Cellulose

microfibrils are mixed with hemicellulose and lignin matrix [11,27]. Therefore, cellulose, lignin, and hemicellulose are the primary elements that alter the structural properties of plants [21,31]. Additionally, oily substances and waxes give fiber protection, and pectin contributes to fiber flexibility. Most microscopic fiber structures are developed from primary, three secondary cell walls, and lumen. These cell walls contain above lignocellulose substances, and the lumen is the cavity that contains air [11]. It reduces fiber density and controls the heat, moisture absorption, and moisture releasing of fiber [21]. Figure 2.5 presents the microscopic structure of the natural fiber.

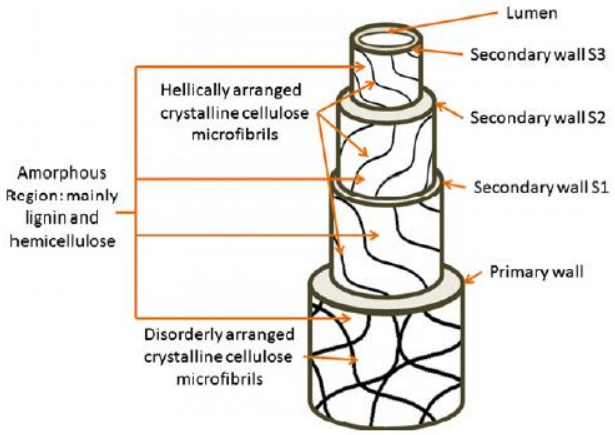


Figure 2.5: Structure of natural plant fiber [11]**.**

*(Reprinted from Material and design, 47, Z. N. Azawa, B. F. Yousif, A. C. Manalo, and W. Karunasena, A review on the degradability of polymeric composites based on natural fibers, 424-442, 2022, with permission from Elsevier)*

A single cellulose chain is arranged by intramolecular hydrogen bonds that form unit cells using intermolecular hydrogen bonds. Linear stability is given by intramolecular hydrogen bonds, and reinforcement is given by intermolecular bonds. Due to many interconnected hydrogen bonds, these cellulose bonds cannot be easily dissolved in moisture and alkaline. Celluloses are hydrophobic [31], and the cellulose content increases fiber stiffness and rigidity. However, fiber flexibility decreases with the cellulose content [27]. These celluloses can be found as thin microfibrils in plants [11], formed by the linear accumulation of unit cells [31]. Such microfibrils provide fiber tensile strength, but the magnitude of the tensile strength depends on the angle which

makes the microfibrils and the central axis of the fiber. This angle is the microfibril angle (MFA) [27].

As the MFA decreases, the tensile strength will increase, reducing the elongation at the break [21]. Figure 2.6 shows the fundamental structure of cellulose.

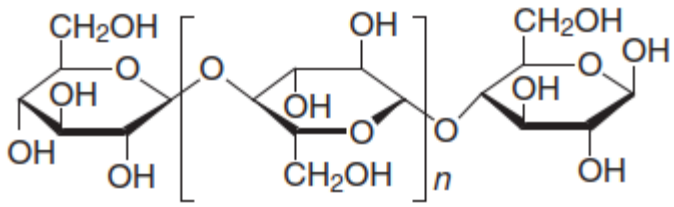


Figure 2.6: Fundamental structure of cellulose [31]

*(Permission is granted subject to an appropriate acknowledgement given to D. D. Stokke, Q. Wu, and G. Han, Introduction to wood and natural fiber composites,Wiley.)*

Hemicellulose acts as a cementitious material between microfibrils in the fiber structure by hydrogen bonds of the hemicellulose molecules [27]. These hemicelluloses can be dissolved in dilute alkaline or acidic solutions and hydrophilic [11]. Figure 2.7 presents the hemicellulose chemical structure.

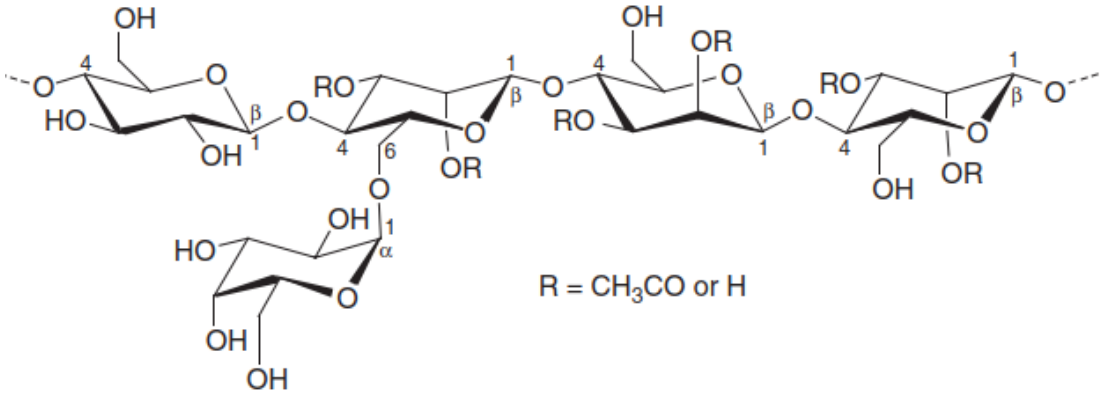


Figure 2.7: Chemical structure of hemicellulose [31]

*(Permission is granted subject to an appropriate acknowledgement given to D. D. Stokke, Q. Wu, and G. Han, Introduction to wood and natural fiber composites,Wiley.)*

Lignin is the next main constituent in the lignocellulose structure. It is mainly identified as amorphous due to various structure types. Lignin has aromatic structures because it contains benzene rings, as shown in Figure 2.8. Lignin is hydrophobic due

to its aromatic structure and crosslinks among the molecules; it acts as a glue between cell walls and gives rigidity to cell walls. Lignin is a thermoplastic material in nature. These advantages can help composite manufacturing [31].

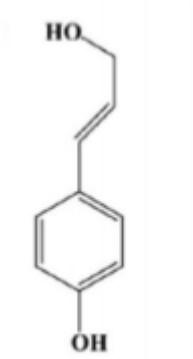


Figure 2.8: Fundamental structure of lignin [31]

*(Permission is granted subject to an appropriate acknowledgement given to D. D. Stokke, Q. Wu, and G. Han, Introduction to wood and natural fiber composites,Wiley.)*

According to the above discussion, the lignocellulose fiber properties depend on the chemical substances on the cell wall. Figure 2.9 shows how to change fiber properties with cell wall substances.

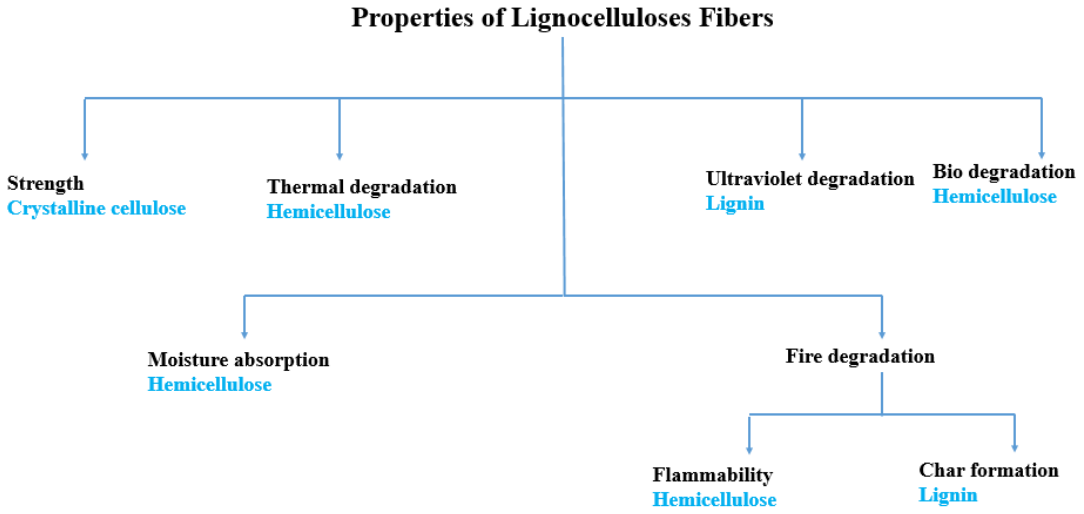


Figure 2.9: Cell wall substances responsible for the properties of natural plant fiber

Chemical substances in the fiber vary between plants. Figure 2.10 provides lignin, hemicellulose, and cellulose percentages of different fibers.

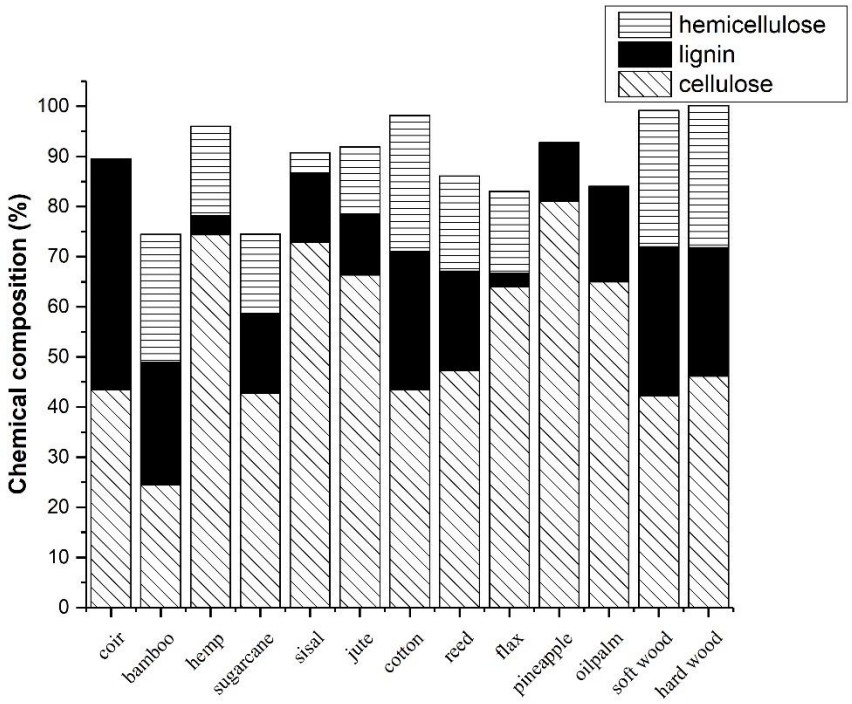


Figure 2.10: Chemical compositions of various plant fibers [11,27]

### 2.2.5 Water absorption of natural fibers

Natural fibers are hydrophilic due to the presence of lignocellulose substances [16]. Therefore, they tend to absorb environmental moisture, resulting in fiber swelling at the matrix. Fiber swelling reduces the matrix's bonding strength [16], affects the desired mechanical and thermal properties, and changes the composite dimension [11,27]. Also, natural fiber composites tend to fail in moist environments, which causes fiber swelling [11].

The water absorption ability of the natural fiber is the crucial parameter for designing a natural fiber-reinforced composite [16]. Hemicellulose in the lignocellulose fiber mainly contributes to moisture absorption. The amorphous region of the cellulose also subscribes to this phenomenon. Water absorption is highly increased by polysaccharide chains in hemicellulose [27], and the hydroxyl groups of substances form hydrogen bonds with moisture. Water absorption rises with the hemicellulose content, affecting fiber biodegradation because high water content influences the microbial attack. Moreover, porosity and hollow cavities decrease fiber density but

increase the moisture absorption of fiber. Dissolving cellulose is difficult in liquid, but these liquids can remain between the microfibrils [11]. Lignin has a much lower water absorption rate than other substances in the lignocellulose fiber [32]. The water absorption rate linearly increases initially and reduces with prolonged duration, following the Fickian behaviour [11].

Two water types can be identified during the moisture absorption process. *Bound water* is found in cell walls and bonds with the hydrogen bonds in the hydroxyl group of substances, whereas *Free water* occurs in voids created by a cell wall [27]. These voids can be identified as a lumen of the cell, small cavities, and micro spaces in the cell wall [31]. This free water is carried by the capillary action or tension forces. However, dimensional changes result from bound water, and free water does not contribute to thickness swelling [27] because secondary bonds break due to water absorption. It produces a hydrogen bond with the hydroxyl group of the lignocellulose fiber. This phenomenon causes fiber swelling [32]. Hence the free water content changes the total mass of fibers but does not affect fiber properties [31].

Khuram studied the behaviour of moisture absorption in sisal, bamboo, jute, and coir [22]. Jute fiber has maximum moisture absorption ability, and its chemical composition makes it the most water-absorbent fiber among the best fibers [29]. The smallest percentage of diameter change was indicated by jute than sisal, bamboo, and coconut fiber. The cellulose content of the jute fiber can absorb moisture without swelling the diameter. Furthermore, a secondary amount of water absorption was observed by sisal fiber due to the high cellulose content. However, coir fiber had the minimum water absorption value [22] since coir fiber is the most lignin-rich fiber among natural fibers [29]. The diameter of the coir fiber increased by 3.53% after water absorption; this was a comparatively small value with the diameter variation of sisal and bamboo fiber.

Moisture absorption of wood fiber was higher than hemp and flax fiber, according to Martin's work [18]. Also, the moisture content of hemp was higher than flax fiber because a large amount of water is absorbed by the high hydrophilic nature of hemp fiber. When hemp is mixed with concrete, it takes a long time to settle and dry with

the excess moisture content of hemp fiber [16]. Hemp fiber can absorb high moisture content, but this value is lower than jute and sisal, as shown in Ikbal's work [19].

In Dewi's experiment, coir fiber and palm fiber were mixed with polyester resin [33]. The required fiber volume of the composite was filled with 100% coir fiber in the first sample. Then the volume of coir was gradually decreased, and the palm fiber volume was increased up to 100% for the next samples. The first sample, which contained 100% coir fiber, provided the least moisture content and the least thickness swelling. It shows that moisture absorption and fiber swelling are lower than palm fiber. Furthermore, the initial coir fiber dimensions can be restored due to lignin and cellulose contents [19]. Coir fiber absorbs less water than pineapple leaf fiber, as in Mittal's work [32], but pineapple absorbs moisture in levels between sisal and jute [29].

Cotton fibers had hydrophilic properties due to their high cellulose content than other natural fibers. Coir fibers contain the highest lignin percentage among other natural fibers [16,29]. Therefore, coconut fibers are relatively waterproof and absorb the least saltwater content than other natural fibers [29].

According to the above discussion, the water absorption behaviour order can be adjusted as coir, bagasse, bamboo, flax, hemp, sisal, pineapple, jute, and cotton [29].

### 2.2.6 Mechanical properties of natural fibers

The mechanical properties of a fiber depend on structure, chemical composition, microfibrillar angle, and defects. Microfibrillar angle is a crucial parameter for defining the mechanical characteristics of fibers. A small microfibrillar angle gives high stiffness and strength values [11] because low angle microfibrillar aligns along with the central axis of the fiber direction and increases the tensile strength [30]. However, the ductility and elongation at the breaking point are increased by a high microfibrillar angle [11,30]. Cellulose has higher strength and stiffness than other lignocellulose substances [29]. Strength is given by the anhydride group and hydroxyl group bond due to the covalent bond in cellulose [16]. Hence, cellulose content and cell dimension increase Young's module and tensile strength of the fiber [11,16]. As mentioned above, the lower the microfibrillar angle, the higher the cellulose content,

the higher length of the cell, and the high degree of crystallinity of cellulose will result in high tensile strength [11]. Additionally, fiber porosity influences mechanical strength because moisture absorption increases with the porosity level [30] and moisture content affects the orientation and degree of crystallinity [11].

Hemp and jute fibers have the highest tensile strength values than other natural fibers [11]. These fibers show the same behaviour for the stress-strain graph [29]. High cellulose content causes the tensile strength to increase, so these fibers can be used for reinforcing applications [16]. Hemp can act as a reinforcing material for various types of applications due to its high stiffness and strength. Flax fiber has good strength because of its high cellulose content. Pineapple leaf fiber has the highest tensile strength among leaf fibers. The microfibrillar angle and high cellulose content are relatively higher than other types of leaf fiber. Bamboo fiber has a high resistance to force, but tensile strength is very low among plant fibers. Palm fibers have the same hardness and toughness behaviour as coir fiber, but the elongation value at the breaking point is higher than other natural fibers due to its highest value for microfibrillar angle [29].

### 2.2.7 Thermal degradation of natural fibers

The chemical composition of lignocellulose fibers alters the mechanical and physical characteristics. Hence the percentage of crystalline cellulose obtains the thermal stability of the fiber. Higher content of hemicellulose and extractives cause fiber degradation at low temperatures [34]. Investigating the lignocellulose fiber degradation is vital because of possible thermal degradation during composite fabrication and prolonged usage. Therefore, prediction and understanding of thermal degradation influence the estimation of composite properties [35].

Natural fibers undergo two or more steps for thermal decomposition. The first stage of decomposition is the evaporation of moisture and the decomposition of low molecular extractives. The hydrophilic nature of fiber affects the first stage of decomposition, and chemically bonded water is not involved in these phenomena [34,36]. Typically, this type of decomposition occurs at a temperature of 50 ºC to 150 ºC. Then hemicellulose degradation can be identified as the second step of degradation between

the temperature range of 200 ºC to 350 ºC. Hemicellulose can be easily removed from the cell structure due to the amorphous and randomness of the structure. CO and $CO_2$ volatiles are generated as a result of hemicellulose degradation. However, the hydrogen bonds between hemicellulose and cellulose increase the thermal stability of hemicellulose. The third stage of decomposition is the paralysation of cellulose. A well-ordered structure and branchless polymer chain affect the high thermal stability at high temperatures. Therefore, cellulose pyrolysis occurs in the high-temperature range of 320 ºC to 400 ºC.

Lignin degradation is identified as the fourth degradation [34]. However, lignin degradation occurs in the entire range of heating from 100 ºC to 900 ºC. Various types of branches with aromatic rings and the function of the chemical bonds lead to a high degree of degradation [34,35].

The most common methods for thermal decomposition analysis are Thermal Gravimetric Analysis (TGA) and Derivative Thermal Gravimetric Analysis (DTGA) [36,37]. Mass loss of the sample relative to time and temperature is analysed by TG and DTG curves. Figure 2.11 indicates the differences between TG and DTG. Cellulose decomposition can be identified from the main peak of a DTG, and the shoulder of the DTG curve indicates the decomposition of hemicellulose. The shoulder peak does not appear in some cases due to the overlapping with the curve's main peak, and the DTG curve's tail shows the lignin decomposition [37].

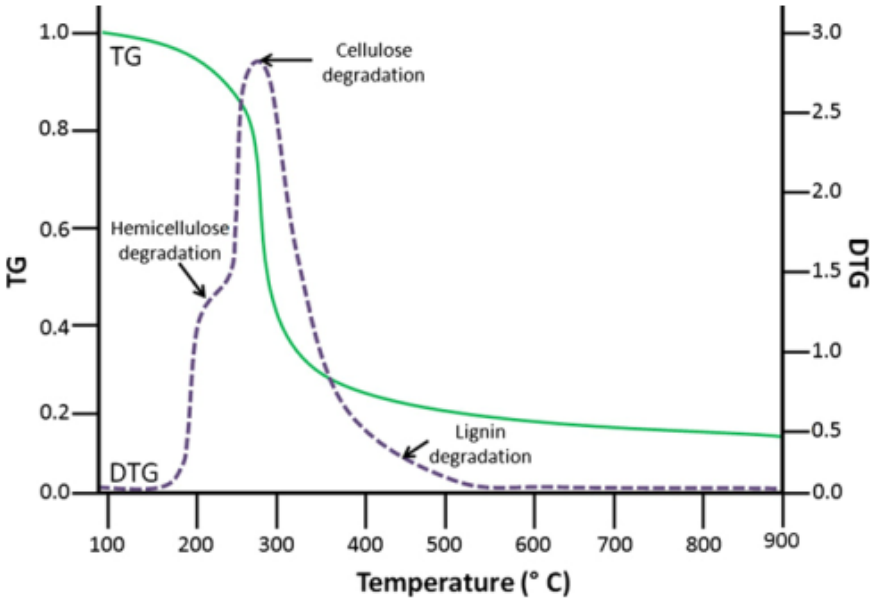


Figure 2.11: Typical TG and DTG curves of natural fibers [11]

*(Reprinted from Material and design, 47, Z. N. Azawa, B. F. Yousif, A. C. Manalo, and W. Karunasena, A review on the degradability of polymeric composites based on natural fibers, 424-442, 2022, with permission from Elsevier)*

Due to their individualistic combination, various types of kinetic techniques are used to analyse the thermal decomposition of lignocellulose fibers [34]. Different types of model-free and model-fitting methods evaluate kinetic parameters taken by TG and DTG. The model-free method is generally used to find kinetic parameters because of its simplicity and accuracy [34,36]. Therefore, the most typical model-free methods such as Kissinger, Flynn Wall Ozawa (FWO), and Friedman are used to determine the activation energy ($E_a$) of plant fibers [34]. The activation energy provides information on the minimum energy required to initiate a reaction. Hence the finding of activation energy for decomposition helps detect the thermal decomposition of natural fibers [37].

Analysing the TGA covers in Poletto's work indicates that jute fiber has higher thermal stability than sisal fiber [34]. A low percentage of bonded water due to the high degree of crystallinity and low content of extractives of jute fiber may have produced this result. The decomposing process of sisal starts at a low temperature. The contrasting properties of jute fibers may have shown this result.

Fei Yao determined the apparent activation energy of selected plant fibers [37]. Bagasse, bamboo, cotton stalk, hemp, and jute were chosen for this review. Here the activation energy of fibers was determined by the above three types of model-free methods. It was suitable for comparison of other fibers. The $E_a$ value of jute fiber was higher than hemp than that of Friedman and FWO, although the behaviour changed in the Kissinger method. However, the $E_a$ values of jute and hemp fibers were at around 180 kJ/mol, and it is higher than the $E_a$ of bagasse, bamboo, and cotton stalk.

Apparent activation energies of coir fibers, sugarcane, banana pseudostem, and pineapple leaf were observed by Siti using three kinds of model-free methods [35]. Here, the Ea values were reduced for coir, pineapple leaf, sugarcane, and banana pseudostem, respectively. Coir fiber showed higher thermal stability than other fibers. The highest content of lignin may have caused this result.

The $E_a$ values of alkaline-treated coir, jute, sisal, and areca were discussed in Shilpa's work [36]. Among these fibers, alkaline-treated coir fiber showed the highest $E_a$ value. The effectiveness of alkaline treatment for fiber will be discussed later in this review.

Furthermore, the $E_a$ value can estimate the lifetime of natural fibers and their composites [38,39]. The Toop's method was proposed as an efficient method for estimating the lifetime of various composites consisting of reinforced coir fibers and flax fibers reinforced in a polymeric matrix [38].

$$lnt_f = \frac{E_a}{RT_f} + \ln\frac{E_a}{\beta R}.P\left(X_f\right) \tag{2.1}$$

Analysing the above equation shows that the estimated lifetime ($lnt_f$) depends on the activation energy of the material [38,39,40]. Therefore, fibers with higher activation energy have a higher lifetime on the thermal. By analysing the result of the previous studies, we identified that coir fiber has a longer lifetime of thermal degradation than jute, sisal, pineapple, bamboo, sugarcane, hemp, and cotton stalk. The highest lignin percentage in coir fiber influences this result because, in fibers, lignin is the most difficult constituent to decompose [35].

### 2.2.8 Embodied energy

The embodied energy is the energy involved in different stages of the material. It involves different stages of extraction, production, transportation, installation, and disposal. Also, embodied energy gives information on embodied carbon. Figure 2.12 presents the embodied energy of different natural fibers [3].

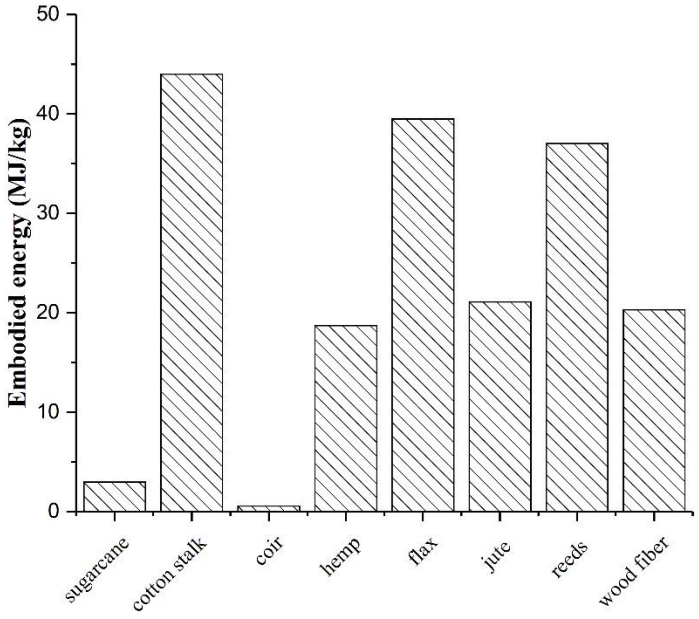


Figure 2.12: Embodied energy of different natural fibers [3]

According to Figure 2.12, coir fibers have a minimum embodied energy of around 0.55 MJ/kg. Therefore, it releases the minimum greenhouse gases throughout the production process. Also, it has a lower production cost due to the lower value of embodied energy [3].

According to this discussion, thermal conductivity, water absorption resistance, thermal degradation, density, elongation at the breaking point, and tensile strength can be summarised using a weight of analysis data as shown in Table 2.1.

Table 2.1: Weight of analysis data for fiber properties

| | Insulation property (25%) | Water absorption resistance (25%) | Resistance to thermal degradation (25%) | Low-density (10%) | Elongation (10%) | Tensile strength (5%) | Average |
|---|---|---|---|---|---|---|---|
| Wood | 2 | 1 | 1 | 1 | 1 | 5 | 1.50 |
| Cotton | 5 | 1 | 2 | 1 | 2 | 2 | 2.45 |
| Flax | 3 | 4 | 2 | 1 | 1 | 4 | 2.70 |
| Coir | 5 | 5 | 5 | 3 | 5 | 1 | 4.75 |
| Sugarcane | 3 | 4 | 2 | 3 | 1 | 1 | 2.85 |
| Oil palm | 2 | 2 | 1 | 4 | 3 | 1 | 2.20 |
| Jute | 1 | 2 | 3 | 2 | 1 | 3 | 2.05 |
| Hemp | 1 | 3 | 3 | 1 | 1 | 5 | 2.25 |
| Bamboo | 4 | 4 | 2 | 5 | 1 | 1 | 3.40 |
| Sisal | 4 | 3 | 2 | 1 | 1 | 4 | 2.70 |
| Pineapple Leaf fiber | 3 | 3 | 2 | 1 | 1 | 5 | 2.50 |

Five types of point scales used in Table 2.1 are given in Table 2.2.

Table 2.2: Five types of point scales

| Grade | Very low | Low | Average | High | Very high |
|---|---|---|---|---|---|
| Score | 1 | 2 | 3 | 4 | 5 |

According to Table 2.1, coir fiber has the highest grade point average among other fibers and shows the minimum value for embodied energy. According to European technical standards, it is suitable for insulation under the pitched type roof cover.

After identifying the fiber type for the composite, we can consider the composite fabrication. However, the composition of each phase (fiber, binder, and void) should be identified before the fabrication. Because the volume ratio of each phase affects the thermal conductivity of the material. The volume ratio of each phase can be identified from the numerical, analytical, and experimental methods. Sections 2.3, 2.4, and 2.5 explain these methods.

## 2.3 A numerical method to analyse the thermal conductivity of composites

The Finite element method (FEM) can be identified as a dominant appliance for finding the closest solution to a mathematical problem in numerical analysis. FEM can adopt different simulation types for various functions of a physical system. FEM generates the finite number of elements to find the unknown variable, and it is given by assuming the closest function of individual elements [41]. Since laboratory experiments generally take a long time to achieve steady-state conditions and much more difficult to maintain those conditions during the investigation, finding a solution through FEM is more effective in analysing the variation of physical parameters.

FEM has a higher degree of flexibility in design enhancement; it is a cost-effective and a faster method of analysing results than experimental methods [42]. In previous experiments, the thermal conductivity of composites was determined by software of the ANSYS package used for finite element analysis [22,41,42,43]. This software has been written by ANSYS Programming Design Language (ADPL) and easily simulates a given problem [43].

A micromechanical model should be created for the ANSYS simulation, and some assumptions were carried out for the simulation of composites in the literature as follows [41,44,45,46].

- The matrix and fibers are microscopically homogeneously distributed throughout the composite.
- The perfect bonding and negligible thermal resistance between fibers and the matrix,
- Fibers having the same shape and size,

- Uniform distribution of fibers, and
- Void-free in the composites

### 2.3.1 Generation of the unit cell

The thermal conductivity of a composite can be changed by either adding reinforced material or changing the molecular orientation of the composite. Frequently, the composition of the fibers or particles changes the thermal conductivity value of the composite. Also, conductivity values depend on fiber orientation, which creates the angle between the heat flux and the fiber [41]. Figure 2.13 shows the longitudinal and transverse arrangement of fibers in a composite [47].

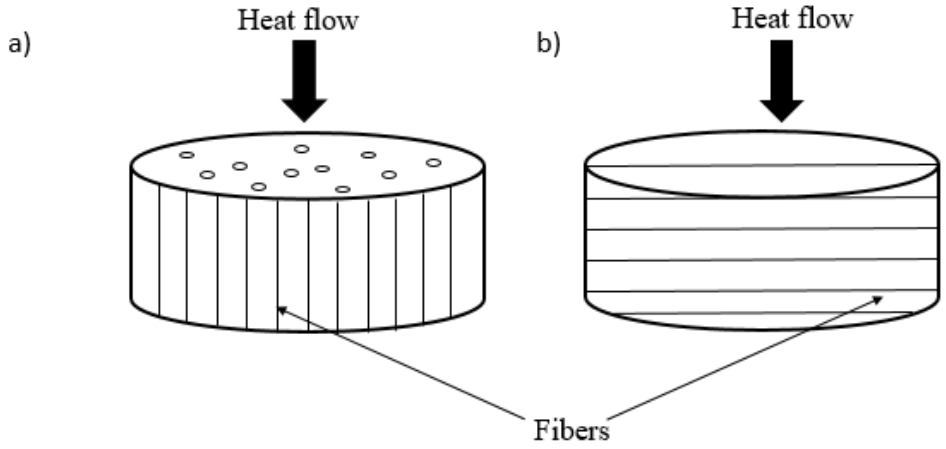


Figure 2.13: Arrangement of the fiber direction - a) longitudinal, b) transverse [47]

Thermal conductivity values for longitudinal (Figure 2.13a) and transverse (Figure 2.13b) directions were considered in previous studies. The longitudinal arrangement showed the highest value for thermal conductivity [41,44,46,48,49] because heat flux is parallel to the fiber arrangement [47]. Analysing the thermal conductivity in the transverse direction is more difficult. It varies due to the arrangement of the crystalline lattice of the cellulose, the vast range of lumens, and fiber walls [49]. In the longitudinal direction, the thermal resistance of the composite lamina is constant [44]. After identifying the fiber orientation, the micromechanical model for FEM should be designed, as shown in Figure 2.14.

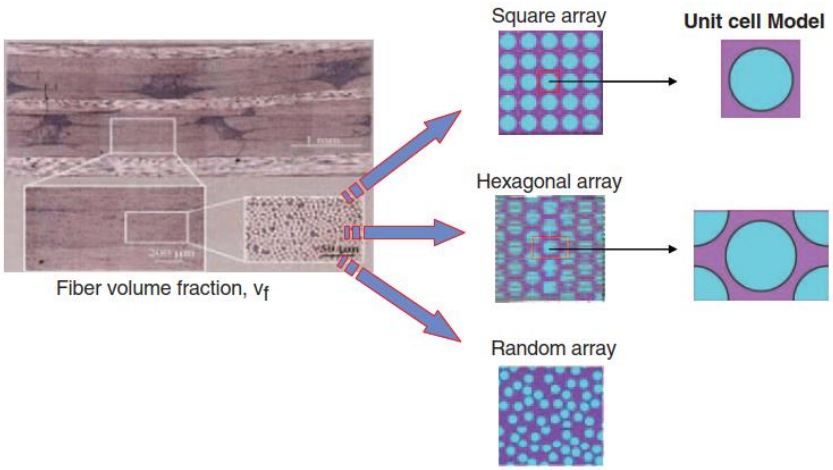


Figure 2.14: Micromechanical arrangement of fiber–reinforced composites [50]

*(Permission is granted subject to an appropriate acknowledgement given to S. Sihn and A. K. Roy, Micromechanical analysis for transverse thermal conductivity of composites, Journal of Composite Materials (vol. 45, no. 11) , pp. 1245–1255, Copyright © 2011 (SAGE Publications) , doi: 10.1177/0021998310382311.)*

The frequent arrangement of fiber arrays can be identified as square or hexagonal unit cells. It can be reduced as a periodic block with a unit cell model description. However, a random array can simulate random fiber arrangement [44,50].

Rao studied the transverse thermal conductivity ($K_T$) of various shapes of fibers using a square unit cell [44]. The centre fiber unit is surrounded by a square matrix, as the square array pattern in Figure 2.14, and models have been extended to different fiber shapes such as circular, square, elliptical, and rhombus. The horizontal elliptical model indicated better insulation properties in the matrix dominated composite than in square and circular fibers. However, elliptical fiber cannot attain a high volume fraction. Therefore, selecting the fiber shape in the unit cell model is essential for thermal performances [44].

The transverse thermal conductivity of hollow manila hemp fibers was simulated in Sihn's work [50]. Thermal properties of circular fiber were compared to a square fiber with the same volume fraction of fiber with a constant volume of the lumen. Equal conductivity values were identified up to 0.5 fiber fractions for both types of fiber shapes. Additionally, the effect of fiber hollowness on $K_T$ was simulated by a square array. Furthermore, the unit cell was reduced to one-fourth of the cell to increase the

simulation efficiency. Here $K_T$ values were decreased by the fiber hollowness of the matrix-dominated composite [46]. The $K_T$ estimation of a fiber-reinforced composite in Priya's work is an example of a hexagonal array [45], and regular and random fiber distributions on $K_T$ were studied in Sangwook's work [50]. The difference between random fiber distribution and regular distribution $K_T$ values was indicated at the higher fiber volume, but the experimental results in Sangwook's work was a well-accepted random distribution [50]. The above studies show that the $K_T$ value changes with the fiber distribution in the matrix, volume fraction, fiber shape, and properties of parent materials [46].

Furthermore, longitudinal thermal conductivity ($K_L$) was simulated by Kumar Sahu and Devieddy [41,43]. The cylindrical fibers of the cube lattice arrays are applied to a 3D model in FEM [41,43]. The short glass fibers and short banana epoxy matrix were taken as two different sets of samples to evaluate the $K_L$ in Kumar Sahu's work [41], and the hybrid composite was made from short banana and jute fibers in epoxy resin in Devireddy's work [43]. These experiments show that FEM is a valuable method for obtaining thermal properties compared to experimental results.

$K_T$ and $K_L$ of the short jute and banana mixed composites have been simulated through a unit cell of the square array [47]. Here the $K_L$ value was slightly higher than $K_T$ because the heat flux was parallel to the fiber orientation in the longitudinal orientation. The percentage error between FEM and experiment was less in the longitudinal direction because fibers touch with other fibers in the investigation, resulting in a lower thermal conductivity of the composite. A cubic lattice array was developed with spheres to evaluate the thermal conductivity of a composite of solid glass spheres and polymer matrix [51].

A thermal evaluation of a composite board was carried out with layer formation of fiber and resin [52]. It is an entirely different approach than the above discussion.

The importance of the role of the unit cell for FEM can be identified from the above discussion, and the identification of unit cell type is essential for studying physical and micromechanical properties. Boundary conditions should be applied after selecting the unit cell.

### 2.3.2 Boundary conditions

There are two approaches to finding the heat distribution through a unit cell [42]. In the first method, the heat load is applied as a temperature of both opposing faces of the unit cell while other faces are assumed to be adiabatic. Many works of literature have followed this method [43,45,46,52]. Then thermal distribution through the composite can be analysed through the Ansys software.

In the second method, the heat transfer coefficient at room temperature is calculated, and heat load is applied as a temperature on a single face of the unit cell. Other faces parallel to heat flow are assumed to be adiabatic [41,42]. Kumar Sahu's work followed this method to analyse thermal distribution [41]. Figure 2.15 shows the boundary conditions in a unit cell according to the first method. Here, temperature loads are applied to the top and bottom faces, and other faces are assumed to be adiabatic.

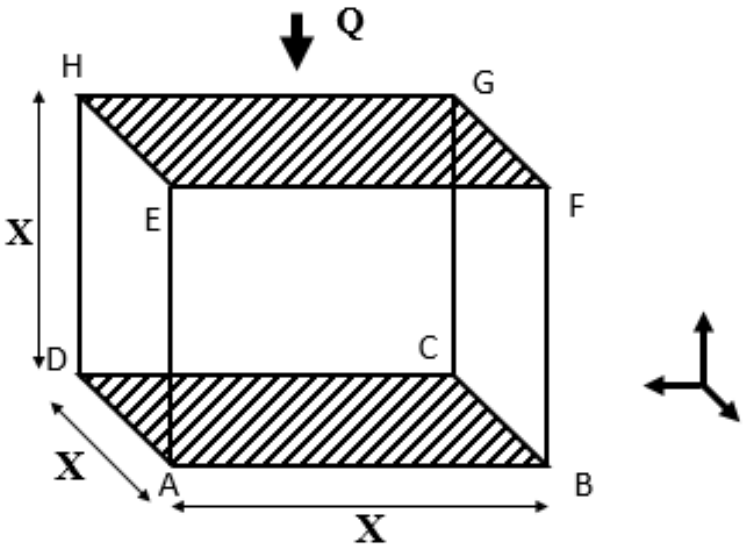


Figure 2.15: Boundary conditions in the unit cell [41]

## 2.4 Analytical method to analyse the thermal conductivity of composites

The thermal conductivity of a material can be evaluated by the analytical method in addition to the experimental method and the numerical method. Various types of analytical models are available to evaluate the thermal conductivity of a composite. This is because the results of the analytical method are more convenient than experimentation. Further, numerical methods have some disadvantages due to the development of complex geometry, and the evaluation is time-consuming. Nevertheless, the FEM method can justify the results taken from the experimental and analytical methods. However, the analytical method is faster and cheaper than other methods. Furthermore, the effective thermal conductivity varies with the size and shape of the fillers, distribution of filler material throughout the matrix, bonding between the particles, and the thermal conductivity of constituents. Therefore, different kinds of basic models and modified and semi-empirical methods are available to evaluate the effective thermal conductivity of the composite material [53,54].

The macroscopic properties can be evaluated by different analytical models of a heterogenic medium using the constituent materials' thermal properties and volume fraction. However, these heterogenic materials are assumed to be microscopically homogenous in analytical models. These models are identified as effective medium approximation (EMA) or effective medium theories (EMT) [53].

Five basic models of Parallel, Series, Maxwell-Eucken model (two forms), and Effective Medium Theory (EMT), were adopted as the main models for developing many thermal conductivity models [54]. Further, past studies have mainly used the Rule of mixtures, Maxwell model, Bruggmen's model, Rayleigh's model, and Lewis Nielsen model to measure the thermal conductivity of composites.

### 2.4.1 Rule of mixtures

Heat flow direction is assumed to be parallel in the material structure in the parallel model and perpendicular in the series model. Commonly these models are called the *Rule of mixtures* [54,55]. These parallel models can be extended to determine the $K_{eff}$ of multi-component composites. These models are called *standard mixture rule* and *inverse mixture rule* [54]. Sahu calculated $K_{eff}$ for short banana fiber/epoxy resin and

short glass fiber/epoxy using the rule of mixtures [41]. The highest deviation relative to the experimental results is given by the rule of mixtures. Also, the calculated $K_{eff}$ value of the rule of mixtures showed the highest deviation for the transverse direction than other models [47,55]. A small deviation has been noted for the rule of mixtures in the longitudinal direction [43,47,55].

### 2.4.2 Maxwell model

The Maxwell model can be identified as the first mathematical model to evaluate the thermal conductivity of a heterogenic medium. Well-dispersion spherical particles in the continuous matrix are the main assumption of the Maxwell model [53,54,56]. However, this model is validated under about 0.25 volume fraction. Thereafter, the development of the Maxwell model was carried out by Eucken to predict the $K_{eff}$ of the continuous matrix, which contains multiple phases of filler particles [53]. However, the $K_{eff}$ of the composite made using epoxy and hollow glass spheres particles shows distant values to the Maxwell model [51]. The short fibers in the epoxy matrix showed a closer agreement with the experimental results but not FEM results [41,57]. The above results signify that the evaluation of thermal conductivity depends on the physical structure of the composite. Therefore, the five basic models do not apply to all applications. As a result of the limitation of the five basic models, empirical and semi-empirical models were introduced to evaluate the $K_{eff}$ of composites. These models were developed based on the sizes, shapes, and distribution of the fillers throughout the matrix [54].

### 2.4.3 Bruggmen's model

Bruggmen developed a model using different assumptions than Maxwell's model [56]. This model can evaluate the thermal conductivity of spherical particles in a homogeneous medium [41,56]. Nevertheless, Bruggemen's model was chosen to predict the $K_{eff}$ of short fibers in the epoxy matrix. However, Bruggmen's and Maxwell's models show more variation in experimental results [41,57]. Bruggmen's model can predict the thermal conductivity of composites and also the thermal conductivity of many forms of materials such as porous materials, nanofluids, and space dust.

### 2.4.4 Rayleigh's model

Rayleigh's model has two forms: one form of Rayleigh's model gives better outcomes than Maxwell's model for high volume fractions with spherical fillers. Another form of Rayleigh's model is important to predict $K_{eff}$ of cylindrical fibers in a continuous matrix [53]. It shows another aspect of predicting the thermal conductivity of composites because fibers act as a filler material in many insulating materials rather than spherical particles. Therefore, it is more interesting to study analytical models that are cylindrical-shaped fillers embedded in a continuous matrix. Moreover, Rayleigh's model can determine the $K_{eff}$ in transverse and longitudinal directions.

### 2.4.5 Lewis Nielsen model

Lewis Nielsen model is a well-known empirical model to predict $K_{eff}$ in composites. It does not consider the interfacial thermal resistance but can give accurate results up to a volume fraction of 0.4. Additionally, it is applicable to a broad range of orientations and shapes of fillers. The simplicity is identified as the main advantage of this model [53]. Lewis Nielsen's model was modified using the Halpin-Tsai model. Hence, this model can determine $K_{eff}$ in the longitudinal and transverse directions [56]. However, Devireddy's work better agrees with the experimental results with less fiber volume fraction in the transverse direction [47].

The above description reveals that the Lewis Nielsen model can be used for composites containing spherical or fibrous fillers embedded in a continuous matrix [43,51,55]. According to Bhaskara's results, the final values of the hexagonal or square packing arrangement in the cubic cell are very close to the unidirectional fiber arrangement [55].

Also, this model can determine a mixture of three components [43,55,56]. The first step is calculating conductivity for a mixture of the matrix and one filler. Next, the total conductivity of the composite can be calculated with the conductivity value of the mixture and the second filler [56]. Also, the Springer and Tsai Semi theoretical model was introduced to find conductivity in the longitudinal and transverse directions [56].

Table 2.3 summarises the filler shape that can be applied to the above mentioned models and the maximum number of phases in that composite.

Table 2.3: Empirical models for analysing the $K_{eff}$ of the composite.

| **Model** | **Filler shape** | **No of phases** |
|---|---|---|
| Rule of mixtures | spheres or cylindrical | Multiphase |
| EMT | spheres | two-phase |
| Maxwell Eucken | spheres | multiphase |
| Bruggmen | spheres | two-phase |
| Rayleigh | cylindrical | two-phase |
| Lewis Nielsen | cylindrical | Multiphase |
| Springer and Tsai semi theoretical model | cylindrical | two-phase |
| Halpsin-Tsai | cylindrical | two-phase |
| Geometric model | spheres | Multiphase |

The Rule of mixtures, Maxwell model, and EMT model are basic empirical models to find $K_{eff}$. Maxwell Eucken and Bruggmen can be applied for spherical particles in a continuous matrix. Further, Rayleigh's model, Lewis Nielsen model, Springer and Tsai Semi theoretical model, and Halpin-Tsai model are significant models for finding the conductivity of cylindrical fillers in a continuous matrix. Additionally, the conductivity of a multiphase component can be evaluated by the Rule of mixtures, Maxwell Eucken, and Lewis Nielsen models. The geometric model can find $K_{eff}$ of a multi-component system [54], but the deviation of results in the geometric model is higher than the rule of mixtures, Halpsin –Tsai model, and the Lewis Nielsen's model in Devireddy's work for hybrid fiber mixtures [43]. However, the Rule of mixtures, Rayleigh's model, and Lewis Nielsen model were frequently applied to evaluate the thermal conductivity of fiber reinforced composite.

The above-discussed empirical models are defined to evaluate the $K_{eff}$ of a solid-solid system. However, it is more important to consider the $K_{eff}$ of a solid-gas system to

develop insulation composites because the thermal conductivity value of a solid material can be reduced by the incorporation of porosity into the material. Here the thermal conductivity of air is lower than in the solid region [58,59]. Therefore, most mineral wool insulators contain over 95% air volume [59]. Hence, 90% volume content of air should be included in 1 W/mK of solid phase to produce materials with thermal conductivity less than 0.1W/mK. However, heat transfer in porous material occurs with vibrational conduction in the solid region, conduction due to the collision of particles within the air gap, and radiation through the large pores or semi-transparent solid region [58]. Therefore, the effective conductivity of a pore is defined as a summation of the true conductivity of the pore and the apparent conductivity value on account of radiation.

Nevertheless, at 4 ºC, the apparent conductivity due to radiation in a 0.25 mm width pore is negligible relative to the conductivity value of air. Also, the thermal conductivity value due to radiation at 482 ºC is considered to be the value of the true conductivity of air at 4 ºC. Further, the apparent conductivity value is equal to the true conductivity for a width of 5 mm pores at 4 ºC temperature [59]. Therefore, the radiation effects should be considered at high temperatures and when large pores are in insulation materials [58]. Moreover, values due to the radiation effect of Ankang's work show negligible changes in the effective thermal conductivity of the open porous polyurethane foam [60]. Also, the effect of radiation on glass wool was neglected in evaluating the thermal conductivity of glass wool insulation [61].

Convectional heat transfer through the pores can be neglected for pore sizes less than 5 mm [58,59] since the natural air movement is negligible when the surfaces are close to each other. Hence the heat transfer through the conduction is greater than the heat transfer through the convection. However, the convection value increases with the width of the air gap, and conduction reduces at this time [62,63]. Therefore, the major portion of the heat transfer below 200 ºC is done by the conduction of air through the insulator [64]. Also, thermal conductivity can be reduced with the increase of porosity, and the results of Russell's work concluded that the conductivity value of materials with continuous air phase is lower than materials with a continuous solid phase [59].

Therefore, most insulators are fabricated with fibrous materials such as glass wool and asbestos wool.

The effective thermal conductivity of a porous material can be predicted using analytical models. It can be derived as a two-phase mixture problem with a function of a void fraction. Effective thermal conductivity of pore materials with 0.04 to 0.95 pore volume fraction (Vp) was analysed through analytical models by Smith [58]. Here the Maxwell-Eucken model shows a better arrangement for the $Vp<0.15$ samples. Also, the $0.15<Vp<0.65$ range of pore volume fraction shows a better arrangement with the Landaure's relation and materials with $Vp>0.65$ shows a better arrangement with the Hashin-Shtrikman upper bond and the Rusell's relation. This is because $Vp<0.15$ materials show close pores behaviour, and $Vp>0.15$ shows open pores behaviour.

In addition to the above models, several theoretical and empirical models are available to find $K_{eff}$ in a porous composite. Progelhof and Throne's empirical model and Topper's theoretical model are some example models to evaluate the thermal conductivity of porous materials [56].

Theoretical models were recently developed to find $K_{eff}$ of two-phase composites. Also, the results of these models were validated by comparing experimental, available theoretical models and FEM [41,43,65,66]. These developed models showed better agreement with experimental results than previously available analytical models.

## 2.5 Experimental procedure to analyse the thermal conductivity of natural fiber composites

The experiment procedure follows two main steps, i.e., *composite processing* and *measuring the thermal conductivity of the fabricated material*. The first step in the fabrication process is the surface treatment for fibers. After that, selecting the binding material and selecting the fabrication process are the critical steps in the fabrication. Finally, thermal conductivity can be measured from the most suitable method. These points are mainly discussed in this section based on past studies.

### 2.5.1 Alkaline treatment for fiber surface

Lignocellulose fibers contain cellulose and hemicellulose as major constitutions. Therefore, these functional groups are highly polarised due to the hydroxyl groups. These hydroxyl groups give a hydrophilic nature to natural fibers because the hydroxyl groups form hydrogen bonds with water.

Industrial applications of natural fibers are limited due to the absorption of moisture from the environment, which results in weak adherence between the hydrophobic matrix and the fibers. This poor adhesion creates a higher void gap between the matrix and the fibers. Hence it leads to the uptake of more moisture into the composite [11,28,32,67]. This moisture absorption causes changes in the stability of the composite dimensions, poor mechanical bonding between the matrix, and the phenomenon of excessive degradation of the composite. Therefore, it is more important to reduce the hydrophilic behaviour of fibers with a suitable pre-treatment process for the fiber that reduces moisture absorption and increases the bonding strength of the matrix and fibrous material [32]. These pre-treatment methods can be identified as a surface coating for the fiber surface and a bulk treatment for the fibers [11]. Bulk or chemical treatment reduces the water absorption of the fibers, thereby reducing the number of reactive groups in the fibers, resulting in a rougher and cleaner surface by removing surface impurities. Hence chemical treatments increase the adhesive properties of fibers and the matrix [28].

The surface coating reduces the moisture absorption rate rather than lowering the water absorption properties of the functional group and removing the impurities in the fibers. From the above point of view, chemical treatment can be chosen as the most suitable fiber pre-treatment method [11].

Different chemical treatments can be identified, such as alkaline, acid, oxidizing, and compiling agents [28,32,68]. The alkaline treatment has been used in past studies as the most popular treatment for lignocellulose fibers [28,32,67] because it is an inexpensive method and can partially remove substances such as impurities, waxes, pectin, hemicellulose, and lignin [32,69]. Sodium hydroxide (NaOH) and potassium hydroxide (KOH) are the most commonly used substances for alkaline treatment, and

NaOH is often used for this treatment [11]. These amorphous and impure substances are sensitive to reacting with alkaline substances. It produces Fiber-ONa by reducing the amorphous region of the fiber, as shown below [69,70].

$$\text{Fiber-OH} + \text{NaOH} \rightarrow \text{Fiber O–Na+} + H_2O + \text{impurities}$$

The above reaction seems to remove the amorphous region of fibers with waxes and oily substances on the fiber surface. As a result, it contains more cellulose to produce better adhesion with the matrix [20,69]. After the alkaline treatment, Fourier Transform Infra-Red Spectroscopy (FTIR) analysis can observe changes in functional groups [28,32,68] because lignocellulose fibers contain different functional groups such as hydroxyl (OH), Carbonyl (C—O), carboxyl (COOH), and methylene (CH2) [28]. Figure 2.16 shows the FTIR analysis of untreated coir fiber [68]. Mittal performed the FTIR analysis for PALF fibers and coir fibers treated with various types of concentrated NaOH [32].

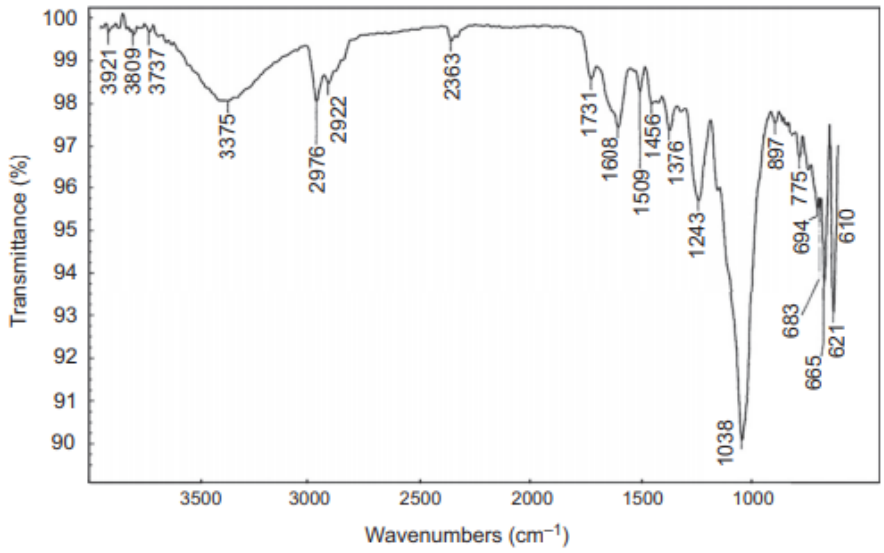


Figure 2.16: FTIR spectrum of untreated coir fiber [68]

*(Reprinted from Handbook of natural fibers, 1, L. Mishra, and G. Basu,, Coconut Fiber: Its structure, properties and applications, 231-255, 2022, with permission from Elsevier)*

According to Figure 2.16, the aromatic C-O stretching for lignin is about 1250 $cm^{-1,}$ and wavenumber 1509 $cm^{-1}$ is associated with aromatic ring stretching of lignin. Also, the peak at 1608 $cm^{-1}$ is represented by lignin [68]. Pectin, hemicellulose, and lignin

show a peak at 1731 $cm^{-1}$ due to the C=O stretching of aldehyde and ester, which disappears after alkaline treatment with NaOH [32]. Also, the stretching vibration of the OH group of cellulose and lignin shows a peak at 3375 $cm^{-1}$ [68]; this provides an active site for the better addition of the fiber-matrix interface. Such peak increases in treated fiber are due to the higher availability of OH groups after removing pectin, wax, and adhesive gummy substances from the surface. Furthermore, the increase in peaks at 1000, 1250, and 1600-1650 conforms to removing surface impurities [32]. The peak at 1038 $cm^{-1}$ shows the cellulose C-O-C stretching. According to Mittal's experiment [32], an increase of peaks is noted at low concentrations of alkaline treatment due to the removal of impurities, and these peaks decrease with increased alkaline concentration. Therefore, it is essential to consider the alkaline solution concentration since excess concentration removes the crystalline region of the fiber structure. Some amount of lignin is removed with the alkaline treatment, but the lignin content does not significantly change the mechanical properties of the fiber, and the researchers believe that the remaining lignin content is sufficient to cover the fiber surface. Hence, the excess amount of lignin does not influence fibers' mechanical properties [16].

Removal of wax and other non-cellulose materials increases the surface roughness of the fiber, as confirmed by the Scanning Electron Microscope (SEM) analysis [28,67]. It also reduces the fiber diameter and increases the fiber aspect ratio. Hence, the fiber tensile strength decreases due to the area reduction.

The surface roughness and the higher aspect ratio give better interface adhesion properties to the matrix and fiber. Moreover, the mechanical properties of composite will increase due to the expansion of the number of reactive sites of the cell wall, and it gives better wetting properties to the matrix and fiber interface. Therefore, the better addition of the composite overcomes the strength reduction of fiber [16,20,28]. Previous studies have observed fiber shrinkage, apart from the mechanical properties of the fiber after the mercerisation process. The reason may be the structural shrinkage of the fiber [16]. Further, the moisture absorption nature of coir, and pineapple leaf fiber with the percentage of NaOH treatment was studied by Mittal [32]. The concentration of this solution was considered as the ratio of NaOH weight to water

volume [32,33,67,69]. Here, water absorption was increased up to the saturation point and reduced after that point. Water is absorbed up to the saturated point by the capillary action because the contact angle and pore diameter change after the alkaline treatment.

Water absorption decreases after the saturated point with the NaOH percentage due to the hydro-elastic property of fibers because excess water penetration interrupts the secondary bond of cellulose and makes a hydrogen bond with cellulose. It increases the fiber swelling and closes the small pores, which reduces the capillary action of the fiber [32]. This water, absorbed by the 2$^{nd}$ action, can be identified as bonded water, which affects the thickness swelling of the fiber [27].

The water absorption percentage with immersion time was studied for treated and untreated fiber in Mittal's work [32]. During the first ten hours, the water absorption rate greatly increases and shows saturated behaviour. Therefore, the immersion time is recommended to be more than ten hours. However, some literature works have taken the immersion time as less than 10 hours [20,28,33].

Agrawal investigated thermal properties with oil palm fiber and phenol-formaldehyde composite [71]. It appears that thermal properties such as thermal conductivity and diffusivity values increased after the alkaline treatment [21,71]. Shalwan [72] observed the insulation characteristics of epoxy and sisal composites, and disclosed that the insulation properties of the treated fiber decreased in the composite (with treated fibers). This allows concluding that chemical treatments of fiber alter the insulation characteristics of the composite because the resin distribution throughout the composite is homogeneous. The air gap at interfacial positions will further decrease, increasing the thermal conductivity of the whole composite. Nevertheless, researchers recommend treated fibers due to the better adhesive properties between the resin and fibrous material [72].

The mercerising process increases the thermal stability of fibers by removing hemicellulose, lignin, and other impurities from the fiber surface. This phenomenon was studied in Kabir's work [69]. Figure 2.17 shows the TGA analysis for treated and untreated jute fibers.

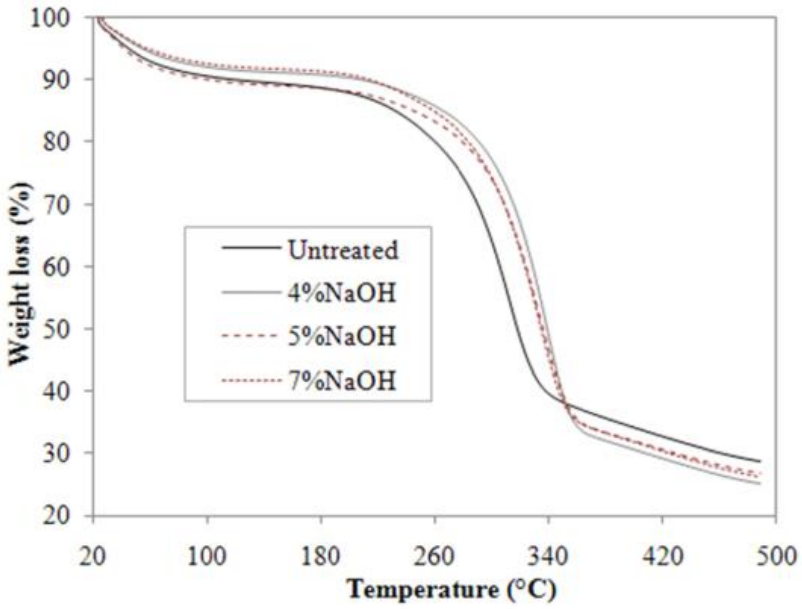


Figure 2.17: TGA analysis for treated and untreated jute fibers [69]

*(Reprinted by permission from M. M. Kabir, M. Islam, and H. Wang, Mechanical and Thermal Properties of Jute Fiber Reinforced Composites, 2013, 71–77.)*

As shown in Figure 2.17, the thermal stability of treated fibers is higher than that of the untreated fibers in the second stage of pyrolysis due to the removal of lignin and hemicellulose from the fiber surface. It increases the activation energy to initiate the reaction [28]. Therefore, increasing the activation energy increases the lifetime of the fiber.

However, excess concentration of the alkaline solution degrades the crystalline cellulose. Hence, the thermal stability of the fiber reduces drastically [28]. Furthermore, the mechanical characteristics of the fiber are decreased as a result of extensive damage to the cell wall [20]. Therefore, it is vital to maintain the appropriate concentrations for fiber treatments.

The above discussion shows that observation of thermal stability and moisture absorption properties with the concentration of alkaline treatment is interesting for future results. The fabrication process can be followed after completing the alkaline treatment, according to past studies. Then adhesive material should be selected at the beginning of the fabrication, and Section 2.5.2 describes the available adhesive materials for coir fibers.

### 2.5.2 Adhesive materials for coir fibers

The matrix's main purpose is to effectively transfer the fiber load throughout the composite by fiber adhesion. Typically, fibers in the composite are the primary media for load-bearing, and the matrix acts as the media to maintain fiber orientation while protecting fibers from environmental effects [73]. Thermoplastic and thermosetting polymers are the existing matrix materials for natural fiber composite processing. Thermoplastic polymer shows a solid-state within the specific temperature range, and then it becomes a rubbery state and liquid state, respectively, with increasing temperature. It will return to the solid-state with subsequent cooling.

Thermosets polymers have chemical reactions beginning with heating resulting in polymerisation into a solid that does not transfer into the liquid state upon heating. Therefore, Thermoset polymers undergo thermal degradation with heating. However, most natural fiber composites are fabricated with thermoset resins [31] because thermosetting resins have a much lower viscosity than thermoplastic polymers, which allows the liquid to be introduced into fibers with low pressure at room temperature. Therefore, these composites can be manufactured by a simple processing method such as hand layup, resin transfer method, compression moulding, and injection moulding method. Also, the thermoset matrix provides better adhesive and mechanical properties with natural fibers such as jute, coir, sisal, flax, and pineapple leaf fibers [73]. Thermoset materials produce a high-cross link density during the polymerisation process, and it increases the composite strength. Therefore, thermosetting resins are the best material to fabricate natural fiber composites than thermoplastic materials. Commonly available thermoset resins are polyester, polyurethane, urea-formaldehyde, and epoxies [74].

However, epoxies show more significant properties than other thermoset polymer resins. Mainly it has the characteristic of sticking to anything [31]. Also, these resins have better chemical and mechanical properties, durability, and high thermal and dimensional stability. These materials contain 100% solids; therefore, solvent content after the curing is negligible. As a result, it shows excellent dimensional stability after curing due to the negligible amount of shrinkage [73,74].

Past research activities have used epoxy resins to fabricate insulation composites with lignocellulose fibers due to their good thermal stability and adhesive characteristics. These composites show better insulation and mechanical properties with lignocellulose fibers. Epoxy resin reacts with lignin and makes crosslinks between resin and lignin after the curing process. This reaction phenomenon can be confirmed by the results of FTIR spectra [75]. Therefore, the better reactive property between the lignin and epoxy will provide an improved adhesive property between lignocellulose fibers and epoxy resin.

However, the non-biodegradability of these synthetic polymers is the main drawback of biocomposite processing [73]. Therefore, researchers are taking steps to use natural based raw materials to process the adhesives. Basically, natural adhesives can be extracted from animals or plants: i.e., milk protein, blood protein, starch and lignin [31]. Among these origins, natural rubber (NR) latex has significant adhesive properties with coir fibers. Therefore, many products like mattresses, automobile parts, and pots are fabricated from NR latex and coir fibers [76].

In general, latex is an emulsion containing polymer microparticles in an aqueous medium with protein, sugar, alkaloids, resins, alkaloids, and gums. NR Latex is found as a milky sap in *Hevea brasiliensis* trees that can be coagulated by espousing to air [26]. The attractive properties of NR latex to use as a natural adhesive are the high tack and tack retention properties, better flexibility, good strength after the vulcanising, and good moisture retention properties [77]. Therefore, it is used to fabricate thermal insulation materials with lignocellulose fibers. Insulation mats were fabricated with coir fibers and NR latex in Srimal's work [25,78,79,80], and the thermal conductivity value was close to the value of glass wool. Likewise, thermal insulation boards were fabricated from pineapple leaf fibers and NR latex in Tangjuank's experiment [23] and Kumfu's experiment [24]. So-me studies have attempted to introduce coir fibers into the NR to fabricate tire treads. Edirisinghe and co-workers [76] introduced NR latex-coated coir fibers into the NR compound. This experiment proved that the compound's mechanical properties could be increased by NR latex-coated fibers than non-coated fibers.

Thuraisingam developed a bio-adhesive with NR-latex and lignin [77]. This compound shows better chemical, mechanical, and morphological properties. Hence, it is concluded that a combination of NR-latex and lignin gives better adhesive properties. Also, lignin is the main compound in coir fibers, and as mentioned above, NR latex is a better adhesive material for coir fibers.

NR latex can be selected as a natural binder for coir fibers, according to the above discussion.

It is also important to study the available fabrication methods for composite fabrication. Section 2.5.3 discusses the available fabrication methods.

### 2.5.3 Fabrication technique for natural fiber composites

The following methods are often employed in composite fabrication.

- Hand layup technique
- Compression moulding technique
- Injection moulding method
- Vacuum-assisted resin transfer moulding technique
- Pultrusion technique

From the above techniques, the hand layup method is the most cost-effective and time-efficient method of producing natural fiber composites [15]. Also, this method is used to fabricate unidirectional or woven fibers with any type of fiber size to fabricate a reinforced fiber composite. Therefore, it can be identified as the oldest method of fabricating woven composites [81]. Hence, it is used to fabricate composite materials for various research activities [41,43,55]. Further, this method can create complex shapes for automobile applications. The fabrication process follows a few steps, such as applying a releasing agent to avoid sticking the sample on the mould surface, then placing fiber layers on the mould surface, and manually applying the resin using a brush. Finally, the trapped air is removed using a roller by pressing the resin and fibers and distributing them evenly through the mould [82]. Figure 2.18 shows the hand layup method for the composite fabrication.

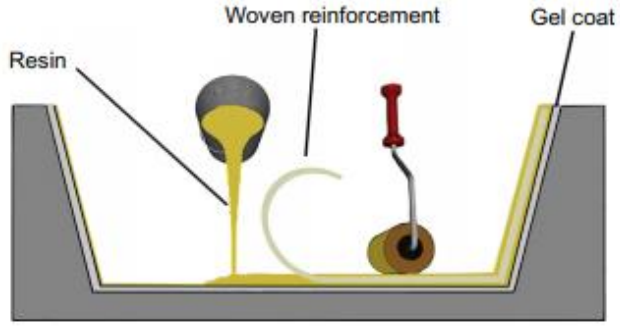


Figure 2.18: The hand layup technique [82]

*(Reprinted from Durability and Life Prediction in Bio composites, Fiber-Reinforced Composites and Hybrid Composites, M. Raji, H. Abdellaoui, H. Essabir, C. A. Kakou, R. Bouhfid, and A. E. K. Qaiss, Prediction of the cyclic durability of woven-hybrid composites, 27-62, 2019)*

Particulate composite can be fabricated by a prepared short fiber. Short fibers are prepared from the chopped long fiber. Then it is mixed with the polymeric resin, and the mixture is poured into the prepared mould [15]. The product quality varies with the operator's skill [81]. The low cost and convenience of the fabrication process make this process widely available for research activities.

### 2.5.4 Experimentally determining the thermal conductivity of insulation material

The two primary methods for determining the thermal conductivity of a material are steady and transient. In the steady-state method, the values are taken after obtaining the absolute thermal equilibrium point of the specimen. At this stage, the temperature of the material does not vary with time. However, this method has disadvantages over the transient method, such as expensive apparatus and time to achieve a steady-state. However, this method gives accurate results for dry materials, while the transient or non-steady method gives the results during heating. Therefore, this method is comparatively faster than the steady-state method.

The temperature range measurement can be divided into three main categories, i.e., below room temperature, room temperature, and above room temperature. Therefore, by considering the operating temperature and the thermal conductivity value of the insulation material, the guarded hot plate (GHP), heat flow meter, and hot disk method can be used to measure the thermal conductivity of insulation materials. The GHP and

heat flow meter methods are steady-state methods, and the hot disk method is a transient method.

**Guarded hot plate**

This is the most common method for finding the thermal conductivity of insulation materials. Also, this is an absolute method since heat loss due to the radiation and convection to the environment and the conduction through the wires of the thermocouples is minimised in this method [83]. A constant temperature gradient is developed in this method for the known thickness, and the heat flow is maintained throughout the sample. The major disadvantages of this GHP method are the extended time duration to achieve a steady-state and the need for a high-temperature difference for the experiment. Besides, the experiment requires a large sample size, which increases the thermal contact resistance between the thermocouple and the sample [83,84].

**Heat flow meter**

Determination of the absolute value of the heat flow through the sample is difficult in the GHP method. Therefore, a comparative technique can overcome this problem without directly considering the heat flow. The heat flow meter method can be identified as a comparative technique. This method has more advantages than the GHP method, such as less time consumption with accurate results, and it is easier to handle when experimenting with insulation materials [85]. In this method, a heat flux transducer determines the sample's thermal conductivity. This transducer is calibrated by the standard specimen with a known thermal conductivity value, and then the measurement of the sample is taken by Fourier's law of heat conduction [83]. This method shows errors in the results of compressible materials because thickness reduction occurs due to the compression load of the transducers. According to Fourier's law, that phenomenon gives completely different results for the experiment. Moreover, this thickness reduction greatly affects the density of the compressible materials. Therefore, the thermal conductivity value changes due to the density variation of the test material.

**Hot Disk method**

This method is similar to the hot wire method, which contains an expanded wire strip. Both thermal diffusivity and thermal conductivity can be measured using the hot wire method. Also, this method is used for the thermal conductivity of electrically conductive materials and insulation materials such as polymer, mineral, ceramics, liquid, powder, glass wool, composites and materials which have anisotropic thermal properties. It shows attractive advantages like negligible contact resistance between the specimen and the sample, faster than the steady-state method, availability of different sensor sizes, and the size of the specimen being smaller than other methods [85].

The metal strip or metal disk is covered with an electrical insulation material with high chemical and mechanical resistance [84]. It should be placed between two identical samples of the specimen, as shown in Figure 2.19. Then the metal strip is heated with a small current passing through the wire. This increases the temperature of the wire disk, and this temperature extremely changes with the properties of the two specimens. Therefore, the temperature properties of the sample can be determined by detecting an increase in the temperature of the metal disk over a short period. This time duration takes a few seconds, which is the main advantage of the hot disk method [83].

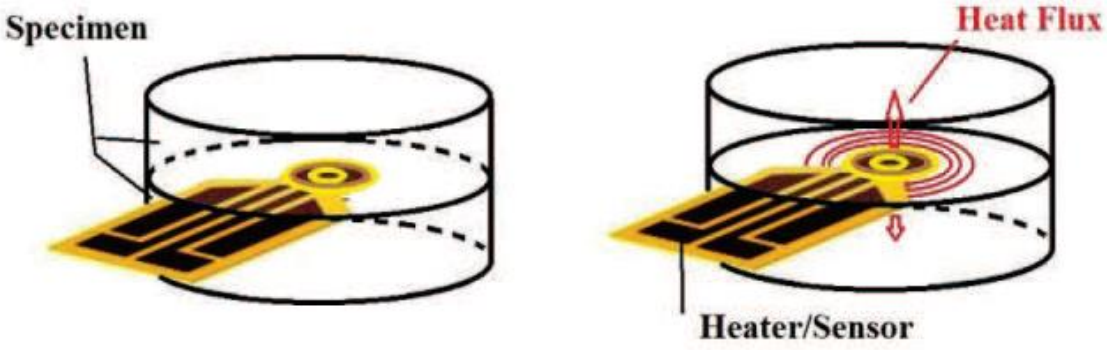


Figure 2.19: Hot disk method [85]

*(2016, N. Yuksel. Originally published in the Review of Some Commonly Used Methods and Techniques to Measure the Thermal Conductivity of Insulation Materials under CC BY 3.0 license. Available from: http://dx.doi.org/10.5772/64157)*

The thermal conductivity of commonly available materials is measured at room temperature using the hot disk method in Saleh's work [84]. Here experiment results

of polyurethane and polystyrene insulation materials show better agreement with the manufacturer's claimed values. Also, the conductivity values of lower and higher density glass fiber samples are 20% and 12% higher than the manufacturer's claimed values, respectively. When the same experiment was conducted for rock wool, it showed better compatibility with the sample with a low-density value. These results indicate that the hot disk method is the most suitable method for measuring the thermal conductivity of compressible insulation materials.

According to the literature review in this chapter (chapter 2), the following conclusions are identified;

The conventional type materials are the most widely available materials for the roof insulation. However, researchers are moving to develop sustainable insulation materials with lignocellulose fibers due to the health and environmental issues of conventional materials. These natural fibers naturally occur in agricultural wastes, grasses, and plant wastes such as sisal, jute, coir, pineapple leaf fiber, oil palm fibers, hemp etc. According to the review, coir fibers exhibits significant properties over other fiber such as low thermal conductivity, low density, high resistance to absorb moisture, higher elongation at the breaking point, and high thermal stability.

Also, for the fabrication process binder material should be added to the adhere fibers. Further, introducing air voids into the fiber and binder combination increases the insulation properties. However, finding the thermal insulation behaviour of the composite with a combination of three-phases is a new approach. So, finding the behaviour of the thermal conductivity with changes in the composition of three-phases by numerical, analytical, and experimental is a new research area currently. Further, validation of the results can be done by the comparison of the results obtained from numerical, analytical, and experimental.

Then the following steps are identified to fulfil the research objectives:

1. Selection of plant fiber for roofing insulation.
2. Identification of the alkaline treatment concentration and studying the thermal stability of coir fiber.
3. Determination of the transverse thermal conductivity of fiber.
4. Determination of the thermal conductivity of latex.
5. Analysing the thermal conductivity of the three-phase composite using the analytical, numerical, and experimental methods.
6. Development of a mathematical model to predict the thermal conductivity of the composite.

# CHAPTER 3

# IDENTIFICATION OF THE CONCENTRATION OF THE ALKALINE TREATMENT AND STUDYING THE THERMAL STABILITY OF THE COIR FIBER.

A comprehensive literature review was performed on lignocellulose fibers to select a suitable fiber for roofing insulation. A set of lignocellulose fibers such as wood, coir, cotton, flax, sugarcane, oil palm, jute, hemp, bamboo, sisal and pineapple leaf fibers were selected for the roofing application. Then the physical, mechanical, and chemical properties were compared to select the best fiber for the roof insulation. Hence, the comparison was based on the thermal conductivity, reactance to moisture absorption, mechanical properties, thermal stability, and embodied energy to select a suitable fiber for roofing insulation. Among the above lignocellulose fibers, coir fibers exhibits significant properties over other fiber such as high resistance to absorb moisture, low density, low thermal conductivity, higher elongation at the breaking point, and high thermal stability. Therefore, coir fibers selected as the fibrous material for this study.

After selecting of coir fibers the first step is the identification of the alkaline treatment and the studying the thermal stability of the fiber. Therefore, these steps are well described in this chapter.

## 3.1 Introduction

The main constituents of coir fibers are cellulose (32%-43%), hemicellulose (0.15%-0.25%), and lignin (40%-45%) [16,21,31]. In addition to that these fibers contain waxy and oily substances on their fiber surface in the natural condition. These lignocellulose substances help to absorb environmental moistures in the natural condition and cause the fiber swelling throughout the composite [16]. It leads to reduce the bonding strength between fiber and matrix [16], change the dimensional stability, mechanical properties and thermal properties of the composite [11,27]. Further, it increases the bio-degradability of fiber due to high microbial attacks in wet conditions [11]. Then it is mandatory to follow a pre-treatment process to remove impurity substances from the

fiber surface before the fabrication. Alkaline treatment is the most popular treatment method for the lignocellulose fibers [28,32,67,83] The reason for that is it removes waxes, hemicellulose, lignin and other impurity substances from the fiber surface and is an inexpensive process [32,69]. Sodium hydroxide (NaOH) are the commonly available methods for alkaline treatment [11]. Following reaction (Equation 3.1) occurs after the alkaline treatment [69,70].

$$\text{Fiber-OH+ NaOH} \rightarrow \text{Fiber O–Na} + H_2O + \text{impurities} \qquad (3.1)$$

Therefore, it is clearly shown that the amorphous region of fiber can be easily removed from the alkaline solution by producing Fiber O–Na+. Thereby, treated fibers contain more cellulose and higher surface roughness, which provides better adhesion between the fiber and matrix [20,69]. However, excessive concentration of alkaline treatment will be caused crack propagation and defibrillation [32]. Hence, the identification of the appropriate concentration of the alkaline solution is a key factor for the fiber pre-treatment.

In this chapter, the appropriate concentration has been identified by analysing SEM images, FTIR spectra, and mechanical properties of untreated and treated fiber samples with different NaOH concentrations. Further, the thermal stability of untreated and treated samples were observed by differential scanning calorimetry (DSC). After identifying the appropriate concentration for NaOH solution, the lifetime analysis was determined for the fibers treated with that concentration.

## 3.2 Methodology

### 3.2.1 Surface treatment for fibers.

Weight to volume ratio of 2%, 4%, 6%, and 8% concentrated NaOH solutions were prepared from 98% NaOH. Then coir fibers were soaked 24 hours at room temperature. Here the solution to fiber weight ratio was maintained at 1:25 [87]. After 24 hours fibers were washed out from deionized water 5 to 6 time until pH value was taken 7. Then fibers were dried at 60 °C for 24 hours to get a constant weight.

Additionally, coir fibers were soaked for 24 hours in deionized water and the same procedure was drying produce was followed to produce untreated fibers

### 3.2.2 Analysing the surface properties of fibers.

Scanning electron microscopy (SEM) images were taken for the treated and untreated fibers with 10 kV of processing acceleration voltage and ×750 magnification.

Fourier transform infrared spectroscopy (FTIR) was used to analyse the surface chemical composition of treated and untreated fibers. FTIR values were taken from Nicolet IS 10 instrument with a wave number range of 600 $cm^{-1}$ to 4000 $cm^{-1}$.

### 3.2.3 Analysing the mechanical properties of fibers.

Changes in the mechanical properties are evaluated by fabricating a composite with epoxy and coir fibers [88]. The mechanical properties change with the fiber volume fraction and fiber length in the composite. Therefore, the tensile strength was observed for various fiber volume fractions and lengths to identify the critical length and the maximum fiber volume fraction that give the highest tensile strength. Various NaOH concentrations were applied to the identified critical length. The composites were fabricated with the identified fiber volume fraction, and the tensile strength of the composites was tested to identify the effect of alkaline treatment. These steps are explained below.

#### 3.2.3.1 Fabrication of the composite.

Fibers (the coir fibers for this research work were selected from the Minuwangoda area in Sri Lanka) were washed with water to remove residual particles and dust and dried at room temperature at 30 °C for 10 min. The purpose was to evaporate excess moisture on the fiber surface before the fabrication process [89].

Coir fibers were cut into various lengths and fabricated composite with epoxy resin to produce different volume fractions of fiber to epoxy resin, as shown in Table 3.1. The conventional hand layup method was applied here. The hardener and epoxy were mixed at the 1:2 weight ratio per manufacturer recommendations, and epoxy resin was poured into the metal mould [250 mm × 125 mm × 25 mm dimensions], so the coir fibers lay upon the epoxy resin. The fiber and epoxy combination was then compressed to 2.5 mm for the desired composite volume. The mould was allowed 24 hours under the compression load to complete the curing process. Figure 3.1 provides the composite fabrication process.

Table 3.1: Fiber length and the volume fractions of the composite.

| Fiber volume fraction | Fiber length | | | | |
|---|---|---|---|---|---|
| 0.1 | 1 cm | 2 cm | 3 cm | 4 cm | 5 cm |
| 0.2 | 1 cm | 2 cm | 3 cm | 4 cm | 5 cm |
| 0.3 | 1 cm | 2 cm | 3 cm | 4 cm | 5 cm |
| 0.4 | 1 cm | 2 cm | 3 cm | 4 cm | 5 cm |
| 0.5 | 1 cm | 2 cm | 3 cm | 4 cm | 5 cm |

1. Fiber layup

2. Compression the fiber – epoxy combination

3. Fabricated composite

Figure 3.1: Composite fabrication process.

Next, the fabricated composite's tensile strength was tested according to ASTM D 3039 standard [90]. For this, the samples were cut into dimensions of 250 mm in length, 25 mm in width, and 2.5 mm in thickness. Figure 3.2 illustrates the sample preparation and the tensile test performance.

1. Sample preparation

2. Prepared sample according to ASTM D 3039

3. Tensile test

Figure 3. 2: Sample preparation and performance of the tensile test

The critical length of the fiber and maximum fiber volume fraction of the composite could be identified after the tensile test. Then a new bundle of coir fiber was cut into

the critical length values and performed the alkaline treatment for the fibers with 2%, 4%, 6%, and 8% of concentrations. The composite samples were prepared with the identified fiber volume fraction, and tensile strength was measured according to ASTM D 3039 standard to compare the effect of alkaline concentration on the tensile properties of the composite [90].

### 3.2.4 Differential scanning calorimetry (DSC)

DSC analysis was conducted by DSC 250 for untreated and treated fibers. The experiment was conducted with the heating temperature range of 0 °C to 400 °C at a heating rate of 10 °C/min in a nitrogen atmosphere.

### 3.2.5 Thermogravimetric analysis (TGA) and activation energy

Appropriate concentration for the fiber treatment can be selected by analysing results of SEM, FTIR, and DSC. Then TGA was carried out on four different fiber samples treated at the identified appropriate concentration. Here, thermal analyser SDT 650 was used for this analysis. The samples (5 mg to 8 mg) were heated to the temperature range of 25 °C to 700 °C with five different heating rates of 5, 10, 12, 15, 20 °C/min in an argon atmosphere [35].

## 3.3 Results and discussion

### 3.3.1 SEM image analysis

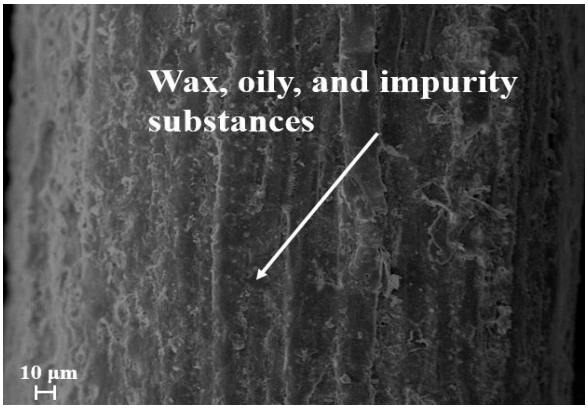


Figure 3. 3: Plane view of untreated coir fiber (×750)

Figure 3.3 shows the plane view of untreated fiber. Waxy and gummy like substances can be seen on the untreated fiber surface. Although, there is no surface roughness on the fiber surface. This leads to reducing the adhesive properties between fiber and

matrix of the composite. Then the SEM image analysis for 2%, 4%, 6%, and 8% is as follows.

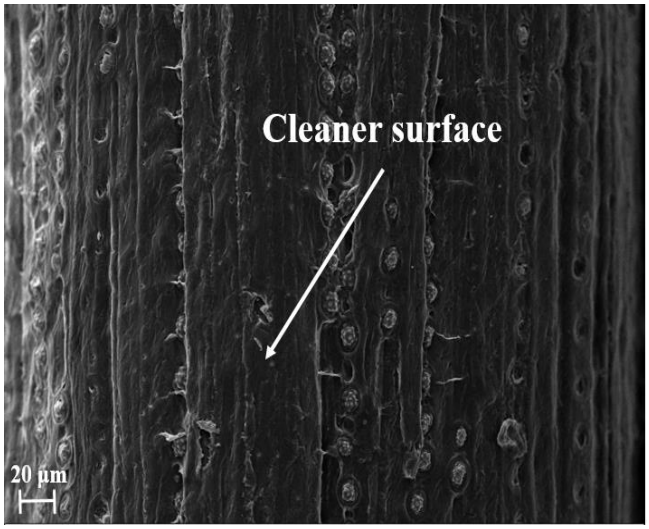


Figure 3.4: Plane view of 2% alkaline treated coir fiber (×750)

Figure 3.4 shows the plane view of 2% alkaline treated coir fiber. The surface roughness of the fiber was increased with regularly distributed pin holes throughout the fiber surface after the alkaline treatment. The reason for that is the removing of waxy, impurities and gummy substances from the fiber surface.

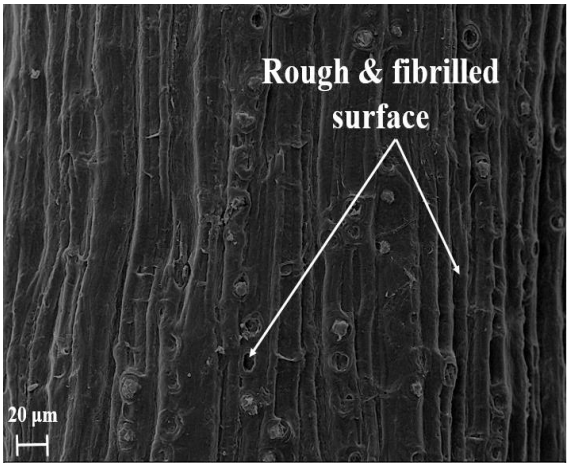


Figure 3.5: Plane view of 4% alkaline treated coir fiber (×750)

Figure 3.5 shows the plane view of 4% alkaline treated coir fiber. The Surface roughness of the fiber is higher than Figure 3.4. Also, there are more number of pin

holes can be seen. It can be concluded that the more amount of substances were removed from the fiber surface than 2% alkaline treatment.

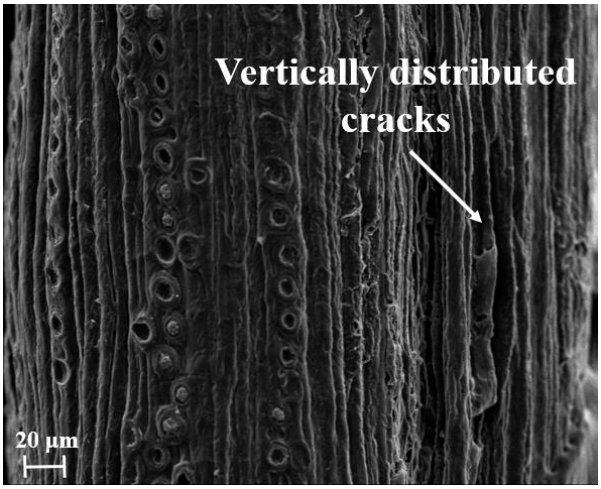


Figure 3.6: Plane view of 6% alkaline treated coir fiber (×750)

Figure 3.6 shows the plane view of 6% alkaline treated coir fiber. Vertically distributed cracks can be seen on the fiber surface. It shows that excess concentration causes to damage the fiber cell. It is due to the much removal of the cellulose content of the fiber [32].

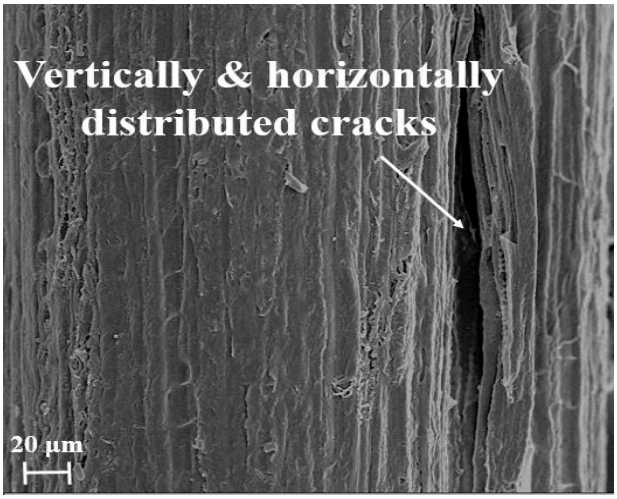


Figure 3.7: Plane view of 8% alkaline treated coir fiber (×750)

Figure 3.7 shows the plane view of 8% alkaline treated coir fiber. The propagation of the surface crack can be seen in vertical and horizontal directions. Also the smooth

appearance of 2% and 4% treated was disappeared at the high concentration of alkaline treatment.

The above results suggest that the alkaline treatment can increase the surface roughness of coir fiber, but excess concentrations will damage the fiber cell structure, causing crack propagation on the fiber surface.

Further, observation of the changes in the chemical composition of the fiber surface is critical to identify the effect of alkaline treatment.

### 3.3.2 FTIR spectrum analysis

The FTIR analysis help to identify changes of various types of functional groups in the coir fibers. The functional groups of carbonyl (-CO), hydroxyl (-OH), carboxyl (-COOH), and methylene ($-CH_2$) in lignocellulose substances on fiber surface were identified from this FTIR spectrum [28,68]. Figure 3.8 shows the FTIR spectrum for untreated and treated coir fibers.

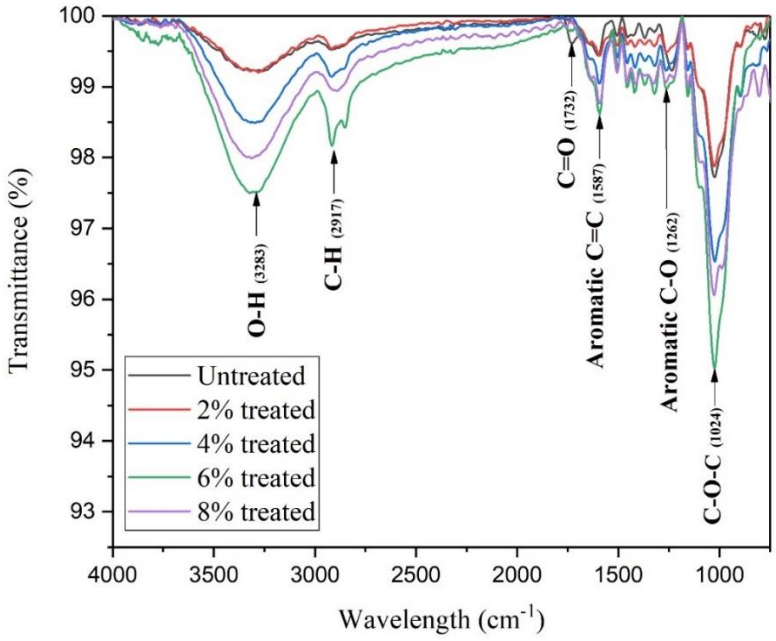


Figure 3.8: FTIR spectrum for untreated and treated coir fibers

A broad distribution of peaks can be identified between 3200 $cm^{-1}$ to 3550 $cm^{-1}$. These peaks are associated with the stretching of intermolecular bonds of O-H stretching for

cellulose and lignin [68]. Also, wavelength 2917 $cm^{-1}$ is related to the C-H stretching of vibration in $CH_2$ and CH groups in hemicellulose and cellulose [86]. Untreated coir fiber contains high amount of Hemicellulose, pectin, and lignin. These compounds contain ester and aldehyde. Therefore, it shows C=O is stretching at 1731 $cm^{-1}$ [32]. Here the peak at 1506 $cm^{-1}$ is related to the stretching of the aromatic ring of the lignin and 1235 $cm^{-1}$ peak is associated to the aromatic C-O stretching of lignin [68]. Moreover, the highest peak at the 1024 $cm^{-1}$ shows the C-O-C stretching of the cellulose [32].

Figure 3.9 compares the changes of the transmittance for the main peaks of the treated fibers compared to the untreated fiber.

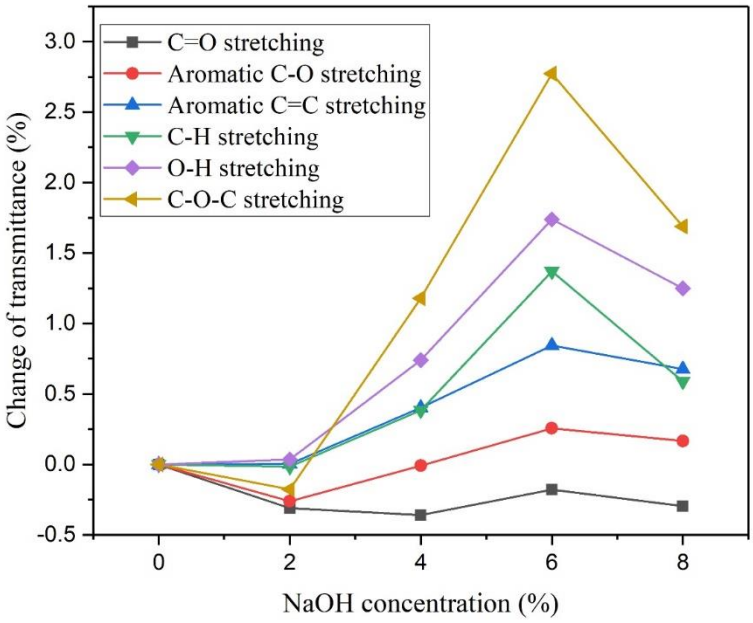


Figure 3.9: Comparison for the changes of the transmittance for the main peaks

The highest peak intensity for the C=O functional group (1732 $cm^{-1}$) is shown by untreated coir fiber sample. It is reduced after the treatment process. It can be confirmed that the reduction of the C=O functional group after the treatment. Therefore, it clearly shows the removal of hemicellulose and pectin from the fiber surface. Nevertheless, the 6% sample shows higher intensity than 2%, 4% and 8%

samples. It might be due to exposure to internal C=O functional groups after crack propagation. But it was reduced after the 8% Treatment due to the excess amount of concentration will be dissolving the internal hemicellulose, pectin, and lignin. However, the minimum intensity value is shown by the 4% concentrated sample. Hence, it concludes that 4% sample has the minimum hemicellulose, pectin, and lignin content on the fiber surface.

Removing of pectin, wax, gummy substances and hemicellulose is confirmed by variation of peak intensity of C=O stretching. Therefore, the intensity of Aromatic C-O stretching, Aromatic C=C stretching, C-H Stretching, O-H stretching of cellulose, and C-O-C stretching is increased to 6% treated sample due to the higher accessibility of infrared energy. However, the peak intensity of these functional groups decreases as the NaOH concentration increases. Therefore, it concluded that excess concentration is caused to propagate cracks on the fiber surface, and it leads to extract excess amount of cellulose and lignin from the fiber surface.

### 3.3.3 Mechanical properties

Figure 3.10 presents the effects of the tensile strength of the composite with various fiber volume fractions and fiber length.

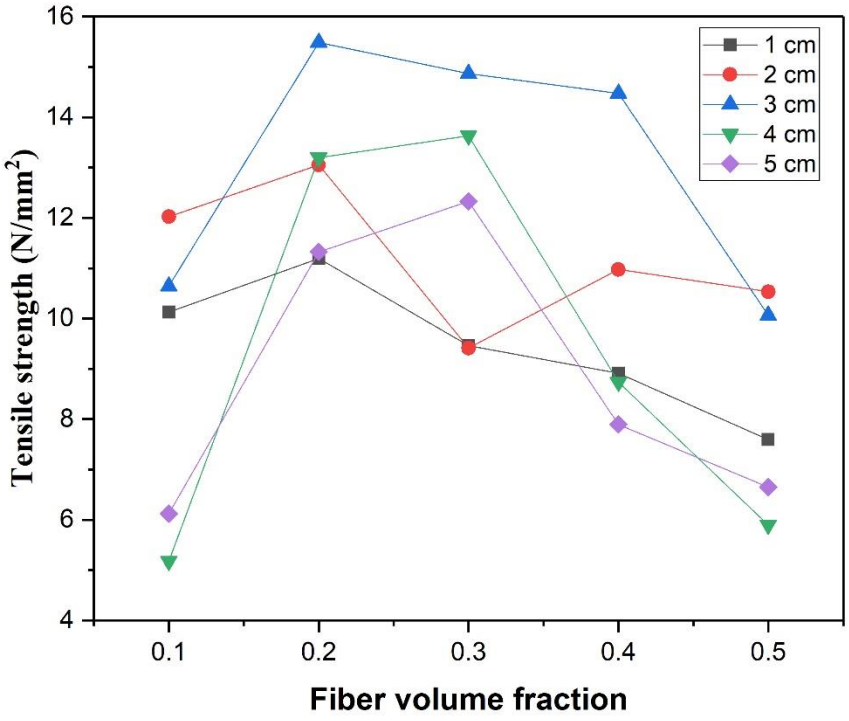


Figure 3.10: Effect of the composite's tensile strength with the fiber volume fraction and fiber length

The tensile strength of the composite changes with fiber length and fiber volume fraction. The tensile strength increases up to 3 cm of fiber length and decreases after 3 cm. The reason is fiber accumulation decreases with fiber length, which reduces the composite's tensile strength. Kuburi [91] studied the effect of coir fiber length on tensile properties with a low-density polyethylene matrix and disclosed that 3 cm length fibers gave the maximum tensile strength [91]. However, the matrix types and fiber properties could change the maximum length.

The tensile strength increases up to 0.2 of fiber volume fraction and decreases after this fiber point because the insufficient filling of the matrix occurs at the high fiber volume fraction, leading to poor adhesion between the fiber and the matrix. Dharmarathne [89] and Prakash [92] evaluated the relationship between the tensile strength and the fiber load in a low-density polyethylene matrix. The maximum tensile strength was given by 20% - 30% of fiber volume fraction in Dharmarathne's work

[89], and the 30% fiber volume fraction produced the highest tensile strength value in Prakash's work [92]

According to the above analysis, 3 cm of fiber length at the 0.2 of fiber volume fraction gives the maximum tensile strength. Therefore, 3 cm is higher than or equal to the critical length, and it can be applied to study the composite mechanical properties further.

A new bundle of coir fiber was cut to the value of 3 cm, and the fibers were subjected to the alkaline treatment with 2%, 4%, 6%, and 8% of concentrations. The composite samples were prepared with a 0.2 fiber volume fraction, and tensile strength was measured according to ASTM D 3039 [90] standard to compare the effect of alkaline concentration on the mechanical properties of the composite.

Tensile strength composites made with treated and untreated fibers were compared, as presented in Figure 3.11.

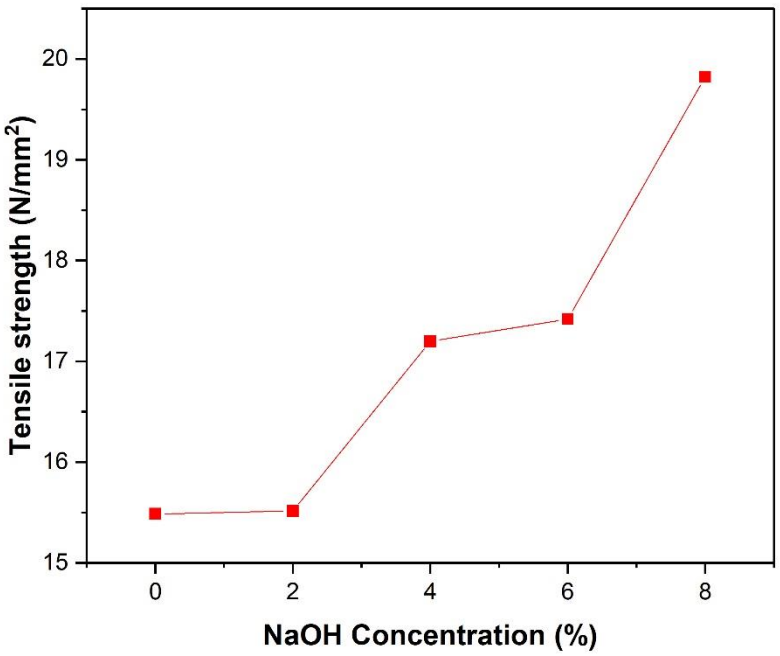


Figure 3.11: Comparison of tensile strength of composites

According to Figure 3.11, the tensile strength of the composite increases with the alkaline concentration, possibly due to the better interfacial bonding between the fiber and the matrix [69]. It may be due to the removal of hemicellulose and impurity materials from the fiber surface, which increases the surface roughness of the fiber [69]. Also, the surface roughness increases with the alkaline concentration, and cracks are formed on the surface at the higher alkaline concentration, according to the SEM image analysis. Therefore, it will increase the bonding strength between the fiber and matrix and cause the transfer of greater strength from fiber to the matrix.

Then the results of sections 3.3.1, 3.3.2, and 3.3.3 can be summarized as follows,
The surface roughness of the fiber surface can be increased by removing of non-cellulose and wax materials from the fiber surface. This surface roughness of the coir fiber increases with the concentration of alkaline solution and excess amount of treatment can damage the fiber cell. This phenomenon can be confirmed by the SEM image analysis.

Also, Removal of wax, non cellulose and cellulose with the concentration of alkaline treatment can be monitored by the FTIR analysis. It confirmed that cellulose and lignin will be removed at excess concentration of the NaOH.

Also, the tensile strength of the composite samples continually increases with the alkaline treatment due to the high surface roughness and removal of impurity substances from the fiber surface. However, the 4% concentration can be selected as the best concentration for the fiber treatment among 0%, 2%, 6%, and 8% weight to volume ratios for coir according to results in sections 3.3.1, 3.3.2, and 3.3.3.

Furthermore, the effect of 3%, 4% and 5% should be studied for the best selection. Following Figure 3.12 shows the SEM images of 3%, 4% and 5% for comparison surface properties.

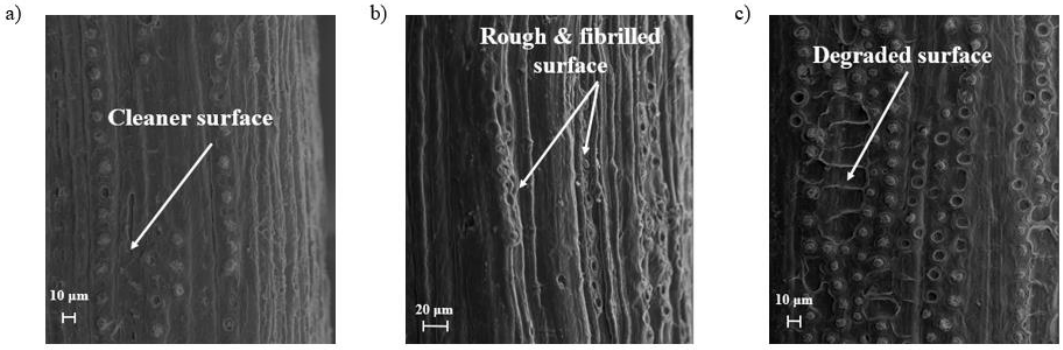


Figure 3. 12: SEM images of coir fibers (×750), a) 3% NaOH treated fiber, b) 4% NaOH treated fiber, c) 5% treated fiber

The surface roughness of Figure 3.12b) of 4% NaOH treated fiber is higher than Figure 3.12a) of 3% of NaOH treated fiber. The fiber shown in Figure 3.12c) for 5% of NaOH treated fiber has started to degrade. Therefore, 4% NaOH shows better surface properties from the SEM analysis. The previous SEM analysis results and FTIR analysis denote that 4% NaOH concentration is the best concentration for the fiber treatment.

### 3.3.4 DSC analysis of coir fibers

The location and magnitude of the exothermic and endothermic peaks of the DSC curve show the material's thermal phase transformation during heating. Endothermic peaks provide the details of sample phase transition, evaporation, dehydration, melting, and pyrolysis [11,69]. Exothermic peaks provide the details of chemical reactions, oxidation, crystallisation, decomposition, and combustion [69].

According to the results of SEM analysis and FTIR analysis, the 8% sample shows a high degradation on the fiber surface. Therefore, the untreated and the treated samples were subjected to thermal analysis with concentrations of 2%, 4%, and 6% by DSC analysis. The results of the DSC analysis are presented in Figure 3.13.

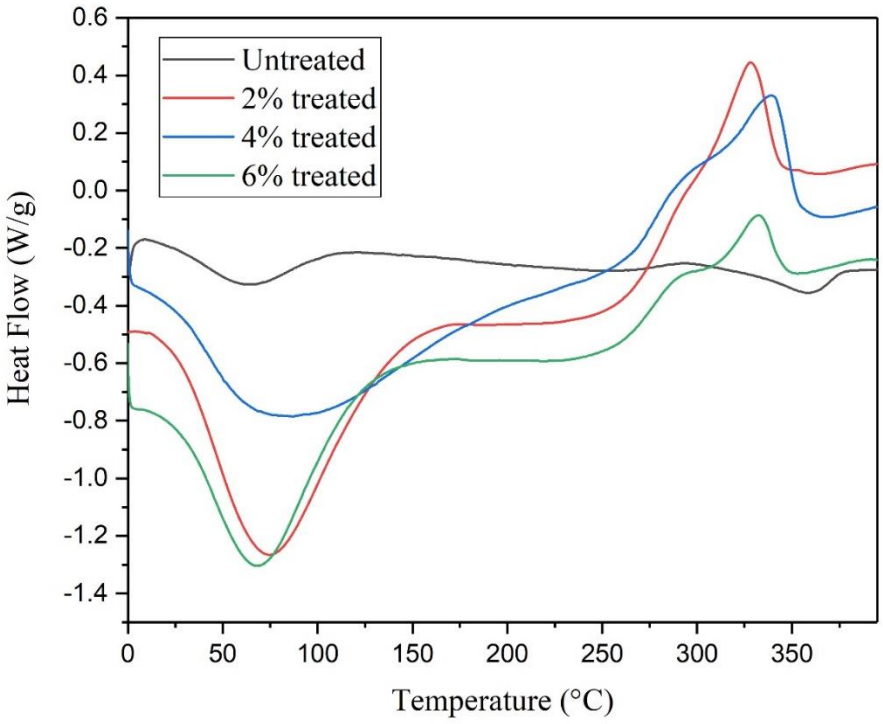


Figure 3. 13: DSC analysis for untreated and treated coir fibers

Both the untreated and treated samples give an endothermic peak between the temperatures of 5 °C to 170 °C. This peak arises due to the evaporation of moisture from the fiber surface [69]. The moisture evaporation temperature of untreated fiber

shows the minimum value. This result concludes that untreated fiber contains the maximum moisture content.

Secondly, both untreated and treated samples show an exothermic peak at the temperature range of 260 °C to 320 °C related to the degradation of hemicellulose [69]. However, the decompose temperature (272 °C) of hemicellulose in treated samples is higher than that in the untreated sample. The decompose temperature of the 4% treated sample shows the maximum value.

Thirdly, untreated fiber shows an endothermic peak at the temperature region 296 °C to 390 °C, whereas the treated fiber shows exothermic peaks at the region 300 °C to 360 °C compared to untreated fiber. These peaks are related to the degradation of cellulose and lignin substances [69]. The untreated fiber contains high amounts of lignin and cellulose. This leads to absorb high energy to degrade the fiber, which causes to show an endothermic peak during the decompose. However, the 4% sample shows the highest temperature value (317 °C) for the third stage decompose. Therefore, according to the discussion of DSC analysis, 4% sample shows the highest thermal stability due to the removal of impurities and hemicellulose from the fiber surface.

The decompose of the fibers followed the first, second, and third decompose stages, as summarised in Table 3.2.

Table 3.2: Thermal analysis of untreated and treated fibers

| **Fiber treatment** | **1st stage - Moisture evaporation temperature (°C)** | **2nd stage -Hemicellulose and lignin decompose temperature (°C)** | **3rd stage - Cellulose decompose temperature (°C)** |
|---|---|---|---|
| Untreated fiber | 17.91 | 264.43 | 305.47 |
| 2% NaOH treated | 25.55 | 271.76 | 306.21 |
| 4% NaOH treated | 20.06 | 272.73 | 317.07 |
| 6% NaOH treated | 24.43 | 265.91 | 313.52 |

The 4% alkaline treated sample shows better surface roughness, chemical composition, and thermal stability according to SEM analysis, FTIR analysis, tensile strength

analysis, and DSC analysis. Further, it is better to study the lifetime of the fiber 4% alkaline treated sample. After identification of the appropriate concentration for the treatment lifetime analysis should be done for that treated sample. The activation energy for the decomposition should be calculated to find the lifetime of the fiber. The following sections are concentrated on how to find activation energies for the decomposition and the lifetime analysis of the treated sample. However, identifyingthe decomposition stages of the degradation is a critical factor. Therefore, the TG analysis was done to identify the decomposition stages.

### 3.3.5 TG analysis

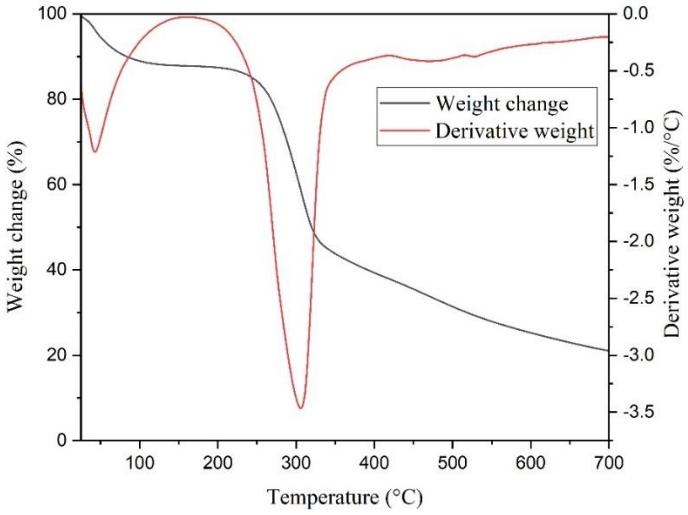


Figure 3. 14: TG and DTG curves for 4% treated fiber at a heating rate of 5 ℃/min

Figure 3.14 shows the TGA curve and differential thermal gravimetric (DTG) curve, obtained at a 5 °C/min heating rate for 4% treated fiber. Two main steps of decomposition could be identified as evaporation of water in the temperature range of 25 °C to 150 °C, and the second stage that follows the decompose of lignocellulose substances in the temperature range of 175 °C to 430 °C [11,35].

### 3.3.6 Activation energy

Mainly, the activation energy ($E_a$) helps to detect the thermal decomposition of lignocellulose fibers. The activation energy provides the minimum energy requirement for initiating the reaction [37]. The model-free method was used to find the kinetic parameters due to the method's accuracy and simplicity [35,36]. The Flynn Wall Ozawa (FWO) method, Kissinger Akahira Sunose (KAS) method, and Friedman method were applied to find the activation energy of the coir sample treated with the appropriate concentration [35].

Here, Thermal analyser SDT 650 was used for this analysis. The samples (5 – 8 mg) were heated to the temperature range of 25 °C to 700 °C with five different heating rates as 5, 10, 12, 15, 20 °C/min in an argon atmosphere [37].

Then the calculations were done using FWO, KAS, and Friedman methods as follows.

Equation 3.2 gives the FWO method,

$$\ln \beta = C - 1.052\, E_a/RT \tag{3.2}$$

Where, $\beta$ is the heating rate in °C/min, $C$ is a constant, $E_a$ is the decomposition activation energy in J mol$^{-1}$, $R$ is the gas constant, and $T$ is the temperature in K. Here, the decomposition activation energy for each conversion rate was calculated by the slope of the line that plotted ln $\beta$ versus *1/T* [35].

Equation 3.3 gives the KAS method:

$$\ln(\beta/T^2) = \ln[AR/(E_a x g(x))] + (1/T)(E_a/R) \tag{3.3}$$

Where x is the degree of conversion as given by $x = (m_o\text{-}m_t)/(m_o\text{-}m_f)$, $m_0$ is the initial sample mass, $m_t$ is the sample mass at time t, and $m_f$ is the final mass. The decomposition activation energy for each conversion rate was calculated by the slope of the line that plotted $\ln(\beta/T^2)$ versus *1/T* [35].

Equation 3.4 presents the Friedman method:

$$\ln(dx/dt) = \ln[Af(\mathrm{x})] - E_a/RT \tag{3.4}$$

*f(x)* is the reaction model. The decomposition activation energy for each conversion rate was calculated by the slope of the line that plotted $\ln(dx/dt)$ versus *1/T* [35].

Figures. 3.15, 3.16, and 3.17 indicate the plots for the FWO method, KAS method, and Friedman method, respectively.

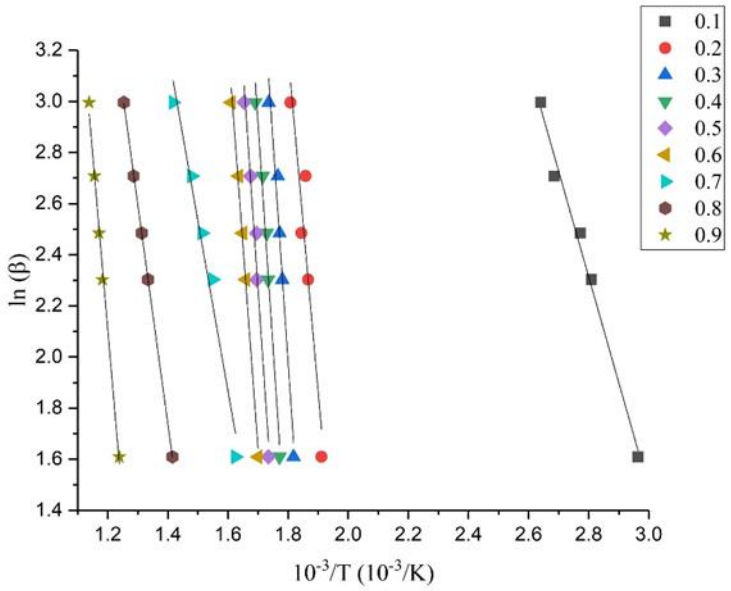


Figure 3.15: Linear plot of FWO method obtained at different degrees of conversion

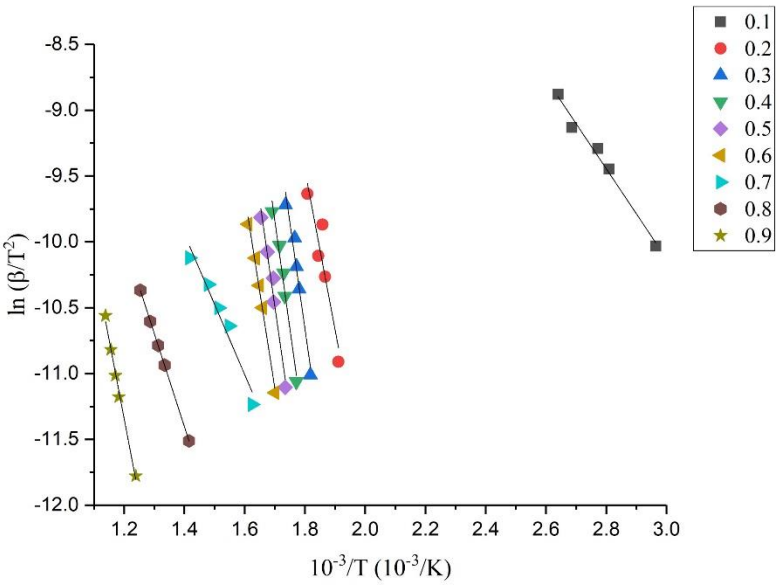


Figure 3.16: Linear plots of KAS method obtained at different degrees of conversion

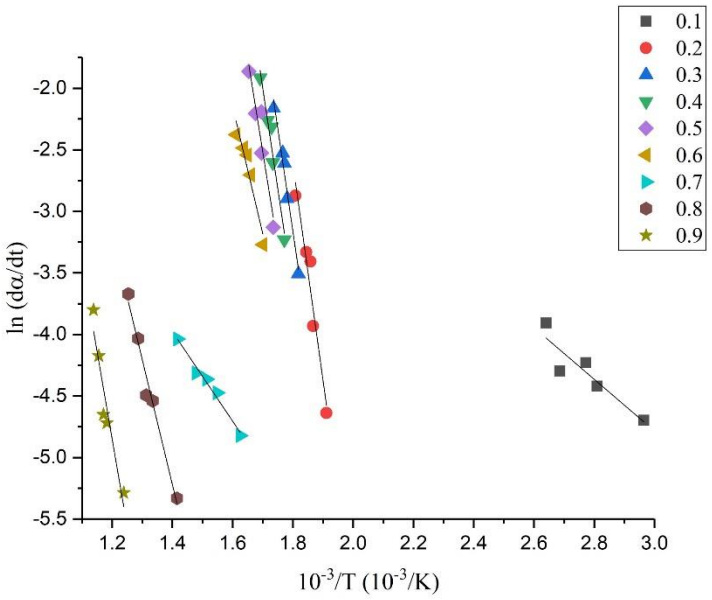


Figure 3.17: Linear plots of Friedman method obtained at different degrees of conversion

The conversion rate of 0.1 gives the activation energy for the first stage decomposition of moisture evaporation. Lines between the conversion rates of 0.2 to 0.6 are parallel to each other in the above three methods, and it implies that the possibility of the single reaction mechanism occurs at that conversion rate with the starting of the second stage of decomposition at the conversion rate of 0.2 [35] However, the reaction mechanism is changed after the 0.6 conversion rate due to the complex reactions of fiber constituents at the high temperature [35].

Table 3.3 summarises the activation energies obtained from the above three methods for the conversion rates of 0.1 to 0.9.

Table 3.3: Activation energies calculated from three methods for conversion rates of 0.1-0.9

| Conversion rate | FWO method | | Kissinger method | | Friedman method | |
|---|---|---|---|---|---|---|
| | $E_a$ (kJ/mol) | $R^2$ | $E_a$ (kJ/mol) | $R^2$ | $E_a$ (kJ/mol) | $R^2$ |
| 0.1 | 34.39 | 0.9901 | 28.45 | 0.9852 | 17.45 | 0.8420 |
| 0.2 | 109.67 | 0.8916 | 100.74 | 0.8738 | 146.22 | 0.9490 |
| 0.3 | 143.22 | 0.9708 | 133.86 | 0.9666 | 138.54 | 0.9791 |
| 0.4 | 145.95 | 0.9811 | 136.35 | 0.9783 | 136.34 | 0.9612 |
| 0.5 | 143.08 | 0.9730 | 133.27 | 0.9689 | 126.81 | 0.9088 |
| 0.6 | 131.69 | 0.9933 | 121.64 | 0.9921 | 85.89 | 0.9256 |
| 0.7 | 55.31 | 0.9743 | 44.37 | 0.9986 | 30.28 | 0.9830 |
| 0.8 | 71.32 | 1.0000 | 58.88 | 1.0000 | 84.45 | 0.9794 |
| 0.9 | 113.65 | 0.9952 | 99.68 | 0.9940 | 118.41 | 0.9179 |

The decomposition activation energy is changing from 109.67 - 145.95 kJ/mol, 100.74 - 136.35 kJ/mol, and 85.89 -146.22 kJ/mol in the FWO method, KAS method, and Friedman method, respectively, in conversion rate of 0.2 to 0.6. The average activation energy (134.72 kJ/mol) obtained from the KAS method is higher than other methods in the conversion rate of 0.2 to 0.6. The same observation can be found in Siti's work, and the activation energy was 200 kJ/mol, obtained from the Kissinger method [35].

### 3.3.7 Lifetime analysis for 4% treated fiber

The life time of the natural fibers can be calculated from the $E_a$ value [38,39], and the estimated lifetime depends on the activation energy of the material, as shown in Equation 3.5 [38,39,40]. Here, Toop's method was used to estimate the lifetime of coir fibers.

$$\log t_f = E_a/2.303RT_f + \log(\ (E_a/\beta R).P(X_f)) \quad (3.5)$$

Where $t_f$ is the estimated lifetime to failure (min), $T_f$ is the failure temperature (K), and $P(X_f)$ is the function that depends on the activation energy at the failure temperature.

The main decompose started at the 0.2 conversion rate. Therefore, it is better to find the lifetime of 4% alkaline treated coir fiber at daytime temperature. The method to find the temperature in the daytime is described in section 3.3.6.1. The average activation energy obtained from the three methods is E=128.88 kJ/mol at the 0.2 conversion rate. The slowest heating rate, 5 °C/min, was selected for this study [94]. The temperature was $T_c$ = 500 K at this heating rate and conversion rate of 0.2. Then the E/RT value was calculated and used to find the log P(Xf) from the numerical integration table in the reference [40]. The antilog value of P(Xf) was calculated next, and the lifetime of the fiber was calculated using Toop's equation [40,94].

### 3.3.6.1 Measuring the daytime temperature under the roofing cover.

Mainly roof insulation materials are installed under the roofing cover. Then, it is better to measure the temperature under the roofing cover in the daytime. Therefore, the temperature under the roofing sheet was measured for five days to find the maximum temperature. Here, the sensor of the thermometer was placed between the asbestos roofing sheet and a wooden ceiling panel. Also, the selected building is located in Homagama, Sri Lanka.

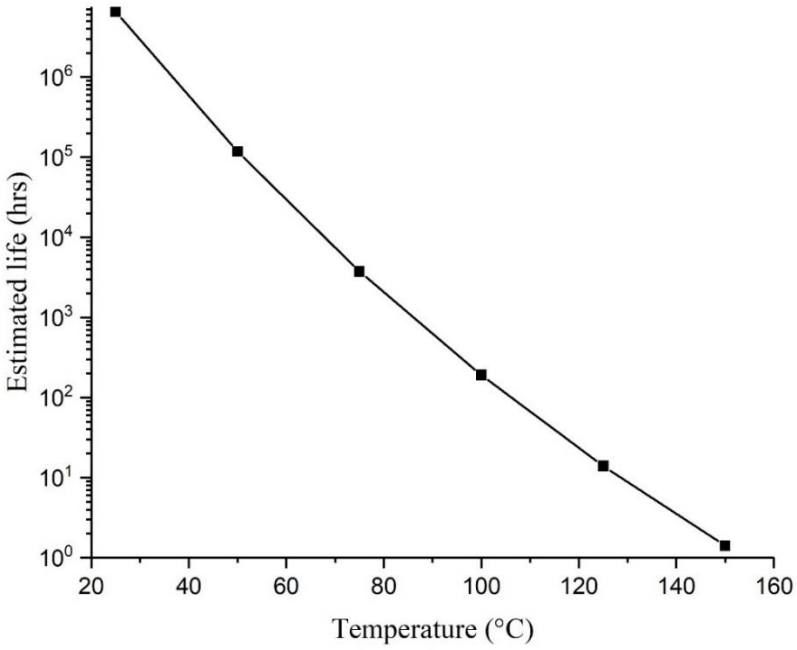


Figure 3.18. The estimated lifetime of 4% treated coir fibers

Figure 3.18 shows the estimated lifetime vs. failure temperature for 4% alkaline treated coir fibers obtained by Toop's method. The maximum average temperature for five days is 49.2 °C. The lifetime value of the 4% treated coir fiber sample is $1.32\times10^5$ hours (15 years) at 49.2 °C. However, the estimated lifetime was analysed from the activation energy value taken from the decompose curves gained at an inert atmosphere without considering mechanical loading and weather conditions [39]. Nevertheless, the above results show that 4% alkaline treated coir fibers have better thermal stability at the daytime temperature.

According to the above results, the 4% alkaline treatment was identified as the appropriate concentration than 2%, 6%, and 8%. Also, it shows a good lifetime at the maximum average temperature of daytime.

After identification of the appropriate concentration for the fiber treatment. It is important to find the transverse thermal conductivity of treated fibers. Because it is used to determine the effective thermal conductivity ($K_{eff}$) of the composite using numerical and analytical methods. Therefore, the chapter 4 describes the way how to find the transverse thermal conductivity of the treated coir fiber.

### 3.4 Conclusion

The alkaline treatment can remove the lignocellulose substances, oil, and wax contained on the surface of untreated coir fibers. This will change the fiber's surface roughness, the chemical composition of the fiber surface, as well as the thermal stability.

The changes in the surface roughness of fiber can be observed using SEM analysis. The concentration of the alkaline solution increases the surface roughness. However, an excess alkaline concentration will damage the fiber surface. Therefore, it will increase the bonding strength between the fiber and matrix and cause to transfer of greater strength from fiber to matrix. Also, the FTIR analysis can confirm the changes in the chemical composition of the fiber surface. It gives the details of the removal of cellulose, hemicellulose, lignin, and other impurities.

Nevertheless, the excess concentration of the alkaline treatment removes the cellulose and lignin from the fiber surface. The fiber thermal stability increases with the alkaline

concentration, but excess alkaline concentration reduces the thermal stability. Therefore, according to the above results, the 4% alkaline treatment was identified as the appropriate concentration than 2%, 6%, and 8%.

The activation energy of the 4% treated fiber could be determined by model-free methods such as FWO, KAS, and Friedman methods. Also, it provides information regarding the minimum energy requirement of the first stage and second stage fiber decomposition. The first stage decomposition occurs at the 0.1 conversion rate and the second stage decomposition occurs at the 0.2 to 0.6 conversion rate. Therefore, the lifetime analysis of the fiber at 0.2 is important before the fabrication process. Then the 4% treated fiber shows $1.32\times10^5$ hours (15 years) at 49.2 °C. The lifetime value reduces with the temperature. Hence, it is critical to maintain the time and the fabrication temperature to avoid fiber degradation.

# CHAPTER 4

# DETERMINATION OF THE TRANSVERSE THERMAL CONDUCTIVITY OF FIBER

## 4.1 Introduction

The thermal conductivity of each phase is required to determine the $K_{eff}$ of the composite using numerical and analytical methods. However, determination of the transverse thermal conductivity of a single fiber is challenging. Therefore, in this chapter, a method is suggested to find the transverse thermal conductivity of a single fiber. In the previous studies the $K_{eff}$ value of the composites has been evaluated from analytical methods by substituting the thermal conductivity of each phase. For this study, the inverse calculation method is used. Here, the $K_{eff}$ of the composite and thermal conductivity of the matrix were determined, followed by analytically defining the thermal conductivity value of fibers. With that aim, two-phase composite was fabricated by coir fibers and epoxy resin with different volume fractions. Then the thermal conductivity was measured for pure cured epoxy and fabricated composite using the hot disk method. Next, the transverse thermal conductivity of the fiber was calculated using Rule of mixtures, Maxwell's model, Lewis Nielsen model, and Rayleigh's model. Then the results were validated by numerical analysis.

The above analytical models were selected based on the accuracy of past studies [41,43,47]. The $K_{eff}$ of a composite can be basically calculated from the Rule of mixture. The Rule of mixture has two types of modes: parallel and series models. In the parallel model, the heat flow direction is supposed to be parallel to the fiber orientation, and the series model fiber orientation is perpendicular to the heat flow in this model [54,55]. Maxwell's model is the first identified analytical model to evaluate the $K_{eff}$ in a heterogenic medium. Mainly it is applicable for a structure with well-distributed spherical particles in a matrix phase [53,54,56]. This model provides accurate results up to 0.25 of volume fraction [53]. Rayleigh's model is a popular model that evaluates the $K_{eff}$ of a composite with continuous fibers. It can also be

applied for mixtures with a higher volume ratio than the Maxwell model [53]. Among these models, Lewis Nielsen's model is an attractive model to determine $K_{eff}$ in transverse and longitudinal directions [56]. This simple model is applicable to a wide range of filler shapes and orientations that gives higher accuracy, up to 0.4 volume fractions, without considering the interfacial thermal resistance [53]. Therefore, transverse thermal conductivity of the fiber was calculated using these models.

Further, it is important to validate the above results using another experimental method. Therefore, a binderless compacted coir fiber disk was prepared, and the thermal conductivity of the disk was measured experimentally. Then the thermal conductivity of coir fibers was calculated using Laundre's equation. The results of this method helped to validate the results of the previous method and it will be discussed in this chapter.

## 4.2 Methodology

### 4.2.1 Density measurement of coir fibers

Coir fibers were pre-treated using 4% concentrated NaOH. Then the density of fibers was measured using the Archimedes method using a 25 ml volume density bottle. The market available canola oil was used as the submerged fluid because it has low viscosity and surface tension which leads to coats the fiber well [95,96]. The fiber density ($P_{fiber}$) was calculated as per Equation 4.1.

$$P_{fiber} = \frac{(W2-w1)}{(W4-W1)-(W3-W2)} \times \frac{W4-w1}{25} \quad (4.1)$$

$W_1$ is the weight of the density bottle, $W_2$ is the weight of the density bottle with fibers, $W_3$ is the density bottle with canola oil and fibers, and $W_4$ is the weight of the density bottle with canola oil. All weighted values are given here in grams (g).

### 4.2.2 Fabrication of the composite

The fiber length should be uniaxial to get uniform distribution [73]. However, if the aspect ratio is higher than 15 then it can be taken uniaxial oriented fibers according to the Lewis Nielsen model [43,56]. But practically, too long fiber gives a curliness and it reduces the uniformity. Therefore, coir fibers were cut into 5 mm length by considering the above parameters. The hand layup method was used to fabricate the

composite. Therefore, fibers were mixed with epoxy resin to produce different volume ratios of fiber to epoxy resin, as shown in Table 4.1. Here, the volume fraction is limited up to 0.1 of fiber to matrix volume fraction. Because values obtained from the analytical models in past studies are well agreed with the experimental values within the fiber to the matrix volume fraction of 0 to 0.1. Then the mixture was poured into the wooden mould with 50 mm× 100 mm × 10 mm dimensions. Here, the hardener and epoxy were mixed as the 1:2 weight ratio as per manufacturer recommendations.

Table 4. 1: The volume fraction of fiber to epoxy resin

| **Sample no.** | **Weight of fibers (g)** | **Volume of epoxy (ml)** | **Volume fraction of fibers ($v_f$) and epoxy ($v_m$)** |
|---|---|---|---|
| 1 | 1.15 | 49 | $V_f$= 0.02, $V_m$= 0.98 |
| 2 | 2.30 | 48 | $V_f$= 0.04, $V_m$= 0.96 |
| 3 | 2.875 | 47.5 | $V_f$= 0.05, $V_m$= 0.95 |
| 4 | 4.60 | 46 | $V_f$= 0.08, $V_m$= 0.92 |
| 5 | 5.75 | 45 | $V_f$= 0.10, $V_m$= 0.90 |

The mould was allowed 48 hours to complete the curing process, and the $K_{eff}$ of the samples were measured using the hot wire disk [83,85], as shown in Figure 4.1. Therefore, each sample was cut into two similar parts as per the requirement of the instrument setup. Then, the sensor of the hot wire disk was placed between the separated sample and the $K_{eff}$ of the composites was measured. Here, the temperature of the sensor was maintained at 30 °C.

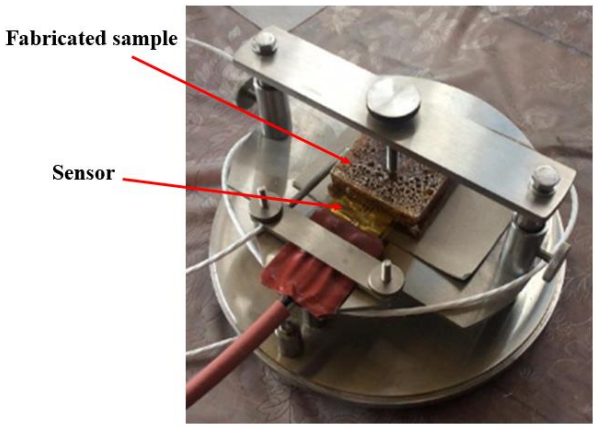


Figure 4. 1: Measuring the thermal conductivity of the fabricated composite

### 4.2.3 Calculation

The thermal conductivity of coir fibers was calculated after measuring the $K_{eff}$ of the composite by using existing analytical models for a solid-solid system. Here, the Rule of mixtures, Maxwell model, Rayleigh's model, and Lewis Nielsen model were used to determine the transverse thermal conductivity of coir fibers.

Here, the fiber orientation is perpendicular to the heat flow. Therefore, a series model was necessary to analyse the $K_{eff}$ in this orientation, as given by Equation 4.2.

$$K_{eff} = \frac{1}{\frac{V_m}{K_m} + \frac{V_f}{K_f}} \tag{4.2}$$

Where $K_m$ is the thermal conductivity of the matrix, $V_m$ is the volume fraction of the matrix, $K_f$ is the thermal conductivity of fiber, and $V_f$ is the volume fraction of fiber.

Equation 4.3 provides the Maxwell's model.

$$K_{eff} = K_m \frac{2K_m + K_f - V_f(K_m - K_f)}{2K_m + K_f + V_f(K_m - K_f)} \tag{4.3}$$

Equation 4.4 gives the transverse thermal conductivity of Rayleigh's model.

$$\frac{K_{eff}}{K_m} = 1 + \frac{2V_f}{C_1 - V_f + C_2(0.30584{V_f}^4 + 0.013363{V_f}^8 + \cdots)} \tag{4.4}$$

Where $C_1 = \frac{K_f + K_m}{K_f - K_m}$ and $C_2 = \frac{K_f - K_m}{K_f + K_m}$

Equation 4.5 presents the Lewis Nielsen's model.

$$K_{eff} = K_m \left[\frac{1 + ABV_f}{1 - BV_f\Psi}\right] \quad (4.5)$$

Where $B = \frac{\frac{K_f}{K_m} - 1}{\frac{K_f}{K_m} + A}$ and $\Psi = 1 + \left(\frac{1 - \varphi_m}{\varphi_m^2}\right) V_f$

The values for the constant 'A' in various systems is given in Table 4.2. Here, the aspect ratio of the fibers is greater than 15. Then the dispersed phase can be taken as uniaxial oriented fibers according to the Lewis Nielsen model. Also, the direction of heat flow is perpendicular to the fiber direction and the 'A' value can be selected as 0.5.

Table 4.2: Values for 'A' for various systems [43,47].

| Type of dispersed phase | Direction of heat flow | A |
|---|---|---|
| Cubes | Any | 2.0 |
| Spheres | Any | 1.50 |
| Aggregate of spheres | Any | $\frac{2.50}{\varphi_0} - 1$ |
| Randomly oriented rods aspect ratio = 2 | Any | 1.58 |
| Randomly oriented rods aspect ratio = 4 | Any | 2.08 |
| Randomly oriented rods aspect ratio = 6 | Any | 2.8 |
| Randomly oriented rods aspect ratio = 10 | Any | 4.93 |
| Randomly oriented rods aspect ratio = 15 | Any | 8.38 |
| Uniaxial oriented fibers | Parallel to fibers | *2I./D* |
| Uniaxial oriented fibers | Perpendicular to fibers | 0.5 |

The values for the constant '$\varphi_m$' in various systems is given in Table 4.3. Also, the packing type can be taken as uniaxial random. Therefore the value of '$\varphi_m$' is equal to 0.82.

Table 4.3: Values for φm for various system [43,47].

| Shape of Particle | Type of Packing | $\varphi_m$ |
|---|---|---|
| Spheres | Hexagonal close | 0.7405 |
| Spheres | Face centred cubic | 0.7405 |
| Spheres | Body centred cubic | 0.60 |
| Spheres | Simple cubic | 0.524 |
| Spheres | Random close | 0.637 |
| Spheres | Random close | 0.601 |
| Rods of fibers | Uniaxial hexagonal close | 0.907 |
| Rods of fibers | Uniaxial simple cubic | 0.785 |
| Rods of fibers | Uniaxial random | 0.82 |
| Rods of fibers | Three dimensional random | 0.52 |

### 4.2.4 Finite element method

The results of the analytical method were validated by the finite element method, using the Ansys software package [22,41,42,43]. Assumptions considered during the simulation are, fibers and matrix are microscopically and homogeneously distributed throughout the composite, fibers have the same shape and size, fiber and matrix have a perfect bonding, thermal resistance between two phases is negligible, and void-free through the composite [22,41,42,43].

Normally, fibers are randomly distributed throughout the matrix in a composite; therefore, the random arrangement is difficult model. Therefore, the micromechanical model can be simplified as an isolated unit cell that has a three-dimensional physical model with a periodic arrangement of cylindrical fibers in epoxy cubes [41,43] because coir fibers have an approximately circular cross-section, as shown in the scanning electron microscope (SEM) image in Figure 4.2. It provides an additional advantage for the analytical and numerical modelling of the composite.

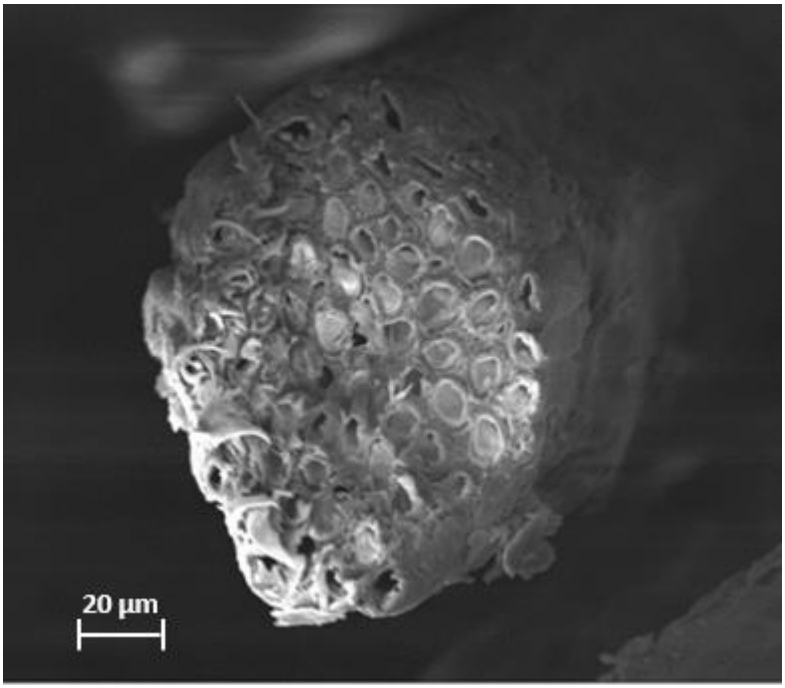


Figure 4.2: Cross section of a coir fiber (×1000)

Further, the fiber distribution of a single unit cell could be identified as a square pattern and hexagonal pattern, as shown in Figure 4.3 [45-47].

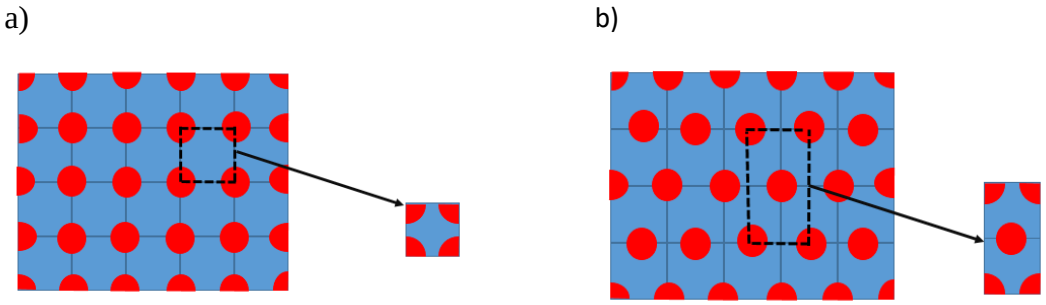


Figure 4.3: Fiber distribution in a) Square pattern, b) Hexagonal pattern

The above unit cells are simplified as a quarter unit cell, as shown in Figure 4.4, to reduce the complexity of geometry and computing time [45]. It is vital to adopt an orthogonal coordinate system that represents the fiber direction on the z-axis; the x-axis is the plane of the unit cell, which is perpendicular to the fibers, and the y-axis is perpendicular to the plane of the unit cell and perpendicular to the fibers. Here, the fiber Diameter was measured using primo star iLED microscope and the average

Diameter was 201.6 μm, and the length of the unit cell was calculated corresponding to the volume ratio of 0% to 0.1%.

a)

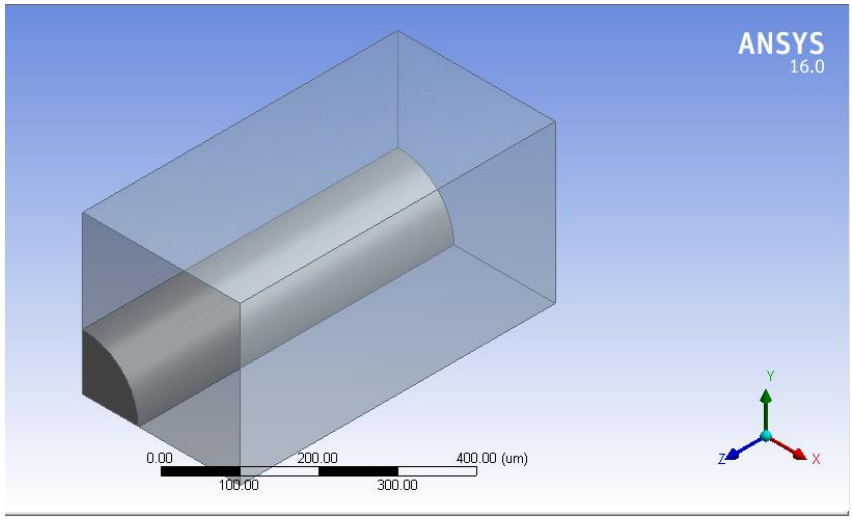


b)

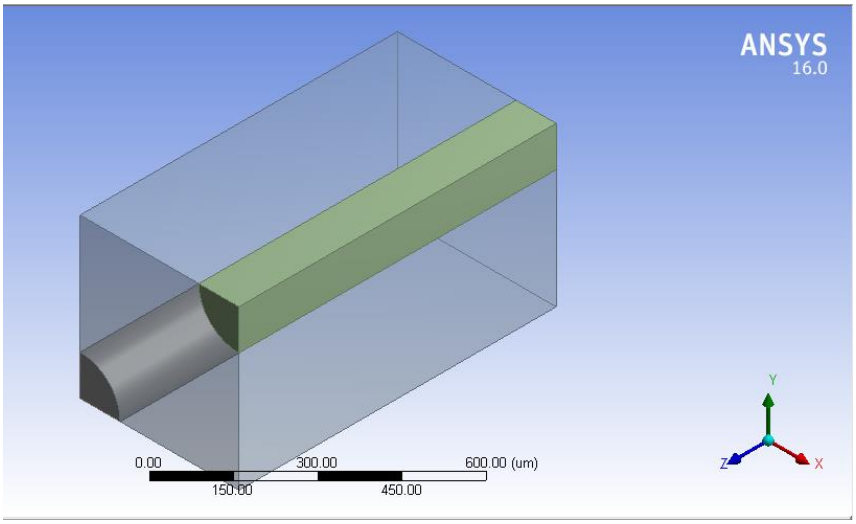


Figure 4. 4: A quarter unit cell of a) Square array, b) Hexagonal array

### 4.2.5 Boundary condition for FEM to analyze thermal conductivity

For finding the $K_T$ of the unit cell, the heat load was applied as a temperature for both plane face (30 °C) and opposite face (25 °C) to obtain a temperature difference of 5 °C. Remaining faces are considered to be adiabatic [44,45,52].

The heat distribution throughout the unit cell was analysed by Ansys software, and the thermal conductivity of the unit cell was calculated by Fourier's law, as shown in Equation 4.6.

$$Q_x = -K\,(dT/da) \qquad (4.6)$$

Where $K$ is the thermal conductivity of the unit cell, $dT/da$ is the temperature gradient in the x-direction, and $Q_x$ is the heat flux along the x-direction.

### 4.2.6 Preparation of coir fiber specimen to measure thermal conductivity.

A cylindrical-shaped specimen was prepared by compressing 5 mm coir fibers without using a binder [98]. Here, a 20 Mpa pressure was applied on 6.61 g coir fibers with a mould diameter of 25 mm. The thermal conductivity reading was obtained from the hot wire disk after removing the specimen from the mould, as shown in Figure 4.5.

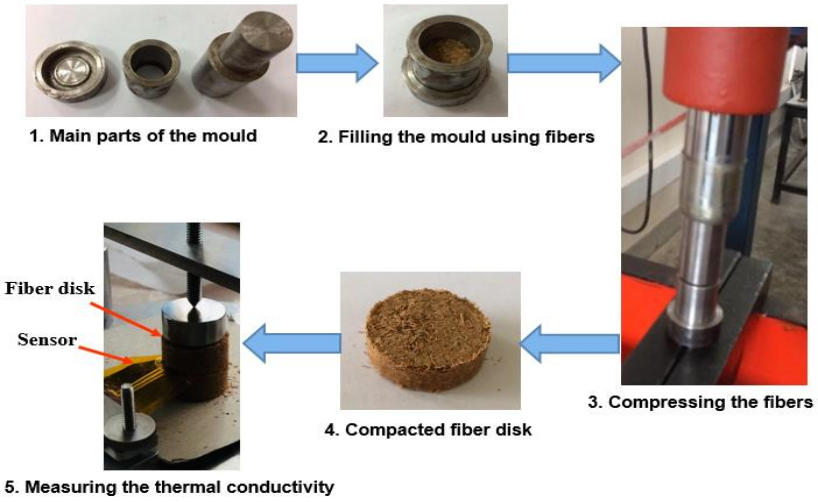


Figure 4. 5: Preparation of binder-less coir fiber disk

## 4.3 Results and Discussion

### 4.3.1 Thermal conductivity of coir fabricated composite

In this study, the $K_{eff}$ of the fabricated composite was experimentally measured by a hot-wire disk. Here, the temperature of the sensor was maintained at 30 °C. Figure 4.6

shows the $K_{eff}$ values of fabricated epoxy based composite with different volume fractions.

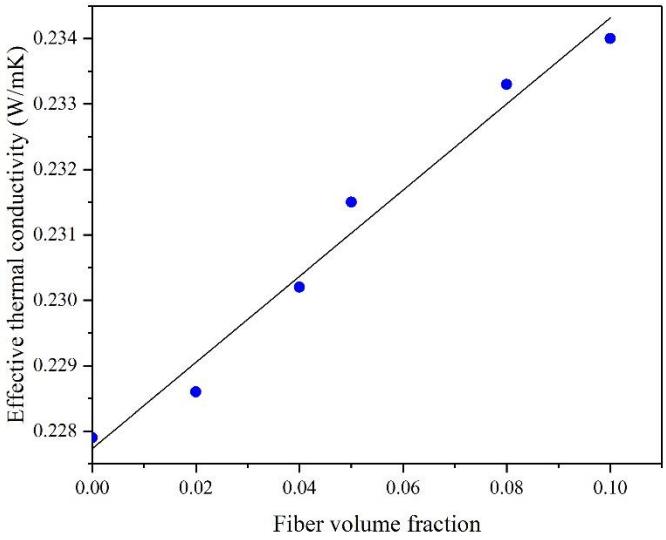


Figure 4.6: The $K_{eff}$ of the epoxy based composite

The effective thermal conductivity of the composite was increased with the fiber volume fraction. It shows that the thermal conductivity of fibers is higher than the thermal conductivity of epoxy.

The transverse $K_{eff}$ of the composite for each fiber loading and the thermal conductivity value of epoxy were substituted to the rule of mixtures, and Maxwell's, Rayleigh's, and Lewis Nielsen's models, to find the fiber thermal conductivity. Table 4.4 summarises the calculated thermal conductivity values of fibers for each volume fraction.

Table 4.4: Thermal conductivity values obtained from each model for the respective fiber volume fraction

| **Fiber volume fraction** | **$K_{eff}$ of composite** | **$K_f$ from Rule of mixture** | **$K_f$ from Maxwell model** | **$K_f$ from Rayleh's model** | **$K_f$ from Lewis Nielsen model** |
|---|---|---|---|---|---|
| 0.02 | 0.2286 | 0.2946 | 0.2815 | 0.2836 | 0.2825 |
| 0.04 | 0.2302 | 0.3172 | 0.2992 | 0.3029 | 0.3049 |
| 0.05 | 0.2315 | 0.3432 | 0.3140 | 0.3199 | 0.3249 |
| 0.08 | 0.2333 | 0.3209 | 0.2960 | 0.2999 | 0.3138 |
| 0.1 | 0.2340 | 0.3133 | 0.2976 | 0.3015 | 0.3028 |
| Average $K_f$ value | | 0.3192 | 0.2977 | 0.3016 | 0.3058 |

Then the calculated average $k_f$ values (0.3192 W/mK, 0.2977 W/mK, 0.3016 W/mK, and 3058 W/mK) obtained from each model were re-substituted to Rule of mixture, Maxwell, Rayleigh's, and Lewis Nielsen models for validation of the results and identification of the value closer to the experimental values. Then the re-substituted $k_f$ values to Maxwell, Rayleigh's, and Lewis Nielsen models could be graphically represented as per Figure 4.7.

a)

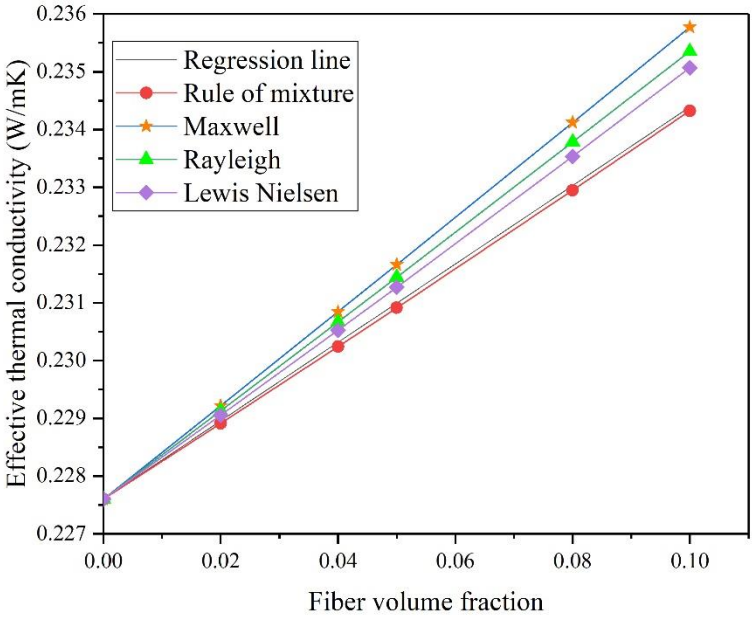

b)

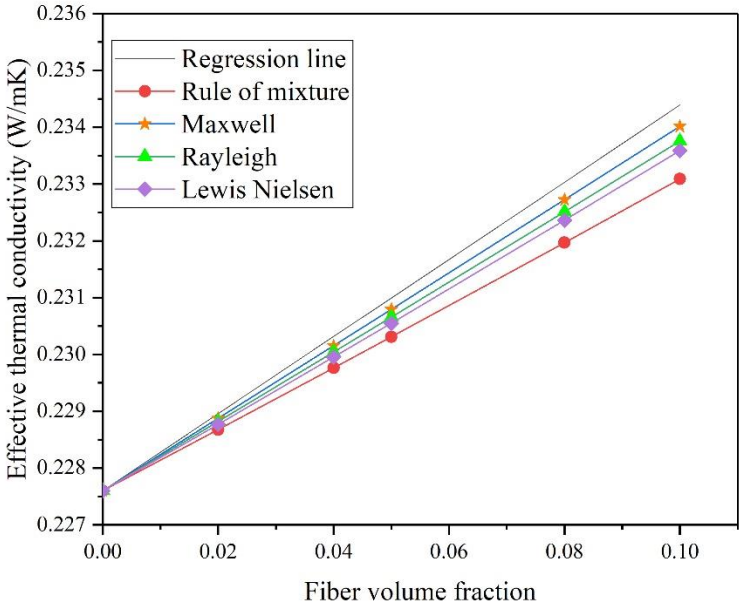
Regression line
Rule of mixture
Maxwell
Rayleigh
Lewis Nielsen
Effective thermal conductivity (W/mK)
0.227
0.228
0.229
0.230
0.231
0.232
0.233
0.234
0.235
0.236
0.00
0.02
0.04
0.06
0.08
0.10
Fiber volume fraction

c)

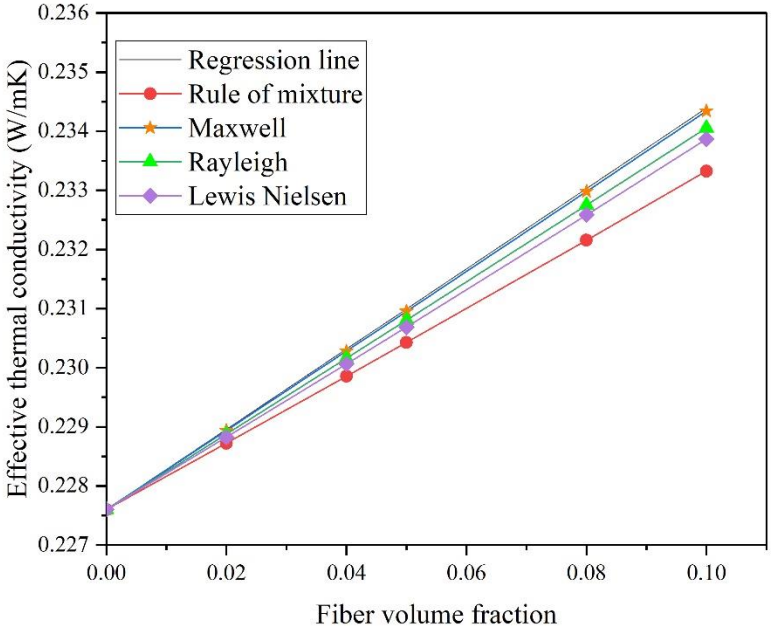
Regression line
Rule of mixture
Maxwell
Rayleigh
Lewis Nielsen
Effective thermal conductivity (W/mK)
0.227
0.228
0.229
0.230
0.231
0.232
0.233
0.234
0.235
0.236
0.00
0.02
0.04
0.06
0.08
0.10
Fiber volume fraction

d)

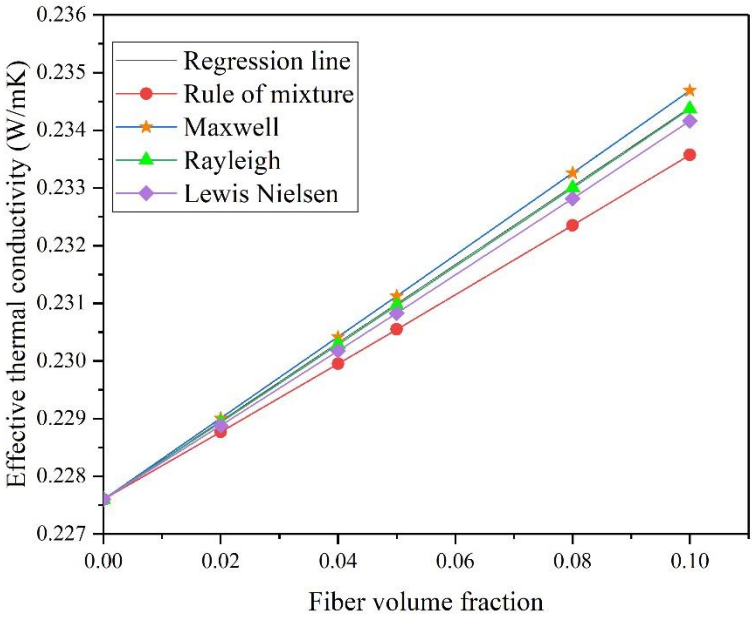


Figure 4. 7: Behaviour of thermal conductivity of fiber with analytical models a) Thermal conductivity value of 0.3192 W/mK, b) Thermal conductivity value of 0.2977 W/mK, c) Thermal conductivity value of 0.3016 W/mK d) Thermal conductivity value of 0.3058 W/mK

The models show a variation with the regression line of the experimental values according to Figures 4.7a) – d). The reason is the difference in the assumption during the development of micromechanical models of the analytical models, such as fiber shape, distribution, and interfacial contact between the matrix and fiber material. Also, void formation in the composite and changes in the orientation of fibers may have caused this situation. Therefore, it is better to consider percentage errors with the regression line, shown in Figure 4.7 a)-d), to select the average $K_f$. Thus, the percentage errors with the regression line in Figure 4.7 a) are shown in Table 5.

Table 4.5: The percentage errors with the regression line in Figure 4.7a)

| **Fiber volume fraction** | **Experimental value (Values on regression line)** | **Percentage error** | | | |
|---|---|---|---|---|---|
| | | **Rule of mixture** | **Maxwell** | **Rayleigh's** | **Lewis Nielsen** |
| 0.02 | 0.2290 | 0.0218 | 0.1136 | 0.0742 | 0.0393 |
| 0.04 | 0.2303 | 0.0347 | 0.2301 | 0.1520 | 0.0912 |
| 0.05 | 0.2340 | 0.0390 | 0.2857 | 0.1905 | 0.1169 |
| 0.08 | 0.2330 | 0.0343 | 0.4678 | 0.3218 | 0.2189 |
| 0.1 | 0.2343 | 0.0299 | 0.5888 | 0.4138 | 0.2901 |
| Average percentage error (X) | | 0.0319 | 0.3372 | 0.2305 | 0.1513 |
| Mean value of average percentage error ($\bar{X}$) | | 0.1877 | | | |

According to Table 4.5, the mean value of average percentage error for rule of mixtures, Maxwell, Rayleigh's, and Lewis Nielsen is 0.0708. The same procedure was followed to find the percentage error in Figure 4.7 b)-d) and results are summarised as Table 4.6.

Table 4. 6: Mean value of $\bar{X}$ in Figure 4.7a) – d)

| **Figure no** | **Substituted $K_f$ value (W/mK)** | **Mean value of $\bar{E}$** |
|---|---|---|
| 4.7a) | 0.3192 | 0.1877 |
| 4.7b) | 0.2977 | 0.2029 |
| 4.7c) | 0.3016 | 0.1321 |
| 4.7d) | 0.3058 | 0.0923 |

The substitution of the $K_f$ value of 0.3058 W/mK produced a minimum percentage error of 0.0923. Therefore, the thermal conductivity of coir fiber can be taken as 0.3058 W/mK. It is important to validate this value using a numerical method, and section 4.3.2 discusses the numerical analysis for the validation.

### 4.3.2 Numerically validating the thermal conductivity of fibers

The value of 0.3058 W/mk was validated from the numerical methods using square array pattern and hexagonal array pattern. Figure 4.8 provides the temperature distribution in square and hexagonal array patterns for the 0.1 fiber ratio.

a)

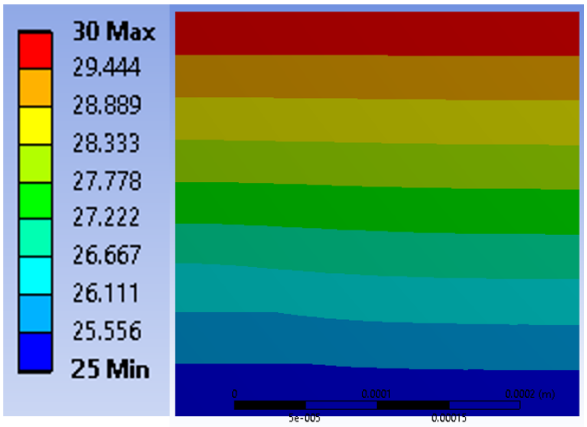


b)

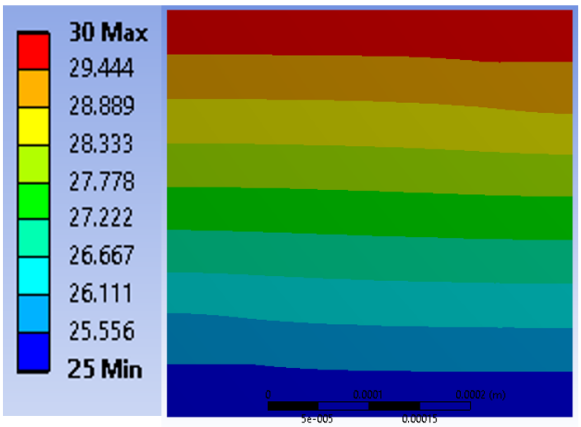


Figure 4.8: The temperature distribution in quarter unit cell a) square array pattern b) hexagonal array pattern

The temperature distribution is uniform in the upper region of Figure 4.8a). However, it shows an uneven distribution around the bottom region of the quarter unit cell due to the presence of fiber. Also, the temperature distribution is uneven in the top and bottom regions of Figure 4.8b) due to the presence of fibers. But it will show a uniform distribution in the middle region of the quarter unit cell.

Figure 4.9 shows the comparison of the experimental, and numerical results.

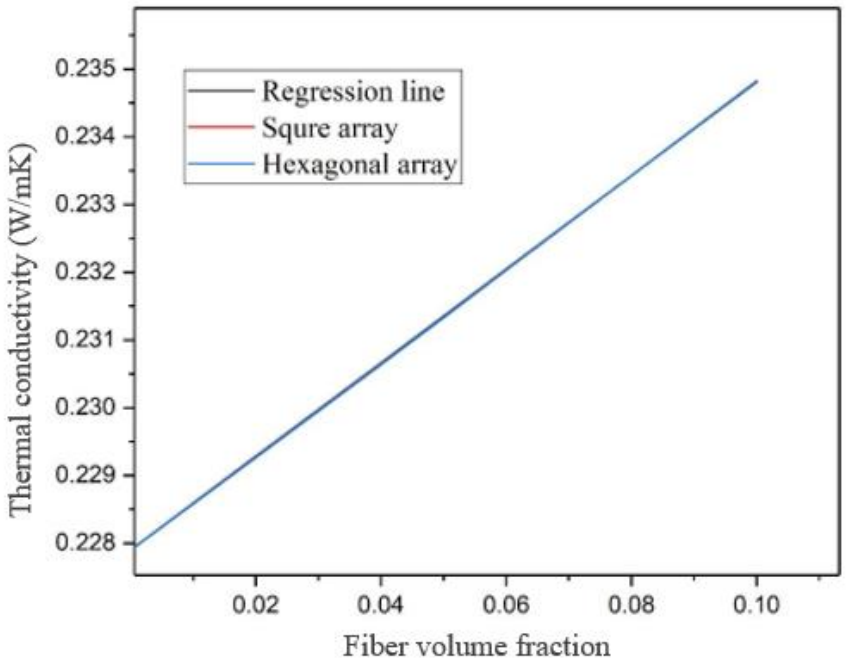


Figure 4.9: Comparison of experimental, and numerical results

According to Figure 4.9, the values obtained from the numerical method overlap with the regression line of the experimental values. Hence, the transverse thermal conductivity of the coir fibers can be accepted as 0.3058 W/mK according to the results of experimental, analytical, and numerical methods.

### 4.3.3 Thermal conductivity of compacted coir fibers

The average thermal conductivity of the compacted coir fiber disk is 0.1982 W/mK, and the density is 0.936 $gcm^{-3}$. According to this density value, the compacted fiber disk contains a 0.2280 volume fraction of air. However, to predict the thermal conductivity of coir fibers, Laundauer's equation was used to calculate the thermal conductivity of coir fibers because the structure is open porous when the volume fraction is in the range of $0.15 < Vp < 0.65$. Equation 4.7 provides the Laundaure's equation.

$$K_{eff} = \frac{1}{4}\left[K_p(3V_p - 1) + K_m(2 - 3V_p) + \left\{\left[K_p(3V_p - 1) + K_s(2 - 3V_p)\right]^2 + 8K_mK_p\right\}^{1/2}\right] \quad (4.7)$$

Where $K_p$ is the thermal conductivity of air at 25 °C, and $V_p$ is the volume fraction of air.

According to Equation 4.7, the calculated value of the thermal conductivity of coir fibers is 0.2797 W/mK. The results obtained from the compacted fiber disk is close to the value of 0.3058 W/mK obtained from Section 4.3.1. However, the variation of the results in the Section 4.3.1 and Section 4.3.3 may be due to the interfacial thermal resistance in the structure.

### 4.4 Conclusion

In this study, a composite material was fabricated using epoxy and coir fibers for different fiber loadings. Then the $K_{eff}$ of the composites was measured. Here, the $K_{eff}$ of the composite was higher than the thermal conductivity of pure epoxy, and the $K_{eff}$ was increased with the increasing fiber loading in the composite. Hence, it concluded that the thermal conductivity of coir fibers is greater than epoxy. Then it is possible to analytically determine the thermal conductivity of coir fibers using the experimentally measured $K_{eff}$ values. Therefore, the analytical models are a practical approach of finding the thermal conductivity in coir fibers due to the close relation with the experimental values. The transverse thermal conductivity of the fiber could be taken as 0.3058 W/mK by the comparison of the results obtained from the analytical models. Additionally, validation of the transverse thermal conductivity value of 0.3058 W/mK using the numerical method will add value to this work. Here, the numerical results and experimental results were overlapped in each other and it proved that the 0.3058 W/mK could be taken as the thermal conductivity of the fiber. Further, a binder-less compacted fiber disk was prepared and measured the thermal conductivity of the disk to validate the results obtained from the previous method. Here, the void content of the disk was 22.8%, which shows an open pores structure. Therefore, the thermal conductivity of fiber was calculated using Laundauer's equation and the value was 0.2797 W/mK. However, this method could be used to validate the value of 0.3058 W/mK, even if the difference between the value of 0.2797 W/mK.

# CHAPTER 5

# DETERMINATION OF THE THERMAL CONDUCTIVITY OF LATEX

## 5.1 Introduction

The attractive properties of NR latex to use as a natural adhesive are the high tack and tack retention properties, better flexibility, good strength after the vulcanising, and good moisture retention properties [77]. Also, NR latex has significant adhesive properties with coir fibers. Therefore, it is used to adhere fibers to each other to maintain the permanence of the composite structure. A combination of NR latex and coir fibers produces many products like mattresses, automobile parts, and pots [76]. Therefore, it is used to fabricate thermal insulation materials with coir fibers in this research work.

The following requirements of the latex compound should be fulfilled for the fabrication [99]:

a) The vulcanising system should be provided with a high-quality cure during the process.
b) A very thin film of latex should be applied on coir fibers, and it will be at the risk of oxidation. Therefore, it is essential to add an effective antioxidant to the compound.
c) Typically, the latex compound should be applied to fibers using spraying. Therefore, it is important to maintain the compound without agglomeration to prevent the spray gun nozzle blockage. Also, the mechanical stability of the compound should be maintained at an adequate level. These objectives can be maintained by adding dispersion media during the compound preparation.
d) Additional wetting agents should be added to the compound to obtain adequate wetting properties. However, an excessive amount of stabilisers and wetting agents will cause a fine mist during spraying. The recommended application is

the slightly large droplets which flow through the fiber surface, and they should join together at the fiber intersection.

Therefore, the following formula is used to produce the latex compound. A suitable formulation is given below [99].

| A suitable formulation is given below. | Parts by weight |
|---|---|
| 60% concentrated NR latex | 167 |
| 10% KOH solution | 5 |
| 20% vulcastab LW | 2.5 |
| 50% Antioxidant TQ (phenolic type) dispersion | 2.0 |
| 50% ZMBT dispersion | 2.0 |
| 50% ZDC dispersion | 2.0 |
| 50% Sulphur dispersion | 5.0 |
| 50% ZnO dispersion | 6.0 |
| 50% China clay | as required |

**5.2 Measurement of the total solid content of the latex compound**

Total solid content (TSC) is the percentage by weight of latex which is non-volatile at a defined temperature. "The standard method is as described in ISO 124:1985 [100]. It involves heating a test sample to constant mass in an oven at 100 °C for 2 hours at atmospheric pressure. The TSC value is calculated using the following Equation 5.1".

$$TSC = \frac{M_1}{M_2} \times 100\% \quad (5.1)$$

Where $M_1$ is the weight of the test portion before heating, and $M_2$ is the weight of the test portion after heating.

Here, the TSC values obtained for the above formula are 58.98%, 58.79%, and 58.90%. The average TSC value is 58.89%.

### 5.3 Determination of the thermal conductivity of latex with aging time

The thermal conductivity of a material can change with the material degradation. Therefore, it is necessary to measure the thermal conductivity of latex with the ageing time. With that aim, eight sheets of 0.2 cm thickness were prepared using the compounded latex batch. These sheets were vulcanised at 150 °C for 40 min. The thermal conductivity of one sample was measured 24 hours after the vulcanisation process (Sample A), and others were subjected to the ageing process up to the maximum duration of 7 days. Table 4.1 provides the prescribed period for the samples. Here, the temperature was maintained at 70 °C following ASTM D 573 standard [101].

Table 5.1: The prescribed period for the samples

| **Sample** | A | B | C | D | E | F | G | H |
|---|---|---|---|---|---|---|---|---|
| **Aging time** | 0 day | 1 day | 2 days | 3 days | 4 days | 5 days | 6 days | 7 days |

Figure 5.1 presents the prepared latex samples after the aging process.

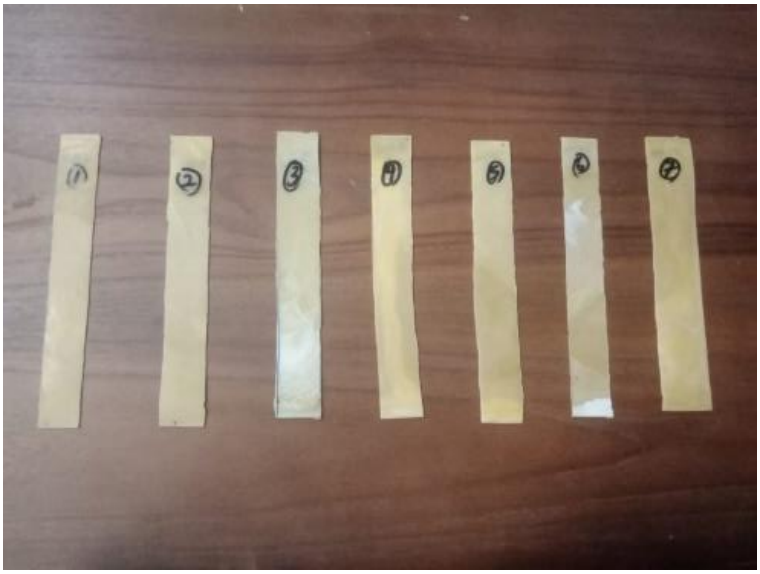

Figure 5.1: Prepared samples after the aging process

Then the thermal conductivity of the samples was measured using the hot-wire disk method. Figure 5.2 presents the thermal conductivity of aged samples.

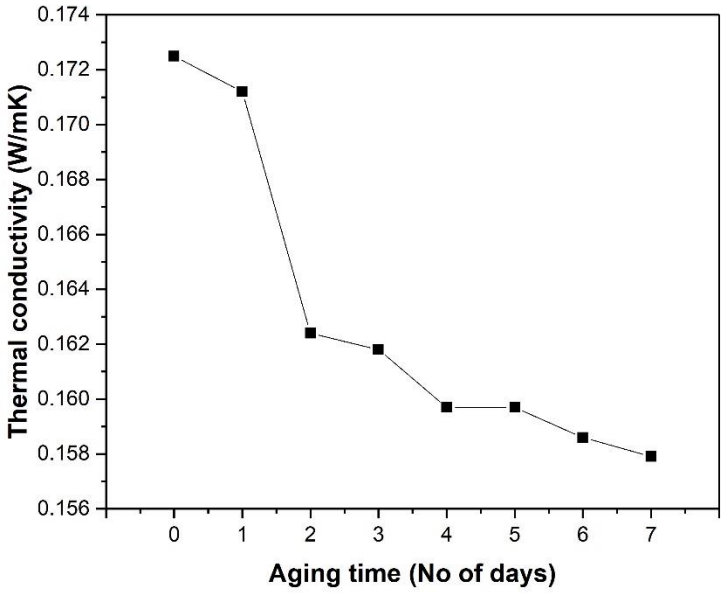


Figure 5.2: Thermal conductivity of aged samples

According to Figure 5.2, sample A, before the ageing process gives the maximum thermal conductivity value, and sample H aged for 7days, gives the minimum thermal conductivity value. Further, the thermal conductivity of the compounded latex reduces with the ageing time, probably due to the reduction of cross-link density of the samples due to oxidation [102] and it will reduce the thermal conductivity of the latex [103]. However, the relative decrease in the thermal conductivity of the H sample with respect to A sample is 8.46%. However, the total reduction of the $K_{eff}$ will be less than 8.46% according to the empirical models, and the modification of the compound is recommended for future studies.

## 5.4 Determination of the thermal conductivity of latex after the vulcanised process.

According to the above formula, the latex compound was prepared and cured for 24 hours. It was heated to 120 ℃ for the vulcanised process for one-and-half hours [99], and the sample's thermal conductivity was measured using a hot wire disk as Figure 5.3.

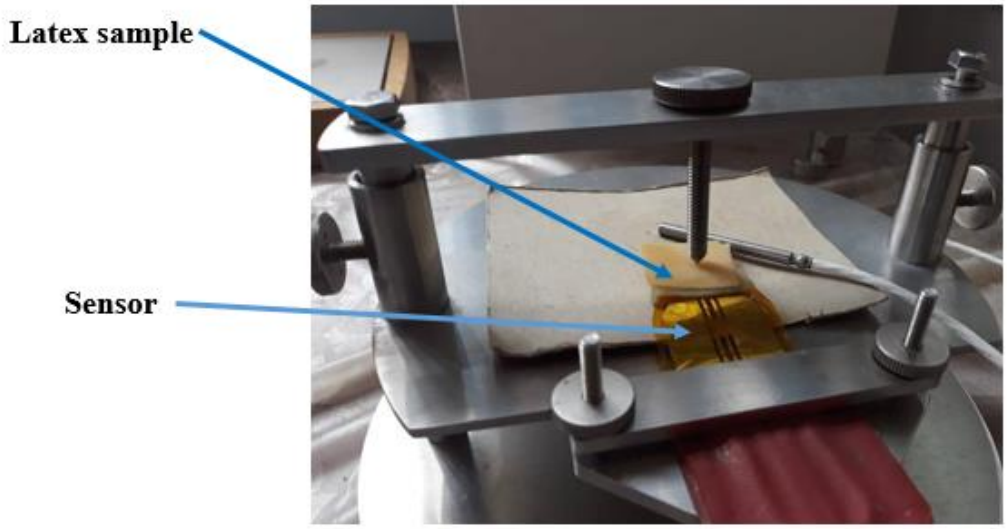


Figure 5.3: Measuring the thermal conductivity of the fabricated composite

### 5.5 Conclusions

Thermal conductivity values

$K_1$ = 0.1758 W/mK

$K_2$ = 0.1725 W/mK

$K_3$ = 0.1725 W/mK

Then the average thermal conductivity = 0.1736 W/mK

Analytical and numerical methods can use to evaluate the $K_{eff}$ of the insulation material after identifying the thermal conductivity of latex and the coir fiber. Chapter 6 discusses evaluating the $K_{eff}$ of the insulation material using analytical, numerical, and experimental methods.

# CHAPTER 6
# ANALYSING THE THERMAL CONDUCTIVITY OF THE INSULATION MATERIAL

## 6.1 Introduction

The mixture of latex (binder material) and the fiber can be identify as a composite material. Further, the insulation properties of this composite can be increased by introducing air voids into the combination of fiber and binder material because the thermal conductivity of air is lower than the solid region [58,59]. Then the material structure will be formulated as a three-phase composite material. After that, the insulation properties of the composite material depend on the volume fractions of each phase (fiber, binder, and air). The $K_{eff}$ mainly decides the material's insulation properties.

The $K_{eff}$ of a composite can be evaluated using experimental, analytical, and numerical methods [41,43]. Analytical and numerical evaluation methods are followed before the experimental methods due to their cost-effectiveness and efficiency [42,54]. In these methods, the first step is to analyse the conductivity of a mixture of matrix and one filler. Then the $K_{eff}$ of the composite can be analysed with the conductivity value of the mixture and the second filler [56]. However, this composite type contains a solid-solid phase (binder and fiber) and a solid-gas phase (binder, fiber, and air). Therefore, it is vital to analyse the $K_{eff}$ with analytical models available to find the $K_{eff}$ in a solid-solid system and the $K_{eff}$ in a solid-gas system.

Maxwell's model, Rayleigh's model, and Lewis Nielsen's model are mainly used to find the $K_{eff}$ of a solid-solid phase as discussed in chapter 4. Additionally, it is essential to study the available analytical model to study the $K_{eff}$ in a solid-gas system. Smith evaluated the thermal conductivity in a porous media analytically and experimentally for the pores fraction 0.04 to 0.95 [58]. Here, different analytical models show closeness with the experimental values for different pore volume fractions ($V_p$). Maxwell Eucken model shows better agreement with the experimental up to $V_p$ of 0.15

because the material can be taken as a close pores structure when the $V_p$ is less than 0.15. Also, Landauer's relation shows a better agreement within the $V_p$ range of 0.15 to 0.65 [58]. Hashin-Shtrikman's upper bond and Russell's relation show better agreement for the $V_p$ higher than 0.65. In addition to these models, some models such as Progelhof and Throne empirical model and Topper theoretical model are available to measure $K_{eff}$ of a pores composite material [56].

In this chapter, the $K_{eff}$ of the solid-solid phase was analysed by analytical and numerical methods. Then the $K_{eff}$ the solid- gas phase (whole insulation material with the latex, coir fibers, and air void) was analysed by the analytical, numerical, and experimental methods.

## 6.2 Evaluation of the $K_{eff}$ of solid-solid phase

In this section, the $K_{eff}$ of the solid-solid phase was measured using analytical and numerical methods. The methodology is described as follows,

### 6.2.1 Methodology

#### 6.2.1.1 Fabrication of the composite.

Microscopically analysis of the cross section of the composite should be carried before the analytical and numerical analysis. Because the development of the analytical and numerical models will depend on the internal structure of the composite. Therefore, the composite should be fabricated to analyse its internal structure. The following steps are described the composite fabrication process. Also, the same fabrication method is used to analyse the $K_{eff}$ of composite using the experimental method.

Uniaxially oriented fibers give an even fiber distribution. Hence it is important to select a fiber length by avoiding the curliness of the fiber. Therefore, fibers were cut into 5 cm length, the fiber layer was a layup, and latex was sprayed on that layer. This procedure was continued until getting the desired volume fraction of fiber and latex. The fiber and latex combination was then compressed to get the designed thickness (1 cm) of the composite [25]. Figure 6.1 shows a cross-section of a composite was observed using an optical microscope.

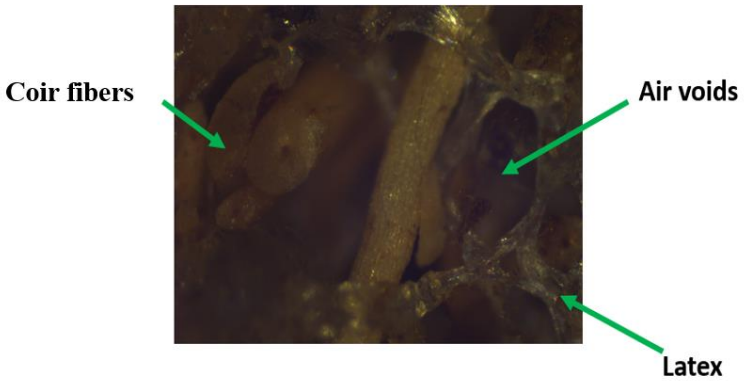


Figure 6. 1: A cross sectional view of the composite (×100)

According to Figure 6.1, the fabricated composite contains a solid-solid phase and a solid-gas phase. Therefore, the first step was to analytically and numerically evaluate the conductivity of a mixture of fiber and latex. Then the $K_{eff}$ of the composite was analytically, numerically, and experimentally evaluated with the conductivity value of the mixture (latex + fiber) and air voids.

#### 6.2.1.2 Analytical methods to find the thermal conductivity of a solid-solid phase

The thermal conductivity of the solid-solid phase was calculated from Maxwell's model, Rayleigh's model, and Lewis Nielsen's model. However, the transverse thermal conductivity was analysed from these models because the transverse orientation of fibers gives the maximum insulation properties. The equations for analysis of transverse thermal conductivity using Maxwell's model, Rayleigh's model, and Lewis Nielsen's model are given in chapter 4. Here the thermal conductivity value is 0.3058 W/mK for coir fibers and 0.1736 W/mK for compounded latex.

#### 6.2.1.3 Development of a unit cell for numerical analysis

The numerical method was used to validate the results obtained from the analytical models. Ansys software package was employed for the numerical analysis in this study, considering the following assumptions: The continuous and the discontinuous phases are microscopically homogeneously distributed, have a negligible thermal resistance between the two phases, and discontinues phase has the same size and shape

[41,43,44,45]. According to Figure 6.1, the fabricated composite contains a solid-solid phase and a solid-gas phase. Therefore, the first step was to numerically evaluate the conductivity of a mixture of fiber and latex.

#### 6.2.1.4 Development of a unit cell for the solid-solid phase

The solid-solid phase contains fibers and latex. Therefore, it can be assumed as a two-phase composite. Latex can be taken as the matrix material. According to Figure 6.1, fibers are randomly distributed throughout the matrix. However, fiber and matrix combinations can be simplified as an isolated unit cell with a periodical arrangement of three-dimensional physical models which contain cylindrical fibers in latex cubes [41,43]. The periodic arrangement of unit cells in a composite could be identified as a hexagonal array pattern and square array pattern [44,47,50]. Further, reducing the computational time and complexity of the geometry is essential. Hence, the hexagonal unit cell and the square unit cell can be simplified as a quarter unit cell, as shown in Figure 6.2 [44].

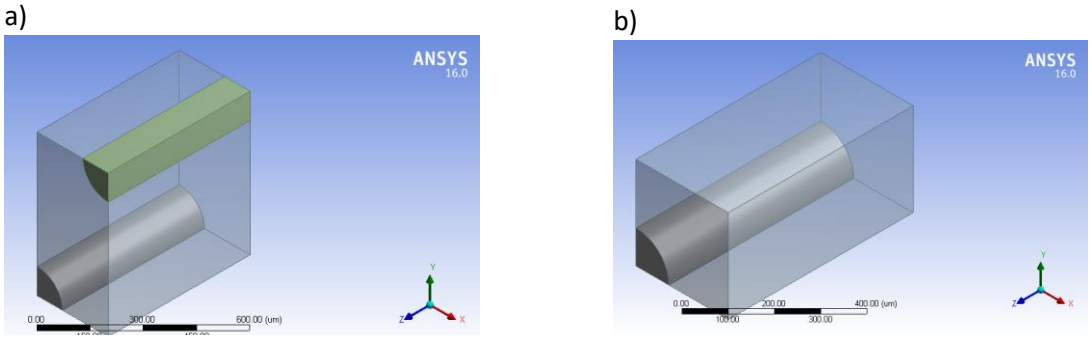


Figure 6.2: A quarter unit cell of a) Hexagonal array b) Square array

Z-axis represents the fiber direction in Figure 6.2, and Y-axis and X-axis represent the perpendicular plane for the fiber. The fiber diameter was 200.16 µm when measured using the primo star iLED microscope, and the unit cell dimensions were calculated corresponding to the volume fraction of fiber to latex.

#### 6.2.1.5 Boundary conditions for unit cell.

The heat load was applied as a temperature in both opposite faces in the XZ plane. A temperature of 30 °C was maintained on the top face in the XZ plane, and 25 °C was applied to the bottom face in the XZ plane. Other faces are parallel to the Y direction,

and those are assumed to be adiabatic [45,46,52]. The heat distribution and the thermal conductivity of the unit cell were analysed using Fourier's law.

### 6.2.2 Discussion

Figure 6.3 illustrates the temperature distribution of the hexagonal model and square model for solid-solid phase at 0.1 fiber volume fraction.

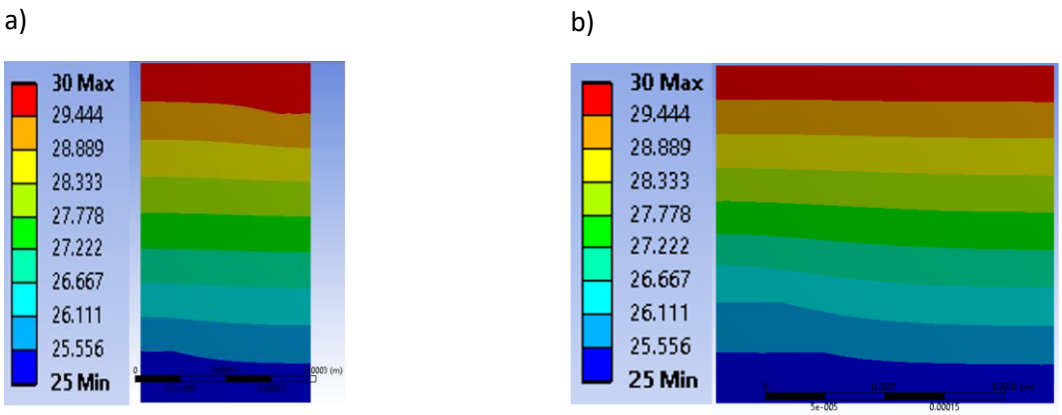


Figure 6.3: The temperature distribution in the quarter unit cell a) Hexagonal array b) Square array

The temperature distribution is uneven in the top and bottom regions of Figure 6.3a) due to the presence of fibers. But it will show a uniform distribution in the middle region of the quarter unit cell. Also, the temperature distribution is uniform in the upper region of Figure 6.3b). However, it shows an uneven distribution around the bottom region of the quarter unit cell due to the presence of fiber.

Figure 6.4 compares $K_{eff}$ of solid-solid phase using analytical methods and numerical methods.

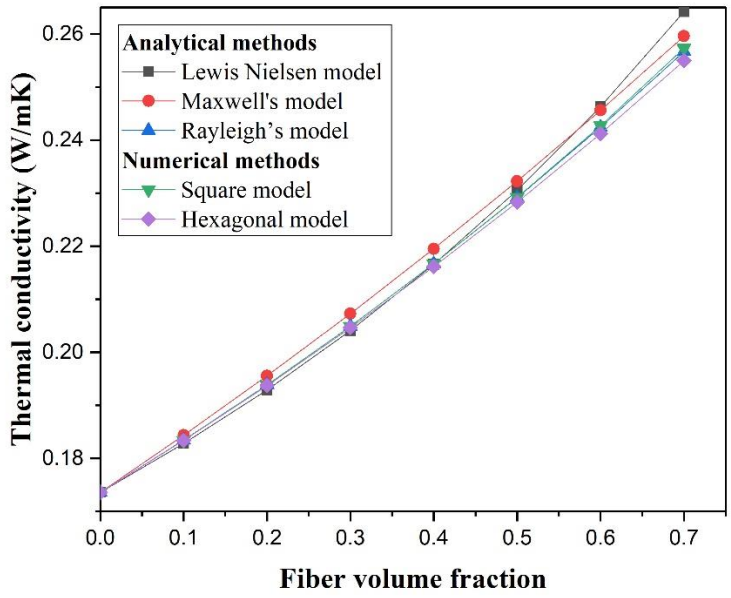


Figure 6.4: Thermal conductivity of the solid-solid phase using analytical, and numerical methods.

The maximum fiber volume fraction of the square unit cell is 0.78. Therefore, the above analysis was made up to the fiber volume fraction of 0.7. However, the $K_{eff}$ of the solid-solid phase is increased with the fiber volume fraction. Except for Maxwell's model, numerical models and analytical models show minor deviations with each other up to 0.4. Maxwell's model is the first analytical model to predict $K_{eff,}$ and the main assumption in the model is well dispersed spherical particles in the continuous matrix. It may give a higher deviation for the results. Also, Sahu analysed the thermal conductivity of short fiber reinforced composite using analytical models. Maxwell's model shows a higher deviation from the experimental results [41]. Lewis Nielsen's model was the most popular model to predict $K_{eff}$ in literature due to good correlation with the experiments [43,47]. However, the Lewis Nielsen model was created up to 0.4 volume fraction, and it gives inconsistent results for the higher volume fractions [53]. Nevertheless, Lewis Nielsen's model is a good analytical model to predict $K_{eff}$ in the composite containing random fiber distribution [43,47]. Therefore, the values obtained from Lewis Nielsen's model are used for further analytical analysis in the solid-gas phase.

Moreover, the main assumption in Rayleigh's model is parallel cylinders embedded in a continuous matrix [53]. It may cause a closer relationship between the square model and Rayleigh's model throughout the variation of the fiber volume fraction. Therefore, this relationship is important to justify the results obtained from the square model. Also, the square model is close to other analytical models than the hexagonal model. Then, the values obtained from the square model are used to further numerical analysis in the solid-gas phase. According to the limitation of the Lewis Nielsen model, the maximum fiber volume fraction is assumed to be 0.4 for further analysis. Therefore, the $K_{eff}$ value in the solid-solid phase is 0.2166 W/mK for the analytical analysis and 0.2167 W/mK for numerical analysis at the 0.4 fiber volume fraction. Also, maximum fiber volume fraction of 0.4 will be taken for the experimental analysis of the composite.

## 6.3 Evaluation of the $K_{eff}$ of solid-gas phase

### 6.3.1 Methodology

#### 6.3.1.1 Analytical methods to find the thermal conductivity of the solid-gas phase

Landaure's equation and Hashin-Shtrikman's upper bond model are used to find the thermal conductivity of the solid gas phase.

Hashin-Shtrikman's upper bond model is given by Equation 6.1.

$$K_{eff} = K_f \left[1 - \frac{3(1 - V_p)(K_p - K_m)}{3K_p - V_p(K_p - K_m)}\right] \quad (6.1)$$

Where $K_p$ is the thermal conductivity of air, and $V_p$ is the volume fraction of air.

#### 6.3.1.2 Numerical method to find the thermal conductivity of solid-gas phase.

***Development of a unit cell for the solid-gas phase***

According to Figure 6.1, the composite contains a solid-gas phase. However, the pore size changed with the volume fraction of the composite [58]. Smith studied the thermal conductivity of porous materials. Here, the low pore density shows a close pore structure, and the high pore density shows the open pore structure [58]. Russell represented cubic model structures to analyse the thermal conductivity of a pores structure [59]. In this study, pores are represented by cubes and surrounded by the uniform thickness of solid walls for the close pores structure. Also, solids are

represented by cubes in the open pores structure, and it is surrounded by the uniform thickness layer of air [59].

Further, if the volume ratio of dispersion media is higher than 0.786, then cubic structures should represent the structure [44]. Therefore, cubical structures are selected to analyse the thermal conductivity of the solid-gas phase. However, the thermal conductivity of the close pore structure and the open pore structure were separately analysed as Figure 6.5.

a) b)

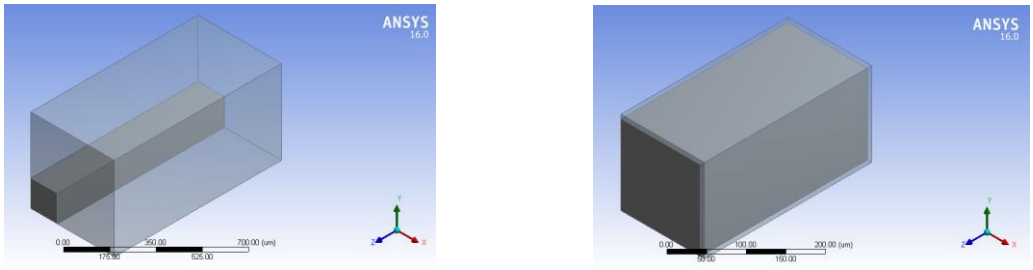


Figure 6.5: A quarter unit cell of a) close pores structure b) open pores structure

As explained in numerical analysis in solid-solid phase, a quarter unit cell was used for the numerical analysis. The air region is represented by the middle cube in 6.5(a), and it is surrounded by solid due to close porosity; the solid region is represented by the middle cube in 6.5(b), and it is surrounded by air due to the open porosity. The thermal conductivity values of the solid region were taken by the solution of numerical analysis in the solid-solid phase for the respective volume fractions of latex and fiber of the composite. The conductivity value of air was taken as 0.0258 W/mK at 30 °C by assuming negligible radiation and convection heat transfer [58,59,60,61]. Also, the boundary conditions are applied as numerical analysis described in section 6.2.1.5.

**6.3.1.3 Experimental method to find the thermal conductivity of solid-gas phase.**

The sample preparation of the composite follows as the methodology given by 6.2.1.1. Also, the composition of fiber, latex and air is given in Table 6.1.

Table 6.1: Composition of the fabricated insulation material

| Volume fraction of fiber : latex | Volume fraction of Void : solid | Weight of the fiber (g) | Volume of the latex (ml) |
|---|---|---|---|
| 0.4 | 0.1 | 207 | 458.48 |
| 0.4 | 0.2 | 184 | 407.54 |
| 0.4 | 0.3 | 161 | 356.60 |
| 0.4 | 0.4 | 138 | 305.65 |
| 0.4 | 0.5 | 115 | 254.71 |
| 0.4 | 0.6 | 92 | 203.77 |
| 0.4 | 0.7 | 69 | 152.83 |

Here, practically the designed thickness (1 cm) of the composite can be obtained up to 0.7 of the void to solid ratio. Therefore, the fabrication is limited to the point of 0.7 of void: solid volume fraction.

The $K_{eff}$ of the insulation material was measured using the hot wire disk method, as shown in Figure 6.6.

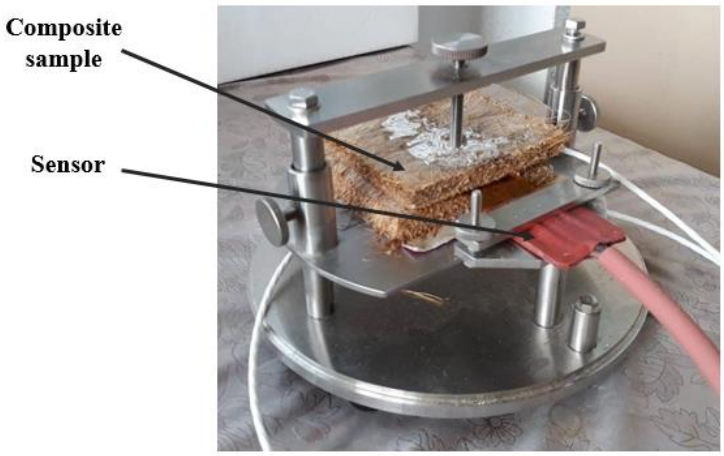


Figure 6.6: Measuring the $K_{eff}$ of the insulation material

### 6.3.2 Discussion

Figure 6.7 presents the temperature distribution of close pores structure and open pores for the solid-gas phase at 0.1 air volume fraction.

a) b)

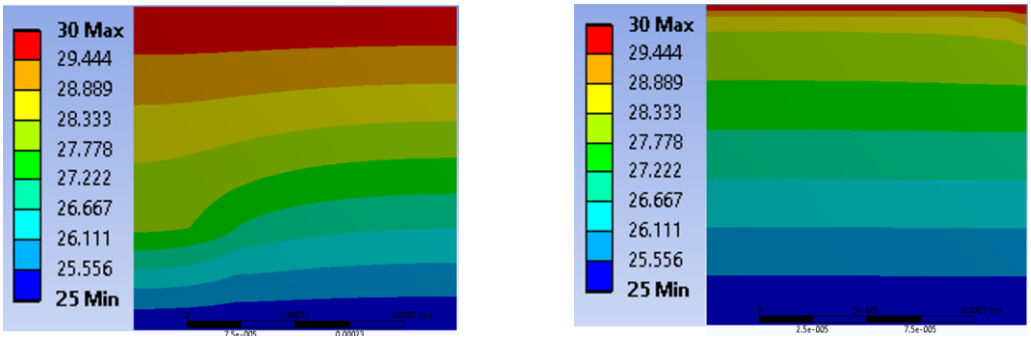


Figure 6.7: The temperature distribution in the quarter unit cell a) close pores structure b) open pores structure.

The temperature distribution is uneven throughout the unit cell in Figure 6.7a). However, Figure 6.7b) shows a negligible uneven distribution at the top end corner of the unit cell. Because the surrounded cubic structure has a negligible thickness compared to the middle cube in the open pores structure.

The numerically obtained results are compared with analytical results in Figure 6.8.

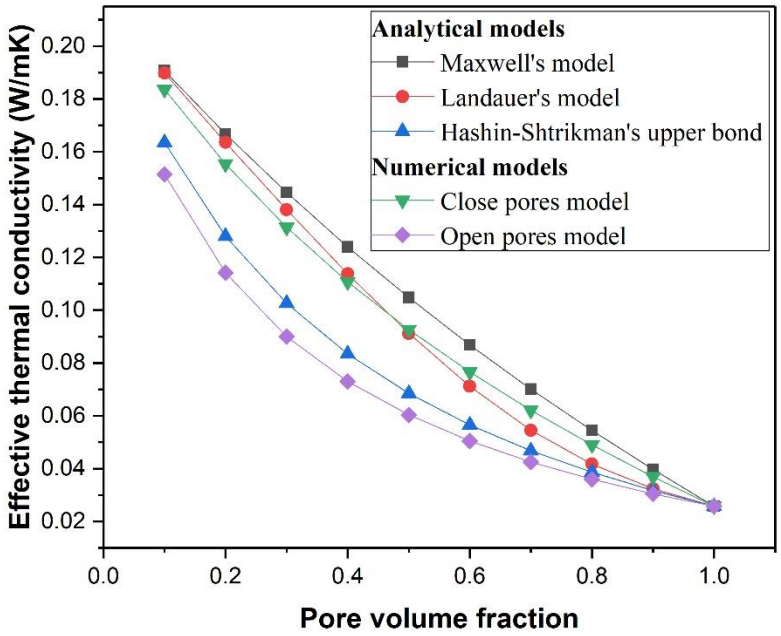


Figure 6.8: The $K_{eff}$ of the insulation using analytical, and numerical methods

The $K_{eff}$ of the insulation material (solid-gas phase) is reduced with the increase of pore (air) volume fraction ($V_p$). However, the results obtained from different models show some variation with each other. The reason is that the models were developed by considering the various types of assumptions such as distribution of discontinuous phase throughout the matrix, size, and shape of the discontinuous phase, bonding between the phases, and the thermal conductivity of constituents. According to Smith's work [58], Maxwell's model has a close porosity for the pore volume fraction less than 0.15. Also, Figure 4.9 within the range $0 < V_p < 0.15$ of Maxwell's model shows a closer relationship with the numerical results in close pores structure [58]. Smith's work shows that the experiment results are closer to the results of Landauer's model [58]. He found that if the $V_p$ is between 0.15 and 0.65, $K_{eff}$ follows Landauer's model.

In our work, the numerical results in close pore structure are closer to Landauer's model. Further, according to Smith's work, experimental results have a closer relationship with Hashin-Shtrikman's upper bond with the high pore fraction above the $V_p > 0.65$. However, the open pore structure shows a closer relationship with Hashin-Shtrikman's upper bond models for the $V_p > 0.65$. Therefore, these results

conclude that the $K_{eff}$ of a pores structure can be analysed through the numerical method. However, the numerical model structure varies with the pore volume fraction.

The accuracy of analytical and numerical results was compared with the experimental results. Figure 6.9 shows the $K_{eff}$ values of fabricated insulation material with different pore volume fractions.

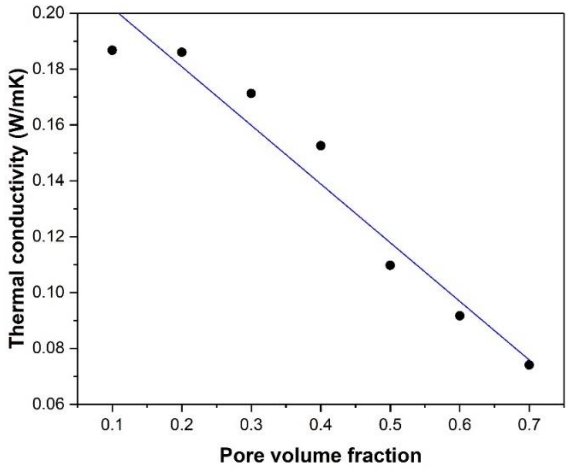


Figure 6.9: Thermal conductivity of the fabricated insulation material

The $K_{eff}$ of the insulation material was reduced with the pore volume fraction. It confirmed that the thermal conductivity of the composite could be reduced by introducing air voids into the solid-solid phase material. Figure 6.10 illustrates the comparison of the regression line of the experimental results with analytical and numerical values.

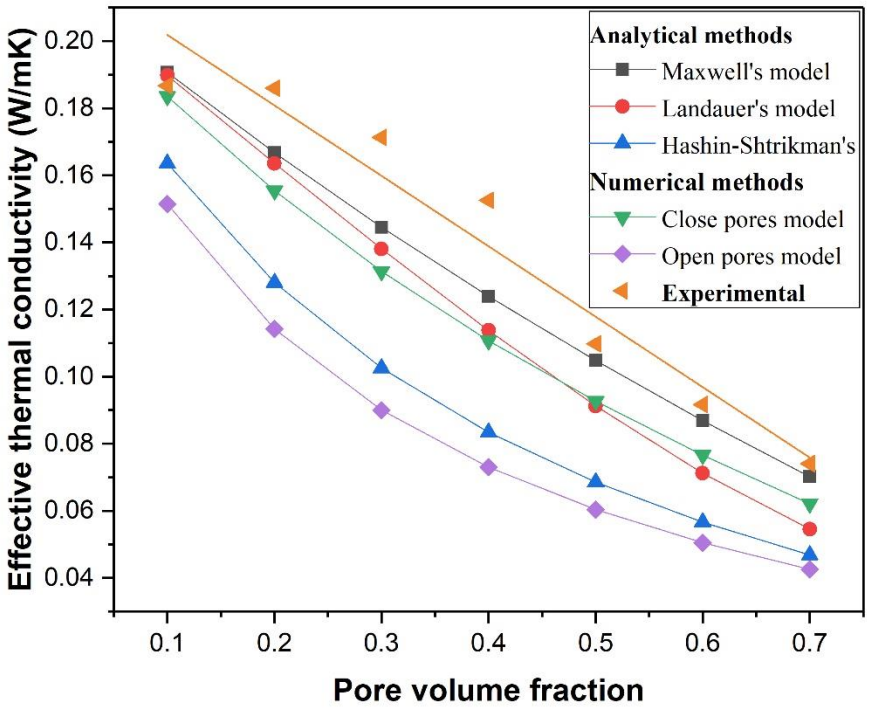


Figure 6.10: Thermal conductivity of the insulation material using analytical, numerical, and experimental methods

The experimental values are slightly higher than those obtained from analytical and numerical models. It may be due to some assumptions considered during the development of analytical models, such as fibers being distributed in the matrix as a regular periodical array. However, fibers are randomly distributed throughout the matrix, and these random fibers can touch each other. Some fibers can also be oriented in the longitudinal direction due to randomness that causes error percentage in the thermal conductivity in experimental and analytical models. This phenomenon can be confirmed by the cross-section view of the composite in Figure 6.1. The moisture content of the composite increases the thermal conductivity. Table 6.2 shows the moisture content of the fabricated composite samples.

Table 6.2: Moisture content of the fabricated composite

| **Pore volume fraction** | 0.1 | 0.2 | 0.3 | 0.4 | 0.5 | 0.6 | 0.7 |
|---|---|---|---|---|---|---|---|
| **Moisture content (%)** | 7.09 | 7.62 | 6.71 | 7.33 | 6.79 | 5.78 | 6.22 |

According to Figure 6.9, the experiment results are closer to Maxwell's model than the other analytical model; in the numerical model, it is closer to the close pores structure. It concluded that the fabricated materials show close pore behaviour in thermal conductivity analysis. However, considering the above factors, the analytical and numerical models used for the close pore structure agree well with the experimental results.

Comparing the $K_{eff}$ of the composite using market-available insulation materials is important. Therefore, Mcfoil and a glass wool sheet were selected to measure $K_{eff}$ using a hot wire disk. Mcfoil is the product name given by Macbertan Private Ltd. Mcfoil is produced from polystyrene, and glass wool sheet is produced from glass wool and thermoset resin. The thermal conductivity of Mcfoil is 0.0446/mK, and the thermal conductivity of glass wool sheets is 0.0475 W/mK. The minimum value obtained from the developed insulation material is 0.0741 W/mK at 0.7 pore volume fraction. However, according to the analytical and numerical model in Figure 6.4, the thermal conductivity of the solid-solid phase increases with the coir fibers. Hence, 0.4 fiber: latex ratio was selected for this experimental analysis. Further, the $K_{eff}$ of the insulation composite can be reduced by lowering the volume ratio of coir fibers, according to Figure 6.4. Therefore, the authors recommended analysing the $K_{eff}$ of the insulation material by decreasing the coir fiber content in future studies.

## 6.4 Conclusion

This study presents a system to find the effective thermal conductivity of a three-phase composite by analytical, numerical, and experimental methods. The process primarily focused on analytical and numerical methods. Here, the composite contains latex, fiber, and air voids.

Evaluating the $K_{eff}$ follows two steps. The first step is calculating conductivity for a mixture (solid-solid phase) that contains the matrix (latex) and one disperse phase (fiber). Next, the total conductivity of the composite can be calculated with the conductivity value of the mixture and the second disperse phase (air). The $K_{eff}$ latex and fiber were evaluated using analytical and numerical methods, and the square array pattern and hexagonal array pattern were employed for the numerical analysis. The results obtained from the square array pattern are used for further numerical analysis due to the closeness with the analytical models than the hexagonal array pattern.

Numerical analysis was performed with the close pore structure model and open pore structure model for the solid-gas phase. These results were compared with the available analytical models. The findings concluded that the experimental analysis has a relationship with the close pores structure. However, experimental results show a slight variation with analytical and numerical results due to the fiber orientation and the moisture content. Nevertheless, numerical and analytical results are useful methods to find $K_{eff}$ of the composite before the experimental methods. Also, the $K_{eff}$ of the developed insulation material is slightly higher than the thermal conductivity of market available materials. However, it could be lowered by reducing fiber volume fraction in the composite material by analysing the numerical and analytical results in the solid-solid phase.

According to Chapter 6, the $K_{eff}$ of the composite can be evaluated using analytical and numerical methods. Here, analytical models are useful to justify the accuracy of the numerical models, but no specific equation is available to find the $K_{eff}$ of the composite. Therefore, Chapter 7 will discuss the development of a mathematical model to predict the $K_{eff}$ of the composite. The development of the mathematical model is based on the models used for numerical analysis in Chapter 6.

# CHAPTER 7

# DEVELOPMENT OF A MATHEMATICAL MODEL TO PREDICT THE THERMAL CONDUCTIVITY OF THE COMPOSITE.

## 7.1 Development of a mathematical model for solid-solid phase.

According to Chapter 6, the internal structure of the composite can be identified as the solid-solid phase and the solid-gas phase. Therefore, models should be separately developed for the solid-solid phase and solid-gas phase. The first step is developing a model for the solid-solid phase. Here, the square unit cell is used to develop the model for the solid-solid phase according to the results of the numerical analysis in chapter 6 [43,47], and also considering the following assumptions: Fibers and the latex phases are microscopically homogeneously distributed, have a negligible thermal resistance between the fiber and latex, and fibers have the same size and shape [43,47]. Figure 7.1 demonstrates the 3D view of the square unit cell for the solid-solid phase.

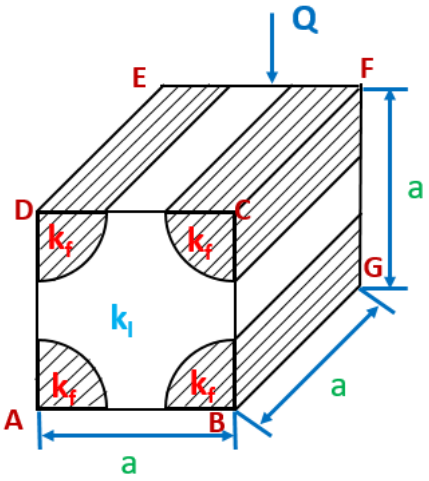


Figure 7.1: The three-dimensional view of a square unit cell for the solid-solid phase

Where Q is the total heat flux, and the heat flow direction is assumed to be top face to bottom face. The thermal conductivity of solid-solid phase, latex, and fiber are given by $k_s$, $k_l$, and $k_f$, respectively. The length of the unit cell is represented by 'a'. Further, the unit cell can be simplified as a quarter unit cell in Figure 7.2.

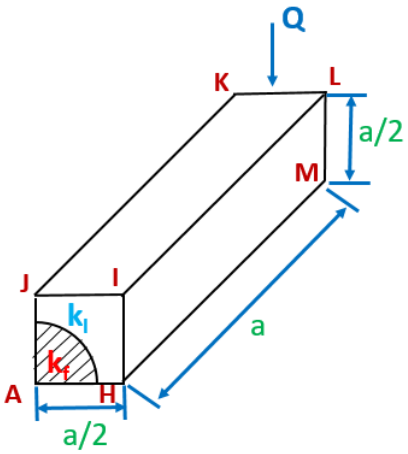


Figure 7.2: The three-dimensional view of a quarter unit cell for the solid-solid phase

**Modelling**

Heat transfer in the quarter unit cell occurred with the combination of series models. The series models in the quarter unit cell should be identified as per Figure 7.3.

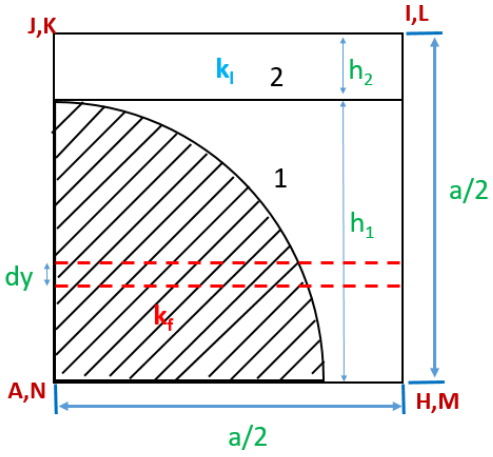


Figure 7. 3: The series models in the quarter unit cell

The above quarter unit cell is divided into two parts. Then the thermal resistance of the element can be calculated by the combination of the resistance of each part. The $K_{eff}$ of the element was calculated using the equal law of specific thermal conductivity.

Part 1 contains latex and fiber (matrix and fiber), and part 2 contains latex. Part 1 and part 2 have the mean conductivity coefficient of $k_1$ and $k_2$, respectively. Also, part 1 has the thickness of $h_1$, which is equal to the radius of the fiber r, and part 2 has the thickness of $h_2$.

**Thermal resistance for part 1**

Part 1 contains the fiber and matrix. Hence the $K_{eff}$ of part 1 is given by the combined effect of the fiber and matrix. Then apply the Fourier's law of heat conduction for the thin piece with the thickness of dy as indicated in Figure 7.3. The thermal conductivity of ($k_1$) of part 1 is given by equation 7.1.

$$k_1 = \frac{Q_l + Q_f}{\left(\frac{dT}{dy}\right)A} = \frac{k_l A_l}{A} + \frac{k_f A_f}{A} \tag{7.1}$$

$A_l$, $A_f$, and A are the cross-section area of matrix, fiber, and part 1, while $Q_l$ and $Q_f$ are the heat flows across the cross-section area of the matrix and fiber, respectively. The temperature difference between the two sides of the thin piece is denoted by dT. Then the thermal conductivity of part 1 can be calculated by integrating equation 7.2 over the complete thickness of part 1.

$$k_1 = \int_0^{h_1} \frac{\left(\frac{k_l A_l}{A} + \frac{k_f A_f}{A}\right) dy}{h_1} \tag{7.2}$$

$$k_1 = \frac{1}{h_1 A}\left(k_l V_l + k_f V_f\right) \tag{7.3}$$

Where, $V_l$ and $V_f$ are the volume of matrix and fiber respectively in part 1.

**Thermal resistance for part 2**

There are no fibers in part 2. Therefore, the value of the matrix material gives the thermal conductivity of part 2.

$$k_2 = \int_0^{h_2} k_l \frac{dy}{h_2} = k_l \tag{7.4}$$

The $K_{eff}$ of the quarter unit cell ($k_s$) is given by the combination of the thermal conductivity of part 1 and part 2, and equation 7.5 provides $k_s$.

$$k_s = \frac{a/2}{RA} = \frac{a/2}{(R_1+R_2)A} \tag{7.5}$$

R, $R_1$, and $R_2$ are the thermal resistance of the quarter unit cell, part 1, and part 2, respectively.

$$R_1 = \frac{h_1}{\frac{1}{h_1 A}(k_l V_l + k_f V_f)A} = \frac{h_1^2}{k_l V_l + k_f V_f} \tag{7.6}$$

$$R_2 = \frac{h_2}{k_l A} \tag{7.7}$$

Substituting equation 7.6 and equation 7.7 into equation 7.5, the $K_{eff}$ of the solid-solid phase is given by equation 7.8.

$$k_s = \frac{1}{\left(\frac{1}{k_l} - \frac{2}{k_l\left(\frac{\pi}{\varphi_f}\right)^{\frac{1}{2}}} + \frac{4}{\pi\left(k_l\left(2\left(\frac{1}{\pi\varphi_f}\right)^{\frac{1}{2}} - 1\right) + k_f\right)}\right)} \tag{7.8}$$

Where $\varphi_f$ is the volume fraction of fiber in the solid-solid phase.

### 7.2 Development of a mathematical model for solid-gas phase.

According to numerical analysis in Chapter 6, close pores structure shows better agreement with the pore volume fraction range up to 0.65. Therefore, the close pores structure is selected for developing the mathematical model. Here, cubes represent pores and are surrounded by the uniform thickness of solid walls for the close pores structure. Figure 7.4 presents the close pores structure for the modelling.

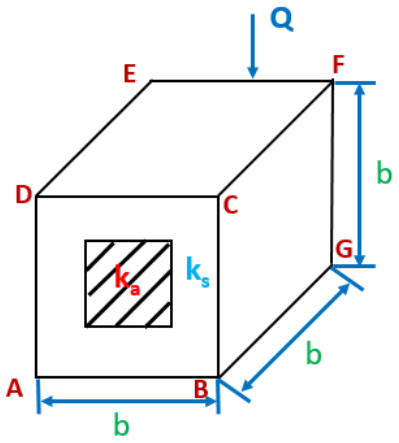


Figure 7.4: The three dimensional view of the close pores structure for solid-gas phase

Where Q is the total heat flux, and the heat flow direction is assumed to be top face to bottom face. The thermal conductivity of the solid-gas phase, solid-solid phase, and the air is given by $k_T$, $k_s$, and $k_a$, respectively. The length of the unit cell is represented by 'b'. The unit cell can be simplified as a quarter unit cell as in Figure 7.5.

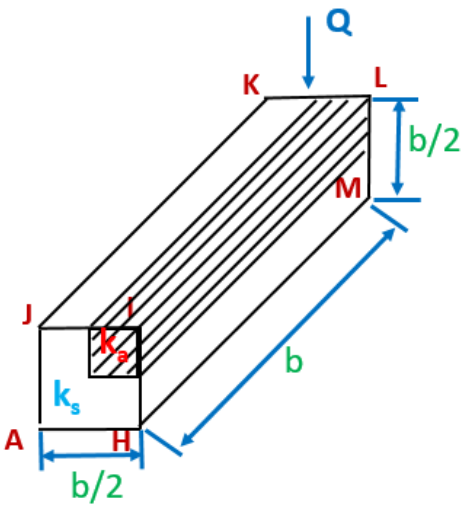


Figure 7.5: The three dimensional view of quarter structure for solid-gas phase

**Modelling**

The heat transfer in the quarter unit cell occurs with the combination of series models. The series models in the quarter unit cell can be identified in Figure 7.6.

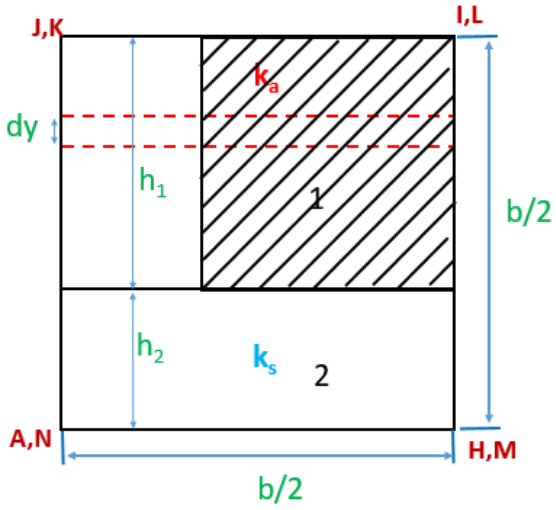


Figure 7.6: The series models in the quarter unit cell for solid-gas phase

The above quarter unit cell is divided into two parts. Then the thermal resistance of the element can be calculated by the combination of the resistance of each part. After that, the equal law of specific thermal conductivity can find the $K_{eff}$ of the element.

Part 1 contains the solid-solid phase and air void, and part 2 contains the solid-solid phase. Part 1 and part 2 have the mean conductivity coefficient of $k_3$ and $k_4$, respectively. Also, part 1 has the thickness of $h_1$, and part 2 has the thickness of $h_2$.

**Thermal resistance for part 1**

Part 1 contains the solid-solid phase and air void. Hence, the $K_{eff}$ of part 1 is given by the combined effect of the solid-solid phase and air void. Then apply the Fourier's law of heat conduction for the thin piece with the thickness of dy. The thermal conductivity of ($k_3$) of part 1 is given by equation 7.9.

$$k_3 = \frac{Q_s + Q_a}{\left(\frac{dT}{dy}\right)B} = \frac{k_s A_s}{B} + \frac{k_a A_a}{B} \tag{7.9}$$

Where, $A_s$, $A_a$, and B are the cross-section area of the solid-solid phase, air void, and part 1. $Q_s$, and $Q_a$ are the heat flows across the cross-section area of the solid-solid phase and air void, respectively. The temperature difference between the two sides of the thin piece is given by dT. Then the thermal conductivity of part 1 can be calculated by integrating equation 7.10 over the complete thickness of part 1.

$$k_3 = \int_0^{h_1} \frac{\left(\frac{k_s A_s}{B} + \frac{k_a A_a}{B}\right) dy}{h_1} \tag{7.10}$$

$$k_3 = \frac{1}{h_1 B}(k_s V_s + k_a V_a) \tag{7.11}$$

Where $V_s$ and $V_a$ are the volumes of the solid-solid phase and air void, respectively, in part 1.

There is no air void in part 2. Therefore, the value of the solid-solid phase gives the thermal conductivity of part 2.

$$k_4 = \int_0^{h_2} k_s \frac{dy}{h_2} = k_s \tag{7.12}$$

Then the $K_{eff}$ of the quarter unit cell ( $k_T$ ) is given by the combination of the thermal conductivity of part 1 and part 2. Equation 7.13 gives the $k_T$.

$$k_T = \frac{b/2}{R_T B} = \frac{b/2}{(R_3+R_4)B} \tag{7.13}$$

Where $R_T$, $R_3$, and $R_4$ are the thermal resistance of the quarter unit cell, part 1, and part 2, respectively.

$$R_3 = \frac{h_1}{\frac{1}{h_1 B}(k_s V_s + k_a V_a)B} = \frac{h_1^2}{k_s V_s + k_a V_a} \tag{7.14}$$

$$R_4 = \frac{h_2}{k_s B} \tag{7.15}$$

By substituting equation 7.14 and equation 7.15 into equation 7.13, the $K_{eff}$ of the solid-gas phase is given by equation 7.16.

$$k_{eff} = \frac{1}{\left(\frac{1}{k_s} - \frac{1}{k_s\left(\frac{1}{\varphi_a}\right)^{\frac{1}{2}}} + \frac{1}{k_s\left(\left(\frac{1}{\varphi_a}\right)^{\frac{1}{2}} - 1\right) + k_a}\right)} \tag{7.16}$$

$\varphi_a$ is the volume fraction of air in the solid-gas phase.

### 7.3 Discussion

Figure 7.7 compares the developed model with analytical and numerical models in the solid-solid phase.

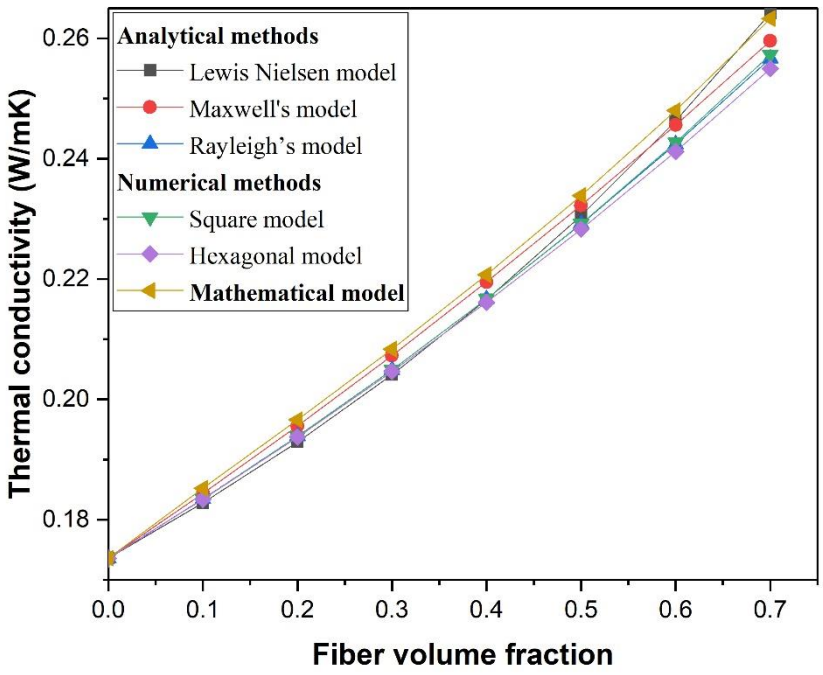


Figure 7. 7: Comparison of the thermal conductivity in the solid-solid phase using mathematical model, analytical, and numerical models

The proposed model deviates from analytical and numerical models at the lower fiber load. However, it shows a closer relationship with the Maxwell model. Further, the model is getting closer to the Lewis Nielsen model at the high fiber load.

The comparison of the developed model with analytical, numerical, and experimental methods in the solid-gas phase up to 0.7 pore volume fraction is given in Figure 7.8. The $K_{eff}$ value in the solid-solid phase is 0.2166 W/mK for the analytical analysis and 0.2167 W/mK for numerical analysis at 0.4 fiber volume fraction, according to Section 4.3. Therefore, the $K_{eff}$ value in the solid-solid phase of 0.2207 W/mK is obtained from

the proposed mathematical model at the 0.4 fiber volume fraction. Therefore, the value of 0.2207 will be used for the comparison in Figure 7.8.

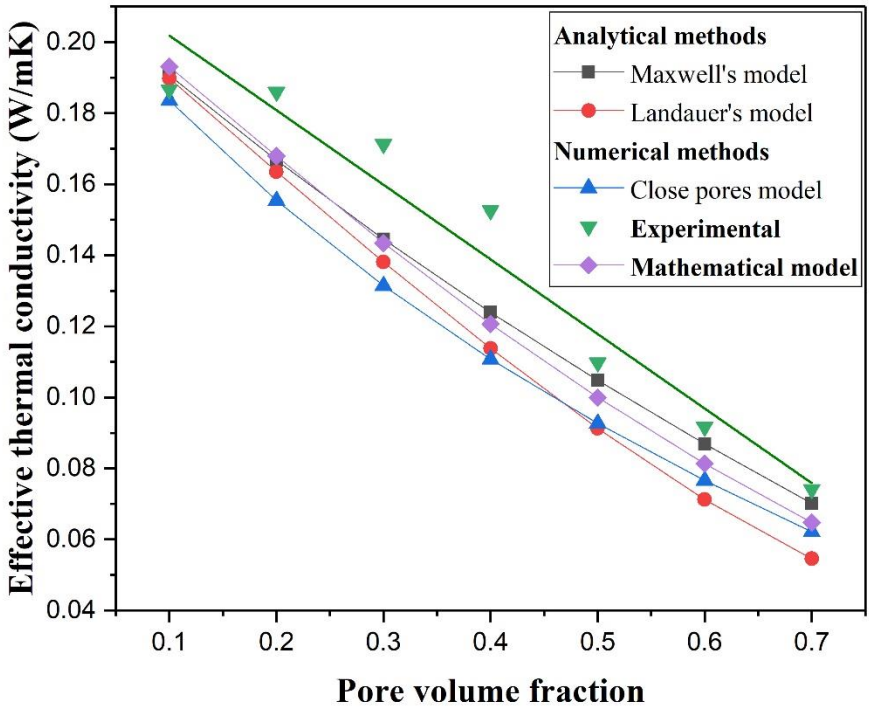


Figure 7. 8: The comparison of the $K_{eff}$ of the insulation material using mathematical model, analytical, numerical, and experiment methods in solid-gas phase

The proposed model shows a better agreement with the Lewis Nielsen model and Maxwell model below the 0.25 pore volume fraction than numerical results. Also, it is closer to the regression line of the experimental results than the Maxwell model below 0.25 pore volume fraction. The deviation between the numerical and the proposed models decreases with the pore volume fraction. However, considering the above results, the proposed model has a closer agreement with the experimental results below 0.25 pore volume fraction, and Maxwell's model agrees more with the experimental results.

The value of 0.2166 W/mK in the solid-solid phase was substituted to Maxwell's model to find the $K_{eff}$ of the solid-gas phase (whole material). The value of 0.2166

W/mK is obtained from Lewis Nielsen's model. Therefore, the analytical values in Figure 7.8 combine two different models. Nevertheless, the proposed mathematical model is developed to find $K_{eff}$ in the solid-solid phase and $K_{eff}$ in the solid-gas phase. Therefore, the model is unique for this application and agrees better with the experimental methods than numerical and analytical methods. This can be used for further analysis in this research area.

## 7.4 Conclusion

A mathematical model was suggested to find the $K_{eff}$ of a three-phase composite based on the numerical analysis in Chapter 6. The proposed model agrees better with the experimental results. Also, the model is used to analyse $K_{eff}$ of solid-solid and solid-gas phases without considering other analytical models. Therefore, it can analyse $K_{eff}$ of fibrous-type insulation materials which contain air voids.

# CHAPTER 8

# CONCLUSIONS AND RECOMMENDATIONS

## 8.1 Conclusions

The conventional type materials are the most widely available materials for roof insulation. However, researchers are developing sustainable insulation materials with lignocellulose fibers due to the conventional materials' health and environmental issues. These natural fibers are found in agricultural wastes, grasses, and plant wastes such as sisal, jute, coir, pineapple leaf fiber, oil palm fibers, and hemp. According to the literature review, coir fibers exhibit significant properties over other fibers, such as low thermal conductivity, low density, high resistance to absorb moisture, higher elongation at the breaking point, and high thermal stability.

Coir fibers contain lignocellulose substances, oil, and wax on the surface of the natural condition. These substances can be removed from the fiber surface by alkaline treatment. However, the excess concentration of the alkaline treatment will damage the fiber surface. Hence, identifying appropriate concentrations is vital before the fabrication.

The appropriate concentration can be evaluated by SEM analysis, tensile properties of the fiber, FTIR analysis, and DSC analysis. According to this analysis, 4% alkaline concentration was identified as the appropriate concentration for the treatment. Also, the activation energy of 4% treated fiber could be determined by model-free methods, and it helps determine the fiber lifetime.

Binder material should be added to adhere to fiber without taking fiber alone. Further, air voids should be introduced into the fiber and binder combination to increase the insulation properties. The $K_{eff}$ of the insulation material can be analysed by analytical, numerical, and experimental methods, and knowing the thermal conductivity of each phase is necessary for analytical and numerical analysis.

However, finding the $K_T$ of the coir fiber is challenging. The two-phase composite was fabricated with coir fibers and epoxy with different volume fractions. Next, the thermal conductivity was measured for the fabricated composite and epoxy using the hot disk method. Finally, the $K_T$ of the fiber was calculated using available analytical models, and the determined value was 0.3058 W/mK. Also, the thermal conductivity of the compounded latex was selected as the binder material, and the value was 0.1736 W/mK. These values helped analyse the $K_{eff}$ of the insulation material by analytical and numerical methods.

The $K_{eff}$ of the insulation material was determined by analytical, numerical, and experimental methods. The microscope image analysis confirmed the fabricated samples have a close pore structure. Further, the behaviour of analytical and numerical models that are used to close pores structure is near to the experimental results. However, a slight difference was noted between the analytical and numerical models with the experimental results due to fiber orientation and moisture content. Still, the numerical and analytical methods were used throughout to find the $K_{eff}$ of the composite before the experimental methods.

There is no specific equation to find the $K_{eff}$ of the composite, which contains fibers and air voids. Therefore, a mathematical model was introduced to find the $K_{eff}$ of the composite. The proposed model shows better agreement with the experimental results. Finally, the behaviour of the $K_{eff}$ of the composite was identified with the variation of the volume fraction of each phase analytically, numerically, and experimentally. It concluded that the $K_{eff}$ of the composite increases with the fiber volume fraction and reduces with the volume fraction of the air voids.

### 8.2 Recommendations

The authors recommended analysing the $K_{eff}$ of the composite by considering moisture content. Then the whole structure will become a four-phase composite. Analysing the $K_{eff}$ of the four-phase composite using numerical and analytical methods is a new research area. Also, the authors recommend analysing the $K_{eff}$ for less fiber volume fraction. It can be fabricated further as a product with a combination of reflective and

mass insulators. Finally, measuring the insulation performance under the roof during the daytime is recommended.

# LIST OF PUBLICATIONS

## Conference proceedings

1. **L.G. Chamath**, L. K. T. Srimal, and G. A. Sewvandi, "Effect of alkaline concentration on the surface properties of coir fibers," National Engineering Research Symposium 2020, National Engineering Research and Development Centre of Sri Lanka, Ja-Ela , Sri Lanka, December 2020.

2. **L.G. Chamath,** L. K. T. Srimal, and G. A. Sewvandi, "Determination of transverse thermal conductivity of coir fibers by analytical methods," Proc. of IESL Young Members Section Technical Conference 2021, Institution of Engineers Sri Lanka (IESL), Colombo, Sri Lanka, October 2021.

3. D.G.G.V. Udayakumara, I.R. De Silva , **L.G. Chamath** , L.K.T. Srimal , R. Gallage, "Design and fabrication of a system in measure thermal conductivity of compressible materials," 19th Academic Sessions, University of Ruhuna, Sri Lanka, March 2022.

4. **L.G. Chamath**, L. K. T. Srimal, and G. A. Sewvandi, "Evaluating the thermal conductivity of three-phase insulation composite using analytical and numerical methods," Mercon 2022, University of Moratuwa, Sri Lanka, July 2022.

## Journal publications

1. **L. G. Chamath,** L. K. T. Srimal, and G. A. Sewvandi, "Assessment of transverse thermal conductivity of coir fibre using experimental, analytical and numerical methods," Journal of the National Science Foundation of Sri Lanka. (Accepted.)

# REFERENCES


[1] F. Asdrubali, F. D'Alessandro, and S. Schiavoni, "A review of unconventional sustainable building insulation materials," Sustainable Mater and Technology, vol. 4, no. 2015, pp. 1–17, 2015, doi: 10.1016/j.susmat.2015.05.002.

[2] L. Aditya, T. M. I.Mahlia, B. Rishmanchi, H. M. Ng, and H. B.Aditiya., "A review on insulation materials for energy conservation in buildings," Renewable and Sustainable Energy Reviews, vol. 73, no. June, pp. 1352–1365, 2017, doi: 10.1016/j.rser.2017.02.034.

[3] D. Kumar, M. Alam, P. X. W. Zou, J. G. Sanjayan, and R. A. Memon, "Comparative analysis of building insulation material properties and performance," Renewable and Sustainable Energy Reviews, vol. 131, no. March, p. 110038, 2020, doi: 10.1016/j.rser.2020.110038.

[4] A. R. Katili, R. Boukhanouf, and R. Wilson, "Space cooling in buildings in hot and humid climates—A review of the effect of humidity on the applicability of existing cooling techniques," in Proceedings of 14th International Conference on Sustainable Energy Technologies (SET), no. August, pp. 25–27, 2015, doi: 10.13140/RG.2.1.3011.5287.

[5] The importance of building science and the building enclosure, Sustainable to architectural designer, 2014 [online] Available: https://www.sustainable.to/news-recognition/2014/9/1/the-importance-of-building-science-and-the-building-envelope.

[6] D. A. Chwieduk, "Some aspects of energy efficient building envelope in high latitude countries," Solar Energy, vol. 133, pp. 194–206, 2016, doi: 10.1016/j.solener.2016.03.068.

[7] Thermal controls in building, Building Science Corparation, 2011 [online] Available: https://www.buildingscience.com/documents/digests/bsd-011-thermal-control-in-buildings.

[8] D. S. Mintorogo, W. K. Widigdo, and A. Juniwati, "Application of coconut fibers as outer eco-insulation to control solar heat radiation on horizontal concrete slab rooftop," Procedia Engineering, vol. 125, pp. 765–772, 2015, doi: 10.1016/j.proeng.2015.11.129.

[9] M. Casini, "Insulation materials for the building sector : a review and comparative analysis," Encyclopedia of Renewable and Sustainable Materials, Elsevier, 2019. doi:10.1016/B978-0-12-803581-8.10682-4 1.

[10] R. Gellert, "Natural fiber and fiber composite materials for insulation in buildings," Materials for Energy Efficiency and Thermal Comfort in Buildings, pp. 229–256, 2010, doi: 10.1533/9781845699277.2.229.

[11] Z. N. Azwa, B. F. Yousif, A. C. Manalo, and W. Karunasena, "A review on the degradability of polymeric composites based on natural fibers," Materials and

Design, vol. 47, pp. 424–442, 2013, doi: 10.1016/j.matdes.2012.11.025.

[12] G. Deshmukh, P. Birwal, R. Datir, and S. Patel, “Thermal insulation materials: a tool for energy conservation,” Journal of Food Processing & Technology,vol. 08, no. 04, 2017, doi: 10.4172/2157-7110.1000670.

[13] D. Bozsaky, “The historical development of thermal insulation materials,” Periodica Polytechnica Architecture, vol. 41, no. 2, p. 49, 2010, doi: 10.3311/pp.ar.2010-2.02.

[14] E. Velichko, E. Tskhovrebov, and A. Shevchenko, “Environmental safety providing during heat insulation works and using thermal insulation materials,” MATEC Web of Conferences, vol. 106, 2017, doi: 10.1051/matecconf/201710603009.

[15] S. K. Santhosh and S. S. Hiremath, "Natural fiber reinforced composites in the context of biodegradability: a review," Encyclopaedia of Renewable and Sustainable Materials, vol. 322, no. 1567. Elsevier, 2020, doi:10.1016/B978-0-12-803581-8.11418-3

[16] L. C. Hao, S. M. Sapuan, M. R. Hassan, and R. M. Sheltami,"Natural fiber reinforced vinyl polymer composites," Natural Fiber Reinforced Vinyl Ester and Vinyl Polymer Composites, Elsevier, 2018, doi: https://doi.org/10.1016/B978-0-08-102160-6.00002-0

[17] K. Manohar, “Experimental investigation of building thermal insulation from agricultural by-products,” British Journal of Applied Science & Technology, vol. 2, no. 3, pp. 227–239, 2012, doi: 10.9734/bjast/2012/1528.

[18] M. Volf, J. Diviš, and F. Havlík, “Thermal, moisture and biological behaviour of natural insulating materials,” Energy Procedia, vol. 78, pp. 1599–1604, 2015, doi: 10.1016/j.egypro.2015.11.219.

[19] I. Cetiner and A. D. Shea, “Wood waste as an alternative thermal insulation for buildings,” Energy and Buildings, vol. 168, pp. 374–384, 2018, doi: 10.1016/j.enbuild.2018.03.019.

[20] S. Sathishkumar, T.K. Naveen, A. Jeevarathinam, V. Karthik, and N.V.A Dhandapani, “Thermal conductivity of natural fiber reinforced plastics,” International Journal of Pure and Applied Mathematics, vol. 118, no. 20, pp. 43–51, 2018.

[21] H. Takagi, “Review of functional properties of natural fiber-reinforced polymer composites: thermal insulation, biodegradation and vibration damping properties,” Advanced Composite Materials, vol. 28, no. 5, pp. 525–543, 2019, doi: 10.1080/09243046.2019.1617093.

[22] K. Rashid, E. U. Haq, M. S. Kamran, N. Munir, A. Shahid, and I. Hanif, “Experimental and finite element analysis on thermal conductivity of burnt clay bricks reinforced with fibers,” Construction and Building Materials, vol. 221, pp. 190–199, Oct. 2019, doi: 10.1016/j.conbuildmat.2019.06.055.

[23] S. Tangjuank, “Thermal insulation and physical properties of particleboards from pineapple leaves,” International Journal of Physical Sciences, vol. 6, no. 19, pp. 4528–4532, 2011, doi: 10.5897/IJPS11.1057.

[24] S. Kumfu and T. Jintakosol, “Thermal insulation produced from pineapple leaf fiber and natural rubber latex,” Advanced Materials Research, vol. 506, pp. 453–456, 2012, doi: 10.4028/www.scientific.net/AMR.506.453.

[25] L. K. T Srimal and S. Baduge, “Value addition for coir fiber as low temperature insulation material,” 12th Academic Sessions, University of Ruhunana, Matara, Sri Lanka, March, 2015, doi: 10.13140/RG.2.2.25891.32808.

[26] Y. M. Yuhazri1, H. Sihombing, A. R. Jeefferie, A. Z. A. Mujahid, A. G. Balamurugan, M. N. Norazman, and A. Shohaimi, “Optimization of coconut fibers toward heat insulator applications,” Global Engineers & Technologists Review, vol. 1, no. 1, pp. 35–40, 2011.

[27] S. R. D. Petroudy," Physical and mechanical properties of natural fibers," Advanced High Strength Natural Fiber Composites in Construction, Elsevier ,pp. 59-83, 2017. doi: http://dx.doi.org/10.1016/B978-0-08-100411-1.00003-0

[28] A. G. Adeniyi, D. V. Onifade, J. O. Ighalo, and A. S. Adeoye, “A review of coir fiber reinforced polymer composites,” Composites Part B: Engineering, vol. 176, no. August, p. 107305, 2019, doi: 10.1016/j.compositesb.2019.107305.

[29] S. K. Ramamoorthy, M. Skrifvars, and A. Persson, “A review of natural fibers used in biocomposites: Plant, animal and regenerated cellulose fibers,” Polymer Reviews, vol. 55, no. 1, pp. 107–162, 2015, doi: 10.1080/15583724.2014.971124.

[30] K. T. Lau, P. Y. Hung, M. H. Zhu, and D. Hui, “Properties of natural fiber composites for structural engineering applications,” Composites Part B: Engineering, vol. 136, no. October 2017, pp. 222–233, 2018, doi: 10.1016/j.compositesb.2017.10.038.

[31] D. D. Stokke, Q. Wu, and G. Han, "Introduction to wood and natural fiber composites,"Wiley, 2013.

[32] M. Mittal and R. Chaudhary, “Experimental study on the water absorption and surface characteristics of alkali treated pineapple leaf fiber and coconut husk fiber,” vol. 13, no. 15, pp. 12237–12243, 2018.

[33] D. O. Rachmawati and I. G. A. Gunadi, “Development of natural fiber composites based on thickness swelling using palm fiber and coconut fiber paper,” Advances in Social Science, Education and Humanities Research, volume 394,Icirad 2019, pp. 294–299, 2020, doi: 10.2991/assehr.k.200115.048.

[34] M. Poletto, H. L. Ornaghi Jnior, and A. J. Zattera, “Thermal decomposition of natural fibers: kinetics and degradation mechanisms,” in Reactions and Mechanisms in Thermal Analysis of Advanced Materials, Wiley Blackwell, 2015, pp. 515–545.

[35] M. S. Alwani, H. P. S. A. Khalil, O. Sulaiman, M. N. Islam, and R. Dungani, "An approach to using agricultural waste fibers in biocomposites application: thermogravimetric analysis and activation energy study," Bio Resources, no. 1, pp. 218-230, 2014.

[36] D.Shilpa and G.Manavendra, "A study of thermal stability and activation energy on natural fibers for bio composite applications," International Journal for Scientific Research & Development, vol. 3, no. 9, pp. 2321-0613,2015.

[37] F. Yao, Q. Wu, Y. Lei, W. Guo, and Y. Xu, "Thermal decomposition kinetics of natural fibers: Activation energy with dynamic thermogravimetric analysis," Polymer Degradation and Stability, vol. 93, no. 1, pp. 90–98, Jan. 2008, doi: 10.1016/j.polymdegradstab.2007.10.012.

[38] B. Enciso, J. Abenojar, G. M. Aparicio, and M. A. Martínez, "Decomposition kinetics and lifetime estimation of natural fiber reinforced composites: Influence of plasma treatment and fiber type," Journal of Industrial Textiles, 2019, doi: 10.1177/1528083719886046.

[39] N. L. Batista, M. L. Costa, K. Iha, and E. C. Botelho, "Thermal degradation and lifetime estimation of poly(ether imide)/carbon fiber composites," Journal of Thermoplastic Composite Materials, vol. 28, no. 2, pp. 265–274, Mar. 2015, doi: 10.1177/0892705713484740.

[40] D. J. Toop, "Theory of life testing and use of thermogravimetric analysis to predict the thermal life of wire enamels," IEEE Transactions on Electrical Insulation, vol. EI-6, no. 1, pp. 2–14, 1971, doi: 10.1109/TEI.1971.299128.

[41] Y. K. Sahu, A. Agrawal, and A. Satapathy, "Heat conduction behavior of short fiber reinforced polymer composites," International Journal of Advanced Technology in Engineering science, vol. 04, no. 1, Feb. 2016

[42] E. M. Sunil and G.Manavendra, "Experimental investigation on thermal properties of bagasse fly ash reinforced epoxy composite," International Research Journal of Engineering and Technology (IRJET),vol 4, no. 4, 2017,

[43] S. B. R. Devireddy and S. Biswas, "Thermo-physical properties of short banana–jute fiber-reinforced epoxy-based hybrid composites," Journal of Materials Design and Application, vol. 232, no. 11, pp. 939–951, Nov. 2018, doi: 10.1177/1464420716656883.

[44] B. R. Rao, V. R. Raju, and K. M. Rao, "Effect of fiber shape on transverse thermal conductivity of unidirectional composites," Sadhana - Academy Proceedings in Engineering Sciences., vol. 40, no. 2, pp. 503–513, 2015, doi: 10.1007/s12046-014-0323-9.

[45] K. B. Priya, M. Abid Ali, and N. G. S. Ram, "Design and analysis of square model unit cell for the prediction of thermal conductivity of fiber reinforced composites," International Journal of Applied Engineering Research, vol. 11, no. 10, pp.7166-7170, 2016.

[46] T. S. Rao, B. R. Rao and V.B.Murthy, "Transverse thermal conductivity of

hollow fiber composites," International Journal of Engineering Technology Science and Research vol. 5, no. 5, pp. 389–394, 2018.

[47] S. B. R. Devireddy and S. Biswas, "Physical and thermal properties of unidirectional banana-jute hybrid fiber-reinforced epoxy composites," Journal of Reinforced plastics and composites,vol. 35, no. 15, pp. 1157–1172, Aug. 2016, doi: 10.1177/0731684416642877.

[48] B. V. Subrahmanyam, S. V. Gopala Krishna, R. Jithedra Kumar, and S. B. R. Devireddy, "Experimental and micromechanical thermal characteristics of jute fiber reinforced polyester composites," Materials Today: Proceedings, vol. 18, pp. 350–356, 2019, doi: 10.1016/j.matpr.2019.06.311.

[49] K. Liu, H. Takagi, and Z. Yang, "Evaluation of transverse thermal conductivity of Manila hemp fiber in solid region using theoretical method and finite element method," Materials and Design, vol. 32, no. 8–9, pp. 4586–4589, Sep. 2011, doi: 10.1016/j.matdes.2011.04.006.

[50] S. Sihn and A. K. Roy, "Micromechanical analysis for transverse thermal conductivity of composites," Journal of Composite Materials, vol. 45, no. 11, pp. 1245–1255, Jun. 2011, doi: 10.1177/0021998310382311.

[51] D. Mishra, A. Satapathy, and A. Patnaik, "Processing and thermal conductivity characterization of solid glass micro-spheres filled polymer composites," Proceedings of 14th International Conference on Advanced Materials and Processing Technologies, Istanbul, Turkey, 2011.

[52] N. P. Ilyas and C. R. Rejeesh, "Modelling and thermal analysis of medium density coir composite boards," International Journal of Engineering and Technical Research, vol. V4, no. 08, Aug. 2015, doi: 10.17577/IJERTV4IS080554.

[53] K. Pietrak and T. Wiśniewski, "A review of models for effective thermal conductivity of composite materials," Journal of Power of Technologies, vol. 95, no. 1, pp. 14–24, 2015.

[54] P. Kosbe and P. A. Patil, "Effective thermal conductivity of polymer composites: a review of analytical methods," International Journal of Ambient Energy, pp. 1–12, 2018, doi: 10.1080/01430750.2018.1557544.

[55] S. Bhaskara and R. Devireddy, "Thesis: mechanical , thermal and physical properties of hybrid banana-jute fibers reinforced epoxy and polyester composites : modeling and experiments mechanical , thermal and physical properties of hybrid banana-jute fibers reinforced epoxy and polyester," Department of Mechanical Engineering, National Institute of Technology Rourkela 2016.

[56] R. C. Progelhof, J. L. Throne, and R. R. Ruetsch, "Methods for predicting the thermal conductivity of composite systems: A review," Polymer Engineering & Science, vol. 16, no. 9, pp. 615–625, 1976, doi: 10.1002/pen.760160905.

[57] Y. K. Sahu, "Thesis: Study on the effective thermal conductivity of fiber

reinforced epoxy composites," Department of Mechanical Engineering,National Institute of Technology, Rourkela, India, 2014.

[58] D. S. Smith, A. Alzina, and J. Bourret, "Thermal conductivity of porous materials," Journal of Materials Research, vol. 28, no. 17, pp. 2260–2272, 2013, doi: 10.1557/jmr.2013.179.

[59] H. W. Russel, "Principal of heat flow in porous insulators," vol. 2, no. Leiden 1961, pp. 220–222, 1982.

[60] K. Ankang and H. Houde, "Effective thermal conductivity of open cell polyurethane foam based on the fractal theory," Advances in Materials Science and Engineering, vol. 2013, no. 1, 2013, doi: 10.1155/2013/125267.

[61] P. D. C. Kumara, M. P. S. Viraj, H. H. E Jayaweera, A. M. Muzathik, and T.R. Ariyaratne, "Experimental investigation of the temperature dependency of the thermal conductivity of glass wool used in a steam generator". Research Symposium 2016 – University of Colombo. Colombo, Sri Lanka.

[62] T.D. Eastop and A. McConkey, Applied thermodynamics for engineering technologists, 5th ed. Harlow: Longman, 1993.

[63] C.P. Arora, Refrigeration and air conditioning, 3rd ed. New Delhi: Tata McGraw-Hill publishing company Limited, 2009.

[64] S. Veiseh, N. Khodabandeh , and A. Hakkaki-Fard ,"Mathematical models for thermal conductivity-density relationship in fibrous thermal insulations for practical applications Article," Asian Journal of Civil Engineering (Building and Housing), vol. 6, no. 4, 2008.

[65] M. Zou, B. Yu, D. Zhang, and Y. Ma, "Study on optimization of transverse thermal conductivities of unidirectional composites," Journal of Heat Transfer, vol. 125, no. 6, pp. 980–987, Dec. 2003, doi: 10.1115/1.1621892.

[66] A. Agrawal and A. Satapathy, "Mathematical model for evaluating effective thermal conductivity of polymer composites with hybrid fillers," International Journal of Thermal Sciences, vol. 89, pp. 203–209, Mar. 2015, doi: 10.1016/j.ijthermalsci.2014.11.006.

[67] R. Shrivastava, A. Telang, R. S. Rana, and R. Purohit, "Mechanical Properties of Coir/ G Lass Fiber Epoxy Resin Hybrid Composite," Materials Today: Proceedings, vol. 4, no. 2, pp. 3477–3483, 2017, doi: 10.1016/j.matpr.2017.02.237.

[68] L. Mishra and G. Basu, "Coconut Fiber: Its structure, properties and applications," Handbook of natural fibers, vol 1, pp. 231-255 , 2020, doi: 10.1016/B978-0-12-818398-4.00010-4.

[69] M. M. Kabir, M. Islam, and H. Wang, "Mechanical and Thermal Properties of Jute Fiber Reinforced Composites,"Journal of Multifunctional Composite, 2013, doi:10.12783/issn.2168-4286/1.1/Islam.

[70] H. Abdellaoui, M. Raji, H. Essabir, R. Bouhfid, and A. E. K. Qaiss, "Mechanical

behavior of carbon/natural fiber-based hybrid composites," Mechanical and Physical Testing of Bio composites, Fiber-Reinforced Composites and Hybrid Composites., pp. 103–122, 2018, doi: 10.1016/B978-0-08-102292-4.00006-0.

[71] R. Agrawal, N. S. Saxena, K. B. Sharma, M. S. Sreekala, and S. Thomas, "Thermal conductivity and thermal diffusivity of palm fiber reinforced binary phenolformaldehyde composites," Indian Journal of Pure and Applied Physics, vol. 37, no. 12, pp. 865–869, 1999.

[72] A. Shalwan, M. Alajmi, and A. Alajmi, "Insulation Characteristics of Sisal Fiber/Epoxy Composites," International Journal of Polymer Science, vol. 2017, 2017, doi: 10.1155/2017/7312609.

[73] T. G. Y. Gowda, M. R. Sanjay, K. Subrahmanya Bhat, P. Madhu, P. Senthamaraikannan, and B. Yogesha, "Polymer matrix-natural fiber composites: An overview," Cogent Engineering, vol. 5, no. 1, 2018, doi: 10.1080/23311916.2018.1446667.

[74] N. Saba, M. Jawaid, O. Y. Alothman, M. T. Paridah, and A. Hassan, "Recent advances in epoxy resin, natural fiber-reinforced epoxy composites and their applications," Journal of Reinforced Plastics and Composites, vol. 35, no. 6, pp. 447–470, 2016, doi: 10.1177/0731684415618459.

[75] P. Yu ,H. He and C. Jiang "Reinforcing styrene butadiene rubber with lignin-novolac epoxy resin networks," Express Polymer Letters, vol. 9, no. 1, pp. 36–48, 2015, doi: 10.3144/expresspolymlett.2015.5.

[76] D. G. Edirisinghe, W. D. M. Sampath, and P. C. Wettasinghe, "Effect of latex coated coconut fiber on cure characteristics and physico mechanical properties of natural rubber-coir composites," Journal of the Rubber Research Institute of Sri Lanka, vol. 95, 2015, doi: 10.4038/jrrisl.v95i0.1832.

[77] J. Thuraisingam, P. Mishra, A. Gupta, T. Soubam, and B. M. Piah, "Novel natural rubber latex/lignin-based bio-adhesive: synthesis and its application on medium density fiber-board," Iranian Polymer Journal (English Edition)., vol. 28, no. 4, pp. 283–290, 2019, doi: 10.1007/s13726-019-00696-5.

[78] K. A. M. Priyadarshani, R. C. Marawanagoda, A. Sirajulhasan, L. K. T. Srimal, B. Sumith, R. Gallage "Development of Coir Mat for Thermal Insulation Purposes", 4th Annual Research Symposium 2016, Faculty of Engineering, University of Ruhuna, Galle, Sri Lanka, 5th January 2017, doi: 10.13140/RG.2.2.11514.62402

[79] L. K. T. Srimal, M. A. R. V. Fernando, and B. Sumith, "Value addition for coir fiber as thermal insulation material", Master of Engineering thesis, Department of Mechanical Engineering, University of Moratuwa, Sri Lanka, March 2014. [Online]. Available: http://dl.lib.uom.lk/handle/123/10957

[80] A.M. Lahiru, L. K. T. Srimal, H.C.P. Karunasena, and B. Sumith, "Value addition for coir fiber as an oil absorbent material", 13th Academic Sessions 2016, Faculty of Agriculture, University of Ruhuna, Matara, Sri Lanka, 2nd

March 2016.

[81] M. Elkington, D. Bloom, C. Ward, A. Chatzimichali, and K. Potter, “Hand layup: understanding the manual process,” Advanced Manufacturing: Polymer and Composites Science, vol. 1, no. 3, pp. 138–151, 2015, doi: 10.1080/20550340.2015.1114801.

[82] M. Raji, H. Abdellaoui, H. Essabir, C. A. Kakou, R. Bouhfid, and A. El Kacem Qaiss, "Prediction of the cyclic durability of woven-hybrid composites," Durability and Life Prediction in Bio composites, Fiber-Reinforced Composites and Hybrid Composites ,pp. 27-62, 2018.

[83] D. Zhao, X. Qian, X. Gu, S. A. Jajja, and R. Yang, “Measurement techniques for thermal conductivity and interfacial thermal conductance of bulk and thin film materials,” Journal of Electronic Packaging, Transactions of the ASME E, vol. 138, no. 4, pp. 1–64, 2016, doi: 10.1115/1.4034605.

[84] S. A. Al-Ajlan, “Measurements of thermal properties of insulation materials by using transient plane source technique,” Applied Thermal Engineering, Transactions of the ASME, vol. 26, no. 17–18, pp. 2184–2191, 2006, doi: 10.1016/j.applthermaleng.2006.04.006.

[85] N. Yuksel, “The Review of Some Commonly Used Methods and Techniques to Measure the Thermal Conductivity of Insulation Materials,” Intech, pp. 13, 2016, [Online]. Available: https://www.intechopen.com/books/advanced-biometric-technologies/liveness-detection-in-biometrics.

[86] G. L. Devnani, and S. Sinha, “Extraction, characterization and thermal degradation kinetics with activation energy of untreated and alkali treated Saccharum spontaneum (Kans grass) fiber,” Composite Part B Engineering, vol. 166, no. October 2018, pp. 436–445, 2019, doi: 10.1016/j.compositesb.2019.02.042.

[87] E. Naveen, N. Venkatachalam, N. Maheswaran N“Alkalichemical Treatment on the Surface of Natural Fibers,” International Journal of Innovative Research in Science, Engineering and Technology, vol. 4, no. 4, pp. 172–178, 2015, [Online]. Available: http://www.ijirset.com/upload/2015/tapsa/25_ME009.pdf.

[88] C. Tezara1, J. P. Siregar, H. Y. Lim, F. A. Fauzi, M. H. Yazdi, L. K. Moey, and J. W. Lim “Factors that affect the mechanical properties of kenaf fiber reinforced polymer: A review,” Journal of Mechanical Engineering and Sciences, vol. 10, no. 2, pp. 2159–2175, 2016, doi: 10.15282/jmes.10.2.2016.19.0203.

[89] Dharmaratne, P.D., Jayasinhge, R.A., Nilmini, A.H.L.R., Galabada, G.H. and Halwatura, R.U., 2021. Preliminary Investigation of the Suitability of Coir Fiber and Thermoplastic Waste as a Construction Material. Engineer: Journal of the Institution of Engineers, Sri Lanka, 54(4), pp.65–74. 2021, DOI: http://doi.org/10.4038/engineer.v54i4.7471.

[90] Standard Test Method for Tensile Properties of Polymer Matrix Composite

Materials, ASTM D 3039/D 3039M, 2017.

[91] L. S. Kuburi et al., “Effects of Coir Fibber Loading on the Physio-mechanical and Morphological Properties of Coconut Shell Powder Filled Low Density Polyethylene Composites,” Procedia Manufacturing , vol. 7, pp. 138–144, 2017, doi: 10.1016/j.promfg.2016.12.036.

[92] B. PrakashReddy, S. Satish, and C. J.ThomasRenald, “Investigation on tensile and flexural properties of coir fiber reinforced isophthalic polyester composites,” International Journal of Current Engineering and Technology, no. 2, pp. 220–225, 2014.

[93] M. E. Ali, and A. Alabdulkarem, “On thermal characteristics and microstructure of a new insulation material extracted from date palm trees surface fibers,” Construction and Building Materials , vol. 138, pp. 276–284, 2017, doi: 10.1016/j.conbuildmat.2017.02.012.

[94] Estimation of Polymer Lifetime by TGA Decomposition Kinetics. TA instruments 2021. [Online] Available: https://www.tainstruments.com/pdf/literature/TA125.pdf.

[95] M. Truong, W. Zhong, S. Boyko, and M. Alcock “A comparative study on natural fiber density measurement,” The Journal of The Textile Institute. 2009;100(6):525–9. doi: 10.1080/00405000801997595

[96] A. Amiri, Z. Triplett, A. Moreira, N. Brezinka, M. Alcock, and C. A. Ulven, “Standard density measurement method development for flax fiber,” Industrial Crops and Products, vol. 96, pp. 196–202, 2017, doi: 10.1016/j.indcrop.2016.11.060.

[97] M. M. Kabir, M. M. Islam, and H. Wang, “Mechanical and thermal properties of wool waste fabric reinforced composites,” Journal of Multifunctional Composites, vol. 22, no. 97, pp. 14–20, 2015, doi: 10.7216/130075992015229703.

[98] N. J. Rodríguez et al., “Assessment of coconut fiber insulation characteristics and its use to modulate temperatures in concrete slabs with the aid of a finite element methodology,” Energy and Buildings, vol. 43, no. 6, pp. 1264–1272, 2011, doi: 10.1016/j.enbuild.2011.01.005.

[99] Manufacture of Rubberized Coir Mattresses, Rubber Research Institute of Sri Lanka, Rathmalana, Srilanka, 2016.

[100] Rubber latices - Determination of total solids content, ISO 124:1985, 1985.

[101] Standard test method for rubber - deterioration in an air oven, D 573: 04, 2019, doi: 10.1520/D0573-04R19.2.

[102] D. Y. Kim, J. W. Park, D. Y. Lee, and K. H. Seo, “Correlation between the crosslink characteristics and mechanical properties of natural rubber compound via accelerators and reinforcement,” Polymers, vol. 12, no. 9, pp. 1–14, 2020,

doi: 10.3390/polym12092020.

[103] A. Vasilev, T. Lorenz, and C. Breitkopf, “Thermal conductivities of crosslinked polyisoprene and polybutadiene from molecular dynamics simulations,” Polymers , vol. 13, no. 3, pp. 1–9, 2021, doi: 10.3390/polym13030315.

# APPENDIX A

## ANALYSING THE MECHANICAL PROPERTIES OF COIR FIBERS EXTRACTED FROM DIFFERENT PLACES

The coir fibers for this research work were selected from the Minuwangoda area in Sri Lanka. A first experiment with a coir fiber epoxy-based composite was described in chapter 3. Here, the tensile strength of the epoxy-based composite was prepared to identify the critical volume fraction and the critical fiber length. However, fiber properties can vary with the place that fibers were extracted. Therefore, it is better to compare the fiber properties with different places that were extracted. Then two more fiber samples were selected from Kurunegala area and Tangalle area. The critical length in chapter 3 was 3 cm and the critical volume fraction was 0.2. Therefore, 3 cm fiber samples were prepared from the other two samples and the composite samples were prepared from the volume fraction of 0.1, 0.2, and 0.3. The results of the tensile strength for samples that were taken from Minuwangoda, Kurunegala, and Tangalle areas shows in Figure A.1.

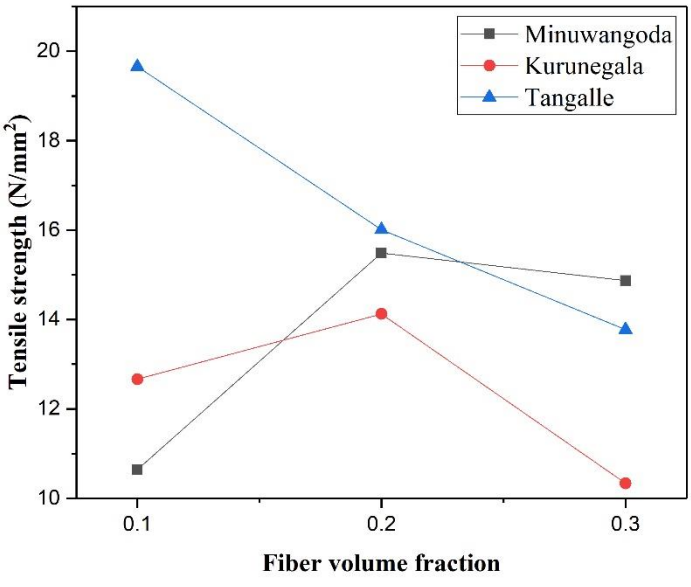


Figure A.1: Effect of the composite's tensile strength with the fiber extracted area.

The highest tensile strength is given by fibers that were taken from the Tangalle area at 0.1 fiber volume fraction. Other samples show the maximum value at 0.2 fiber volume fraction. Therefore, results concluded that the properties of composite change with the place of the fiber which was taken for the experiment.